OSCILLATION PHYSICS WITH A NEUTRINO FACTORY

M. Apollonio[1], *A. Blondel*[2], *A. Broncano*[3],*M. Bonesini*[4], *J. Bouchez*[5], *A. Bueno*[6], *J. Burguet-Castell*[7], *M. Campanelli*[2,*], *D. Casper*[8], *G. Catanesi*[9], *A. Cervera*[10], *S. Cooper*[11],*M. Donega*[2],*A. Donini*[12], *A. de Gouvêa*[13], *A. de Min*[14], *R. Edgecock*[15,16], *J. Ellis*[17], *M. Fechner*[18], *E. Fernandez*[19], *F. Ferri*[4], *B. Gavela*[3], *G. Giannini*[1], *D. Gibin*[14], *S. Gilardoni*[2,16], *J. J. Gómez-Cadenas*[2,7], *P. Gruber*[16], *A. Guglielmi*[14], *P. Hernández*[17], *P. Huber*[20], *M. Laveder*[14], *M. Lindner*[20], *S. Lola*[17,†], *D. Meloni*[12], *O. Mena*[3], *H. Menghetti*[21], *M. Mezzetto*[14], *P. Migliozzi*[22], *S. Navas-Concha*[6], *V. Palladino*[23], *I.Papadopoulos*[24], *K.Peach*[15], *E. Radicioni*[9], *S. Ragazzi*[4], *S. Rigolin*[17], *A. Romanino*[25], *J. Rico*[6], *A. Rubbia*[6], *G. Santin*[1], *G. Sartorelli*[21], *M. Selvi*[21], *M.Spiro*[5], *T. Tabarelli*[4], *A. Tonazzo*[4], *M. Velasco*[26], *G. Volkov*[27], *W. Winter*[20], *P. Zucchelli*[10,28]

[1] University of Trieste and INFN Trieste, Italy
[2] DPNC, University of Geneva, Switzerland
[3] Dep. de Física Teórica, Univ. Autónoma de Madrid, Madrid, Spain
[4] University of Milano 2 Bicocca and INFN Milano, Italy
[5] DAPNIA, CEA Saclay, France
[6] ETH Zurich, Switzerland
[7] University of Valencia and IFIC Valencia, Spain
[8] University of California, Irvine, California, USA
[9] INFN Bari, Italy
[10] CERN EP, Geneva, Switzerland
[11] Oxford University, Oxford, United Kingdom
[12] University of Roma I and INFN Roma I, Italy
[13] Fermilab, Batavia, Illinois, USA
[14] University of Padova and INFN Padova, Italy
[15] Rutherford Appleton Laboratory, United Kingdom
[16] CERN PS, Geneva, Switzerland
[17] CERN TH, Geneva, Switzerland
[18] Département de Physique de l'Ecole Normale Supérieure, Paris, France
[19] Universidad Autonoma de Barcelona, Spain
[20] Tech. U. München, Munich, Germany
[21] University of Bologna and INFN Bologna, Italy
[22] INFN Napoli, Italy
[23] University of Napoli, Italy
[24] CERN IT, Geneva, Switzerland
[25] Scuola Normale Superiore, Pisa, Italy
[26] Northwestern University, Evanston, Illinois, USA
[27] IFVE, Protvino, Russia
[28] INFN Ferrara, Italy
[†] now at HR division, CERN, Geneva, Switzerland

[*] Editor: Mario.Campanelli@cern.ch

CERN-TH/2002-208, hep-ph/0210192

Abstract

A generation of neutrino experiments have established that neutrinos mix and probably have mass. The mixing phenomenon points to processes beyond those of the Standard Model, possibly at the Grand Unification energy scale. A extensive sequence of of experiments will be required to measure precisely all the parameters of the neutrino mixing matrix, culminating with the discovery and study of leptonic CP violation. As a first step, extensions of conventional pion/kaon decay beams, such as off-axis beams or low-energy super-beams, have been considered. These could yield first observations of $\nu_\mu \rightarrow \nu_e$ transitions at the atmospheric frequency, which have not yet been observed, and a first measurement of θ_{13}. Experiments with much better flux control can be envisaged if the neutrinos are obtained from the decays of stored particles. One such possibility is the concept of beta beams provided by the decays of radioactive nuclei, that has been developed within the context of these studies. These would provide a pure (anti-)electron-neutrino beam of a few hundred MeV, and beautiful complementarity with a high-intensity, low-energy conventional beam, enabling experimental probes of T violation as well as CP violation. Ultimately, a definitive and complete set of measurements would offered by a Neutrino Factory based on a muon storage ring. This powerful machine offers the largest reach for CP violation, even for very small values of θ_{13}.

Contents

1 INTRODUCTION

Neutrino experiments over 30 years [1], culminating with the Super-Kamiokande atmospheric neutrino data [2], have provided, for the first time, unambiguous evidence for the existence of physics beyond the Standard Model. This comes from the fact that the ν_μ to ν_e flux ratio is far from theoretical expectations, in combination with the nontrivial angular dependence of the atmospheric ν_μ flux. This 'atmospheric neutrino puzzle' cannot be explained by standard means, such as changing the cosmic ray spectrum, or improving the atmospheric neutrino flux computations. Furthermore, the Super-Kamiokande result is in good agreement with other, less precise, measurements of the atmospheric neutrino flux [3].

On a different front, solar neutrino experiments [4, 5] have consistently been measuring solar ν_e fluxes which are significantly smaller than those predicted by theory [6]. It is equally hard to explain this 'solar neutrino puzzle' by traditional means (dramatically modifying the currently accepted solar models, questioning the estimation of systematic effects by some of the experiments, etc.). The recent measurement of the solar neutrino flux via neutrino – deuteron scattering performed by the SNO Collaboration in both charged-current and neutral-current processes provides unambiguous evidence (at the five-sigma level) that there are active neutrinos other than ν_e coming from the Sun [5, 7].

Neutrino oscillations provide the simplest and most elegant solution to *both* the atmospheric and solar neutrino puzzles. Neutrino oscillations take place if neutrinos have non-degenerate masses and, similar to what happens in the quark sector, the neutrino mass eigenstates differ from the neutrino weak, or flavour, eigenstates. Although less standard solutions to the atmospheric and the solar neutrino puzzles, such as exotic neutrino decays, or flavour-violating interactions [8] may still be advocated, no satisfactory single solution to both anomalies other than neutrino oscillations is known.

The implications of the neutrino data are extremely interesting, since they point towards non-zero neutrino masses, which are *prima facie* evidence for physics beyond the Standard Model. In the absence of right-handed neutrinos, ν_R, no Dirac neutrino mass can be generated, while the transformation properties of the left-handed neutrinos, ν_L, under $SU(2) \times U(1)$ also forbid a renormalisable Majorana mass term. On the other hand, non-zero neutrino masses arise naturally in many extensions of the Standard Model, which generically contain an extended lepton and/or Higgs sector, and possibly new lepton number-violating interactions.

A large number of analyses of the solar, atmospheric and reactor neutrino data can be found in the literature [9], including two-flavour and three-flavour analyses of the solar data [10], two-flavour analyses of the atmospheric data [11], three-flavour analyses of the combined atmospheric and reactor data [12] and combined analyses of all neutrino data [13]. It turns out that both the solar and the atmospheric neutrino deficits can be accommodated in minimal schemes with three light neutrinos, which may have either of the following hierarchical patterns of masses:

(a) The normal hierarchy, in which the masses are fixed by the mass differences required for the atmospheric and solar deficits. The atmospheric neutrino data require $m_3 \approx 10^{-1}$ to $10^{-1.5}$ eV, while m_2 is determined by the solar neutrino squared-mass difference.

(b) Inverted hierarchy solutions, in which $|m_1| \sim |m_2| \gg |m_3|$, where $m^2_{1,2} \sim \Delta m^2_{atm}$ and $\Delta m_{12} = \Delta m^2_{sun}$.

Since oscillation experiments are only sensitive to mass differences of two neutrino species and not to the absolute values of the masses, normal and inverted solutions with near-degenerate masses are also allowed.

Information about the absolute neutrino mass scale can be derived from direct searches, and experiments looking for neutrinoless double-beta decay if neutrinos are Majorana particles, are sensitive to neutrino masses $\mathcal{O}(\mathrm{eV})$ or below. If the masses are close to the upper boundary of this limit, neutrinos may still provide a significant component of hot dark matter; next generation experiments looking for direct neutrino mass will probe this scenario, which is however disfavoured by the most recent cosmological observations.

Neutrino oscillations (and other types of new physics in the neutrino sector) can potentially be observed in terrestrial neutrino experiments, by studying, for example, the flux of $\bar{\nu}_e$ coming from nuclear reactors [14] or studying the ν_μ flux from pion or muon decays [15]. The K2K experiment has reported first results that are consistent with the atmospheric neutrino data [16]. So far, no other terrestrial evidence for oscillations has been confirmed, although the current results significantly constrain the neutrino oscillation parameter space. However, the LSND Collaboration has reported an anomalous flux of $\bar{\nu}_e$ from μ^+ decays, which may be interpreted as evidence for $\bar{\nu}_\mu \leftrightarrow \bar{\nu}_e$ oscillations [17]. This experimental evidence has not yet been independently confirmed, but will be put to the test in the near future [18].

The minimal schemes with only three neutrino masses allow only two independent mass differences, and thus the oscillation interpretation of the LSND result cannot be considered, unless a light sterile neutrino is introduced [19]. In this case, one has to take into account the constraints from cosmological Big Bang Nucleosynthesis: a sterile neutrino that mixes with an active one, thus being in equilibrium at the time of nucleosynthesis, can change the abundance of primordially produced elements, such as ^{4}He and deuterium. The larger the mixing and the mass differences between the sterile and active neutrinos, the bigger the deviations from the observed light element abundances. This implies that models where the sterile component contributes to solar rather than atmospheric neutrino oscillations are accommodated more easily within the standard nucleosynthesis scenarios. However, recent data on solar neutrino oscillations disfavor the sterile solution also in this case. In our discussion, we focus on the minimal schemes with only three light neutrinos. The physics programme of the Neutrino Factory would be even richer if there were more light neutrinos.

We can hope that future neutrino data will provide important information on the possible models. Indeed, the main goals of the next generation of neutrino experiments include the determination of neutrino mass-squared differences and leptonic mixing angles. If neutrino oscillations are indeed the solution to the neutrino puzzles, the measurement of these fundamental parameters is of utmost importance. Moreover, in general we may expect that $P(\bar{\nu}_\alpha \to \bar{\nu}_\beta) \neq P(\nu_\alpha \to \nu_\beta)$ and that we may look for CP violation in a neutrino factory [20] by measuring observables of the type

$$A_{CP} \equiv \frac{P(\nu_e \to \nu_\mu) - P(\bar{\nu}_e \to \bar{\nu}_\mu)}{P(\nu_e \to \nu_\mu) + P(\bar{\nu}_e \to \bar{\nu}_\mu)}. \tag{1}$$

In the near future, it is essential to:

• Confirm the atmospheric neutrino puzzle in a terrestrial experiment and determine the 'atmospheric' mixing parameters. This is one of the driving forces behind the accelerator-based long-baseline neutrino experiments, namely the K2K experiment [16], which started taking data in 1999 and already has presented some results, the Fermilab NUMI/MINOS [21] project, which is under construction and is supposed to start data-taking in 2005, and the CNGS (CERN neutrinos to Gran Sasso) project [23], which should start running in 2006. The CNGS effort also aims to determine whether $\nu_\mu \leftrightarrow \nu_\tau$ is the dominant oscillation channel responsible for the atmospheric neutrino anomaly, by searching for the appearance of τ leptons from an initially pure ν_μ beam.

• Establish that the solar neutrino puzzle is indeed due to neutrino oscillations and determine what are the 'solar' mixing parameters. This is one of the goals of the SNO experiment [24]. Other experiments will also contribute significantly to these goals, such as KamLAND [25], which may provide terrestrial confirmation for the solar neutrino puzzle as long as the solar oscillation parameters lie in the LMA region, and GNO, which may observe anomalous seasonal variations of the solar neutrino flux [26]. New experiments, such as Borexino [27], which is already under construction and should start taking data in 2003, and a possible upgrade of the KamLAND [25] experiment, may also observe anomalous seasonal variations [28] or a day-night variation [29] of the ^{7}Be solar neutrino flux. It should also be mentioned that a 'background-free' version of Borexino, or an experiment to measure the pp solar neutrino flux, similar to the HELLAZ [30] proposal, should also be able to detect the presence of

neutrinos other than ν_e coming from the Sun [31].

It is very likely that, after the present and the next rounds of neutrino experiments, both the atmospheric and solar neutrino puzzles will be unambiguously established as signals for new physics. Moreover, neutrino flavour conversions would also be confirmed. Neutrino oscillations, and therefore unambiguous evidence for neutrino masses and mixing, will be more difficult to establish explicitly by the observation of an oscillating pattern. However, the K2K data offer a hint of an oscillation effect in their energy spectrum, KamLAND [25] has an opportunity when studying reactor neutrinos, and this is also an objective of the MINOS experiment. For atmospheric neutrinos, a possible option for better observations in the future is to build a new generation of larger atmospheric neutrino detectors with higher performance. Current detector studies include target materials as different as iron [32], liquid argon [23] and water [33].

We set out in this review a multi-step programme for exploring neutrino oscillations and related physics. This includes:

• An intense hadron source, such as could be provided by the Superconducting Proton Linac (SPL) project at CERN, which could yield a low-energy neutrino super-beam.

• The beta-beam concept, which envisages the production of pure ν_e and $\bar{\nu}_e$ beams via the decays of radioactive nuclei stored in a ring.

• The Neutrino Factory itself, in which pure ν_e and $\bar{\nu}_\mu$ beams, or pure ν_μ and $\bar{\nu}_e$ beams, are produced via the decays of muons stored in a ring.

As we discuss in this report, this multi-step programme represents a systematic scheme for exploring neutrino physics. There are significant synergies between successive steps in the programme. It also offers unique prospects for short-baseline neutrino physics and studies of rare decays of slow and stopped muons, that are discussed elsewhere [34, 35]. Moreover, in the longer term, the Neutrino Factory is an essential stepping-stone towards possible muon colliders, as also discussed elsewhere [36].

2 CURRENT STATUS OF NEUTRINO MASSES AND OSCILLATIONS

2.1 Neutrino Masses

2.1.1 Laboratory limits

Direct laboratory limits on neutrino masses are obtained from kinematical studies. The most stringent current upper limit is that on the $\bar{\nu}_e$ mass, coming from studies of the end-point of the electron energy spectrum in Tritium beta decay [37]

$$m_{\bar{\nu_e}} \leq 2.5 \text{ eV}$$

For some time, these experiments tended to prefer a negative mass squared, but this problem has now disappeared, as has the previous report of a spectral feature near the end-point. The proposed KATRIN experiment aims to improve the sensitivity to $m_{\bar{\nu_e}} \sim 0.3$ eV [38]. Constraints on the mass of ν_μ are derived from the decay $\pi^+ \to \mu^+ + \nu_\mu$, which leads to the bound [39]

$$m_{\nu_\mu} \leq 170\,\text{keV}$$

This upper limit could be improved by careful studies using the high fluxes provided at the front end of a neutrino factory. Finally, the mass of ν_τ is constrained by τ decays into multihadron final states: $\tau^- \to 2\pi^-\pi^+\nu_\tau$ and $\tau^- \to 3\pi^-2\pi^+\pi^0\nu_\tau$. The current limit is [40]

$$m_{\nu_\tau} \leq 15.5\,\text{MeV}$$

and experiments at B factories may be sensitive to $m_{\nu_\tau} < 10$ MeV. We note that the distinction between neutrino flavour and mass eigenstates is unimportant for the above direct upper limits, as long as the mass differences indicated by oscillation experiments are much smaller.

An important constraint on Majorana neutrino masses arises from neutrinoless double-β decay [41], in which an (A, Z) nucleus decays to $(A, Z+2) + 2\,e^-$, without any neutrino emission. This could be generated by the following quark-level interaction:

$$d + d \to u + u + e^- + e^-$$

which violates lepton number by two units ($\Delta L = 2$). Such a transition could be generated by an exotic, beyond the Standard Model interaction, and any such interaction would necessarily generate a non-zero Majorana neutrino mass [42]. Assuming that this dominates the neutrinoless double-β decay matrix element as illustrated in Fig. 1, it can be used to constrain the combination

$$< m_{ee} > \equiv |\sum U_{ei}^{*2} m_i|, \tag{2}$$

which involves a coherent sum over all the different Majorana neutrino masses m_i, weighted by their mixings with the electron flavour eigenstate, which may include CP-violating phases, as discussed below. This observable is therefore distinct from the quantity observed in Tritium β decay.

The interpretation of neutrinoless double-β decay data depends on calculations of the nuclear matrix elements entering in this process. The strictest limit that had been reported until recently came from a study of the ^{76}Ge isotope by the Heidelberg-Moscow Collaboration [43]:

$$< m_{ee} > \ \leq \ 0.2 \text{ eV}$$

Subsequently, the data of this experiment have been reanalysed in [44], where evidence for neutrinoless double-β decay at a rate corresponding to a mass

$$< m > = (0.11 - 0.56) \text{ eV},$$

has been reported, with a preferred value of 0.39 eV. However, this interpretation is not yet generally accepted. We note that there are proposals capable of improving the sensitivity of neutrinoless double-β decay experiments by an order of magnitude.

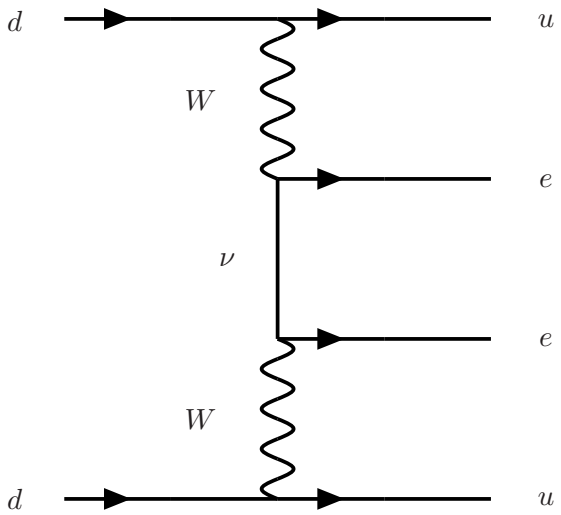

Fig. 1: *Diagrammatic representation of the possible role of a Majorana neutrino mass in generating neutrinoless double-β decay.*

2.1.2 Astrophysical and cosmological constraints on neutrino masses

For a review of cosmological and astrophysical limits on neutrino masses, see [45]. Neutrinos much lighter than 1 MeV have relic number densities that are essentially independent of their masses, yielding a relic energy density that is linear in the sum of their masses [46]:

$$\Omega_\nu h^2 \; = \; \left(\frac{\sum_i m_{\nu_i}}{94 \; \mathrm{eV}} \right), \tag{3}$$

where $\Omega_\nu \equiv \rho_\nu / \rho_c$, ρ_ν is the neutrino energy density and ρ_c the critical density, h parametrises the uncertainty in the Hubble parameter and is probably in the range $0.6 \leq h \leq 0.9$, and the sum in (3) is over all conventional electroweak doublet neutrinos, which are assumed to be metastable [1]. Cosmic microwave background data and large-redshift supernovae indicate a total matter density $\Omega_m < 0.5$, corresponding to $\sum_i m_{\nu_i} \lesssim 30$ eV. Theories of large-scale structure formation suggest that $\Omega_\nu \ll \Omega_m$, with the remainder of Ω_m dominated by cold dark matter [47], and a recent global analysis of data on the cosmic microwave background radiation, large-scale structure, big-bang nucleosynthesis and large-redshift supernovae yields

$$\sum_i m_{\nu_i} \leq 2.5 \; \mathrm{eV}.$$

The small differences in neutrino masses-squared indicated by the oscillation data discuss later then imply that each neutrino species must weigh $\lesssim 0.9$ eV.

Cosmological nucleosynthesis additionally imposes constraints on possible oscillations between conventional active neutrinos and any additional light sterile neutrinos [48]. If these are sufficiently strong that the relativistic density of additional neutrinos is comparable to that of the active neutrinos, the rate of expansion of the universe is affected during nucleosynthesis, and hence the produced abundance of ^{4}He in particular. The success of conventional calculations of primordial nucleosynthesis suggests that

$$\delta m^2 \; \sin^2 \theta < 10^{-6} \; \mathrm{eV}^2$$

[1] There are also constraints on the lifetimes of unstable neutrinos obtained by requiring that the energy density of the relativistic decay products be below the critical density, and late decays should also satisfy constraints from the cosmic microwave background radiation and light-element abundances.

for the mass-squared difference δm^2 and mixing angle θ between any active and sterile species.

Additional limits on neutrino masses and mixing are obtained from astrophysical processes, such as supernova physics [49, 50]. The arrival times of neutrinos from SN 1987a have been used to derive upper limits of about 20 eV on neutrino masses. Oscillations inside a supernova must be considered in connection with the r-process, and also for the interpretation of any future neutrino signal from a galactic supernova. As a final point in this short discussion, we note that one of the favoured scenarios for generating the baryon asymmetry in the universe is leptogenesis [51]. In this scenario, CP violation in the decays of massive singlet neutrinos create a lepton asymmetry, which is subsequently recycled by non-perturbative electroweak interactions into a baryon asymmetry. We discuss later the possibility that the parameters of such a leptogenesis scenario may be related to neutrino and/or charged-lepton parameters that may be measurable in experiments.

2.1.3 General principles for neutrino masses

There is no fundamental theoretical reason why neutrinos should not have masses and mix with one another. It is generally thought that particles are massless if and only if they are associated with an exact gauge symmetry. Examples include the photon and gluon, which are thought to be massless because of $U(1)$ and $SU(3)$ gauge symmetries, respectively. There is no exact gauge symmetry associated with lepton number L, so it is expected that lepton number should be violated at some level. If L is violated by two units: $\Delta L = 2$, then neutrino masses may arise.

On the other hand, the particle content of the minimal Standard Model, in conjunction with gauge invariance and renormalisability, allows neither a Dirac nor a Majorana neutrino mass term. A Dirac mass of the form $m(\bar{\nu_L}\nu_R + \bar{\nu_R}\nu_L)$ cannot arise in the absence of a singlet ν_R field, whilst a Majorana term $m\nu_L^T\sigma_2\nu_L$ has weak isospin $I = 1$, and hence would violate $SU(2)$ gauge invariance. However, it is possible to introduce Majorana neutrino masses into the Standard Model, even without postulating any new particles, at the price of postulating a higher-order non-renormalizable interaction linking two left-handed doublet neutrino fields and two Higgs doublets:

$$\frac{(H.L)(H.L)}{M}, \tag{4}$$

where H denotes a Higgs doublet field, L denotes a generic lepton doublet field, and M is some (large) mass parameter that is required for dimensional reasons. An interaction of the form (4) would yield neutrino masses of order

$$m_\nu \sim \frac{< 0|H|0 >^2}{M}, \tag{5}$$

which would be $\ll m_{q,\ell}$ if $M \gg < 0|H|0 >$. However, an interaction of the type (4) is not satisfactory from a theoretical point of view, because it is non-renormalizable. Therefore, we need to understand the presence of such a term in the framework of well-motivated extensions of the Standard Model.

The minimal such possibility is to add three heavy singlet-neutrino fields ${N^c}_i$ to the Standard Model, often called right-handed neutrinos, without necessarily expanding the gauge group. Then the following neutrino Dirac and Majorana mass terms are allowed in the Lagrangian:

$$\mathcal{L} = N_i^c(M_{\nu_D})_{ij}L_j + \frac{1}{2}{N^c}_i(M_{\nu_R})_{ij}N_j^c + h.c. \tag{6}$$

where the indices i, j run over three generations, $M_{\nu_D} = Y_\nu < 0|H|0 >$ is the Dirac mass matrix, and M_{ν_R} is the Majorana mass matrix for the right-handed isosinglet neutrino sector. The most general neutrino mass matrix is then

$$\mathcal{M} = \begin{pmatrix} 0 & M_{\nu_D} \\ M_{\nu_D}^T & M_{\nu_R} \end{pmatrix}. \tag{7}$$

The entries in M_{ν_D} require electroweak symmetry breaking, and so must be $\lesssim m_W$, whereas the entries in M_{ν_R} may be arbitrarily large. Assuming that $M_{\nu_R} \gg M_{\nu_D}$, the light eigenvalues of M are given by

$$m_\nu^{light} \simeq \frac{M_{\nu_D}^2}{M_{\nu_R}}$$

and therefore are extremely suppressed, as is also obvious from the associated diagram shown in Fig. 2. This is the well-known seesaw mechanism [52], which explains naturally why the neutrinos are so much lighter than the other known fermions.

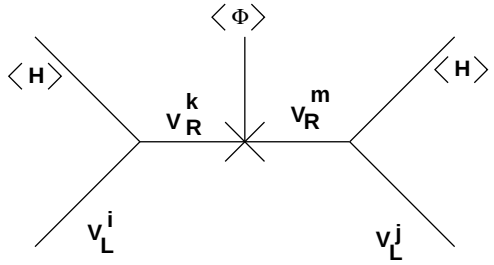

Fig. 2: *Diagrammatic representation of the seesaw mechanism for generating small neutrino masses.*

Neutrino mixing arises from the mismatch between the mass eigenstates and the current eigenstates that couple via the weak interactions to charged leptons of definite flavour. The neutrino mixing matrix is therefore given by

$$V = V_\nu^\dagger V_\ell, \tag{8}$$

where V_ℓ diagonalizes the charged-lepton mass matrix, and V_ν diagonalizes the light neutrino mass matrix m_ν^{light} [53]. As a unitary 3×3 matrix, V would seem to have 9 parameters *a priori*, but 3 of these can be absorbed by phase transformations of the charged-lepton fields, yielding a net total of 6 parameters, of which 3 are light-neutrino mixing angles $\theta_{ij} : 1 \leq i \neq j \leq 3$ and 3 are CP-violating light-neutrino mixing phases, including the oscillation phase δ and two Majorana phases $\phi_{1,2}$ that appear in the neutrinoless double-β decay observable. Thus, the total number of neutrino parameters that are in principle observable at low energies is 9: 3 light-neutrino masses m_ν^{light}, 3 real mixing angles and 3 CP-violating phases.

However, the minimal seesaw model contains a total of 18 parameters, even after taking into account the possible field redefinitions. In addition to the 9 parameters mentioned above, there are additionally 3 heavy Majorana neutrino mass eigenvalues M_{ν_R}, 3 more real mixing angles and 3 more phases associated with the heavy-neutrino sector [54]. As illustrated in Fig. 3, 12 of these parameters play a role in generating the baryon number of the universe via leptogenesis, but these do not include θ_{ij}, δ and $\phi_{1,2}$. Since the lepton number density involves a unitary sum over the light neutrino and lepton species, it is insensitive to the values of these light-neutrino mixing angles and phases. However, as also shown in Fig. 3, 16 of the 18 neutrino parameters contribute to renormalization effects that are, in principle, measurable in a supersymmetric version of the minimal seesaw model.

2.1.4 Aspects of models for neutrino masses and mixing

Our experimental knowledge of the 18 neutrino parameters introduced above is limited so far to 4: 2 neutrino mass-squared differences, and 2 mixing angles. As we discuss later in more detail, the data indicate that these 2 measured neutrino mixing angles are probably both quite large, possibly even maximal, whilst the third angle is relatively small. Since the seesaw mechanism suggests that the origins of neutrino masses and mixings are different from, and more complicated than those of quarks, we should, in retrospect, perhaps not have been so surprised that some neutrino mixing angles are larger than those

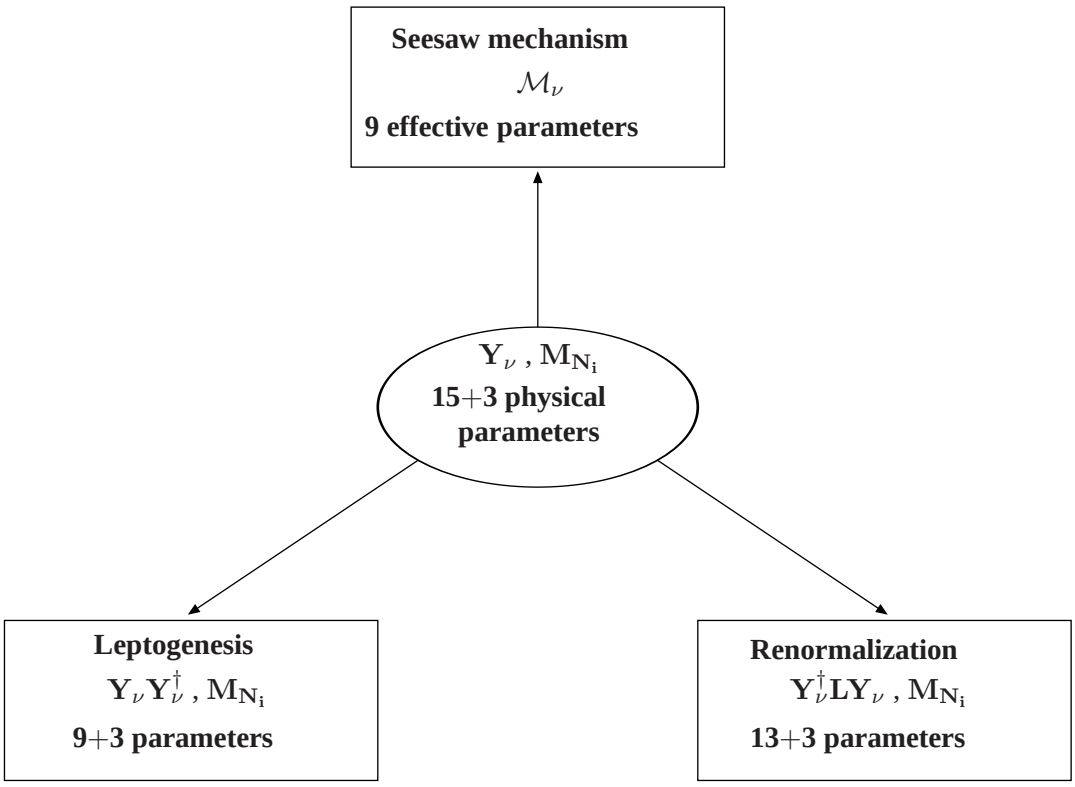

Fig. 3: *Roadmap for the physical observables derived from Y_ν and N_i.*

in the quark sector. The spate of experimental information on neutrino masses and mixing, and their unexpected nature, has spawned many theoretical models, some of whose general features we review below. The neutrino factory is uniquely well placed to provide crucial input for distinguishing between such models, in particular via neutrino-oscillation experiments. Models for neutrino masses and mixing typically incorporate ideas for family (or generation) symmetries and/or grand unification schemes linking quarks and leptons, and we now give examples of each.

$U(1)$ *Flavour Symmetries*

The left- and right-handed components of quarks and leptons may be assigned various $U(1)$ charges, as are the Higgs fields, such that only one or a limited number of entries in the mass matrices can be generated by renormalizable terms in the effective Lagrangian [55]. Additional entries become permitted if the symmetry is broken, for example by one or more vacuum expectation values $\mathcal{V}$ for fields that appear in non-renormalizable terms in the mass matrices, scaled by inverse powers of larger masses M. This type of scheme provides a perturbative expansion in powers of some small parameter $\epsilon \equiv \mathcal{V}/M$. In a popular class of realizations, only the (3,3) element of the associated mass matrix is non-zero at leading order, whilst other terms arise with various powers of ϵ, that are fixed by the $U(1)$ charge assignments:

$$\mathcal{M} \sim \begin{pmatrix} \epsilon^m & \epsilon^n & \epsilon^p \\ \epsilon^q & \epsilon^r & \epsilon^s \\ \epsilon^t & \epsilon^u & 1 \end{pmatrix} \tag{9}$$

In such models, each term in the mass matrix has a numerical coefficient that may be calculated only with a more complete theory.

In its absence, there are numerical ambiguities in the predictions of such a model, but mixing angles are generically powers of ϵ. There are two possible ways to obtain large mixing angles in such

a perturbative $U(1)$ framework. One of the mixing matrices may contain more than one entry appearing with the same power of ϵ, for example perhaps the (3, 3) and (3, 2) entries in (9) might both be $\mathcal{O}(1)$. Alternatively, the numerical coefficients might be such as to compensate for the 'small' expansion parameter ϵ.

Grand Unified Theories

In a generic scheme, there is a lot of freedom in assigning the various $U(1)$ flavour charges. However in Grand Unified Theories, quark and lepton fields that belong in the same GUT multiplets have the same flavour charges. This introduces additional constraints, thus increasing predictivity [56]. For instance, in $SO(10)$ models, all quarks and leptons are accommodated in a single $\mathbf{16}$ representation of the group, implying left-right symmetric mass matrices with similar structures for all fermions. As a consequence, such GUT models predict $V_{\mu\tau} \approx V_{cb}$, which is inconsistent with the data. Hence, in order to construct a viable $SO(10)$ solution, one must consider the effects of the additional Higgs multiplets that break $SO(10)$ down to $SU(3) \times SU(2) \times U(1)$. However, this introduces additional parameters, thus decreasing predictivity.

The situation is different in $SU(5)$ unification, where the $(q, u^c, e^c)_i$ fields (for left-handed quarks, right-handed up quarks and right-handed charged leptons, respectively) belong to $\mathbf{10}$ representations, the $(\ell, d^c)_i$ fields (for left-handed leptons and right-handed down quarks, respectively) belong to $\overline{\mathbf{5}}$ representations, and the N_i (singlet neutrinos) to singlet representations of the group. In this case, the up-quark mass matrix is symmetric, there is a lot of freedom in chosing the neutrino mass matrices, and the charged-lepton mass matrix is the transpose of the down-quark one. Hence the mixing of the left-handed leptons is related to that of the right-handed down quarks, and not with the small CKM mixing of the left-handed quarks. Thus, $SU(5)$ can in principle accommodate large MNS neutrino mixing at the same time as small CKM quark mixing, without any tuning of parameters.

In left-right symmetric models, one has identical $U(1)$ flavour charges for the left- and right-handed fields, as in $SO(10)$ unification, but quarks and leptons need not be correlated. This leads to symmetric quark, lepton and neutrino mass matrices, but allows the lepton mixing to be independent of that in the quark sector.

Non-Abelian Flavour Symmetries

Specific $U(1)$ flavour models may yield one relatively large neutrino mixing angle, but tend to favour small values of the other mixing angles and hierarchical neutrino masses. Thus, such models are comfortable with the small value of θ_{13}, but could be embarrassed if the current preference for the LMA solar solution is confirmed. This feature of models with Abelian flavour symmetries may be traced to the lack of charge quantization and arbitrary coefficients, making it difficult to obtain accurate cancellations between the various entries of the mass matrices, unless extra assumptions are made, for example in the heavy singlet-neutrino sector.

The situation is reversed in non-Abelian models. To illustrate this, consider a simple case in which the lepton fields are $SO(3)$ triplets. In this case, degenerate lepton textures are to be expected. Subsequently, one may break $SO(3)$ so that there are large mass splittings for charged leptons, but not for the light neutrinos [57]. This means that, in schemes with non-Abelian flavour symmetries, solutions with degenerate neutrinos and bimaximal mixing can be generated in a natural way. On the other hand, the understanding of any small mixing angles and phases might then become an issue.

2.1.5 Testing models of neutrino masses

The neutrino oscillation measurements that can be made at a neutrino factory, notably the magnitudes of θ_{13} and δ, will provide important constraints on models of neutrino masses. For example, as just discussed, the expected size of δ and other CP-violating phases may be rather different in Abelian and non-Abelian flavour models.

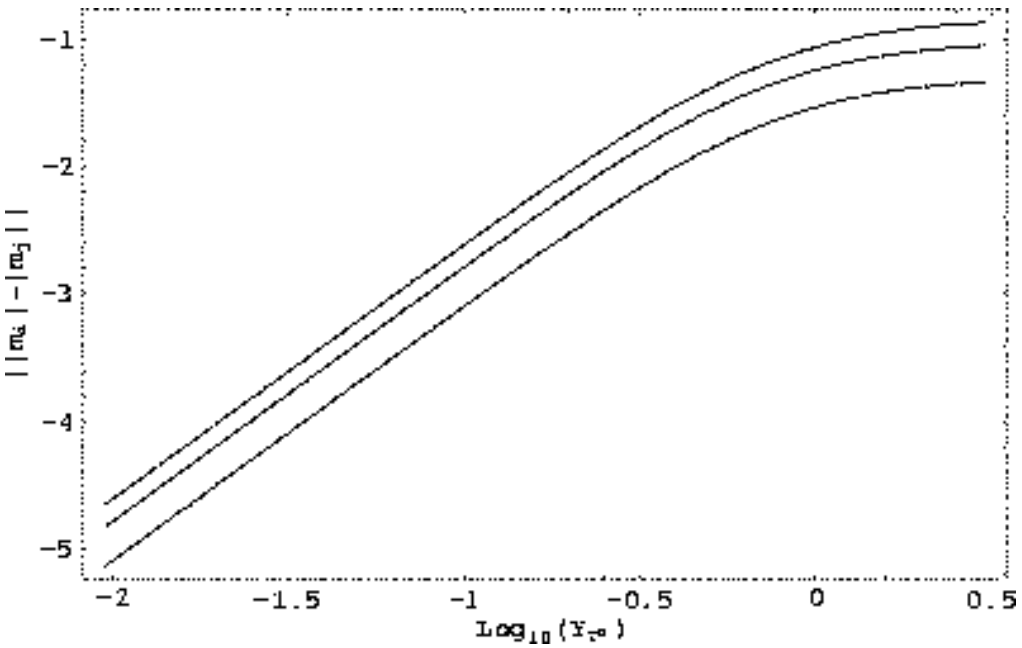

Fig. 4: *Renormalization of m_{eff} eigenvalues in a model which would seem to lead to bimaximal mixing. The range of initial values of the τ Yukawa coupling chosen correspond to values of tanβ in the range 1 to 58, assuming $M_N = 10^{13}$ GeV.*

When comparing model predictions with data, care must be taken to include the effects of quantum corrections in the neutrino parameters, which cause them to vary as functions of energy [58]. To leading order, entries in the neutrino mass matrix are renormalized by multiplicative factors [59]:

$$m_\nu^{light}(Q)^{ij} = m_\nu^{light}(M_N)^{ij} \times I_i \times I_j \,, \tag{10}$$

where the $m_\nu^{light}(M_N)^{ij}$, $i = e, \mu, \tau$ denote the initial mass entries at the high-energy energy scale where the neutrino mass matrix is generated, and the

$$I_i \equiv \exp[\frac{1}{16\pi^2}\int_{t_0}^{t} Y_i^2 dt] : \; t \equiv \ln \mu \tag{11}$$

are integrals determined by the running of the charged-lepton Yukawa couplings Y_i as functions of the renormalisation scale μ. This effect implies that the neutrino mixing can be amplified or even destroyed, as we go from high to low energies, and the neutrino mass eigenvalues may also be altered significantly. Although these renormalization effects are not significant for schemes with hierarchical neutrino masses, they are potentially large in models with degenerate neutrinos and may be important in models with bimaximal mixing. For instance, for the neutrino mass texture

$$m_{nu}^{light} \propto \begin{pmatrix} 0 & \frac{1}{\sqrt{2}} & \frac{1}{\sqrt{2}} \\ \frac{1}{\sqrt{2}} & \frac{1}{2} & -\frac{1}{2} \\ \frac{1}{\sqrt{2}} & -\frac{1}{2} & \frac{1}{2} \end{pmatrix}$$

which would seem to lead to bimaximal mixing, Fig. 4 indicates a large change of the eigenvalues when running from high to low energies [59], and analogous large effects may also occur in the mixing angles.

In supersymmetric seesaw models, quantum corrections may provide other ways of measuring neutrino parameters and testing models via lepton-flavour-violating processes. In the minimal seesaw

model without supersymmetry, the amplitudes for processes such as $\mu \to e\gamma$, μ-e conversion in nuclei, $\mu \to eee$ and $\tau \to \ell\gamma, 3\ell$ [60, 34, 61] where $\ell = e, \mu$ denotes a generic light charged lepton, are proportional to the neutrino mass-squared difference, and so are many orders of magnitude smaller than the existing experimental bounds. This is no longer the case in supersymmetric theories, due to the existence of loop diagrams with internal sparticles, that may violate charged-lepton numbers. This may happen either because sfermion masses are not diagonal in the lepton flavour basis already at the input scale M_{GUT}, in which case very large lepton-flavour violating rates are generically predicted [60], or because flavour-violating effects are induced by quantum corrections [62].

These are generic in the Minimal Supersymmetric Standard Model with heavy singlet neutrinos, because the Dirac Yukawa couplings to neutrinos and charged leptons cannot, in general, be diagonalized simultaneously. Since both these sets of lepton Yukawa couplings appear in the renormalization-group equations, the slepton mass matrices receive off-diagonal contributions. In the leading-logarithmic approximation, in the basis where the charged-lepton Yukawa couplings are diagonal, these are given by

$$\left(\delta m^2_{\tilde{\ell}}\right)^i_j \propto \frac{1}{16\pi^2}(3+a^2)\left(Y^\dagger_\nu\right)^i_k L_k \left(Y_\nu\right)^k_j m_0^2, \tag{12}$$

where $L_k \equiv \ln \frac{M_{GUT}}{M_{N_k}}$, the singlet-neutrino mass M_{N_k} is the scale above which the Dirac Yukawa coupling Y_ν appears in the renormalization-group equations, a is related to the trilinear mass parameter, and m_0 is the common value of the scalar masses at the GUT scale.

In this class of models, the rates predicted for processes violating charged-lepton flavour may be close to the current experimental bounds, and are in principle sensitive to up to 16 of the 18 parameters in the minimal seesaw model, as indicated in Fig. 3 [54]. Therefore, different models predict in general different rates for the different charged-lepton flavour-violating processes: the larger the lepton mixing and the larger the neutrino mass scales, the larger the rates. Consequently, schemes with degenerate eV neutrinos and bimaximal mixing generally yield significantly larger effects than schemes with hierarchical neutrinos and small mixing angles.

The prospects for measuring some of these processes at the front end of a neutrino factory are discussed elsewhere [34]. Here we just note that the present experimental upper limits on the most interesting of these processes are $BR(\mu \to e\gamma) < 1.2 \times 10^{-11}$ [63] and $R(\mu^- Ti \to e^- Ti) < 6.1 \times 10^{-13}$ [64], and that projects are underway to improve these upper limits significantly. An experiment with a sensitivity $BR(\mu \to e\gamma) \sim 10^{-14}$ is being prepared at PSI [65] and the MECO experiment with a sensitivity to $R(\mu^- N \to e^- N) \sim 10^{-17}$ has been proposed for BNL [66], whilst the PRISM project [67] and a neutrino factory [34] may reach sensitivities to $BR(\mu \to e\gamma) \sim 10^{-15}$ and $Br(\mu \to eee) \sim 10^{-16}$. The latter sensitivity may open the way to measuring the T-odd, CP-violating asymmetry $A_T(\mu \to eee)$. Other measurements that may be sensitive to CP violation in the lepton sector include those of the electric dipole moments of the electron and muon, and a neutrino factory would also have unique sensitivity to the latter [34].

In this way, the front end of the neutrino factory could contribute to determining as many as 16 of the 18 parameters in the neutrino sector, via their renormalization of soft supersymmetry-breaking parameters (see Fig. 3). Any such information would therefore provide useful constraints on neutrino models. Moreover, the combination of such front-end data with oscillation data from the neutrino factory may enable the baryon number of the universe to be calculated, if it is due to leptogenesis in the minimal supersymmetric version of the seesaw model.

2.2 Oscillation Physics

Neutrino oscillations in vacuum would arise if neutrinos were massive and mixed [68] similar to what happen in the quark sector. If neutrinos have masses, the weak eigenstates, ν_α ($\alpha = e, \mu, \tau, ...$), produced in a weak interaction are, in general, linear combinations of the mass eigenstates ν_i ($i = 1, 2, 3, ...$). We now review the basic physics of neutrino oscillations in vacuum and in matter.

2.2.1 *Relativistic approach to the two-family formula*

In the simpler case of two-family mixing, one has:

$$\begin{pmatrix} \nu_\alpha \\ \nu_\beta \end{pmatrix} = \begin{pmatrix} \cos\theta & \sin\theta \\ -\sin\theta & \cos\theta \end{pmatrix} \begin{pmatrix} \nu_1 \\ \nu_2 \end{pmatrix} \tag{13}$$

We use the standard approximation that $|\nu\rangle$ is a plane wave and consider its propagation in a one-dimensional space. A mass eigenstate produced at t,x=0, will evolve in space and in time as:

$$|\nu_i(t,x)\rangle \quad = \quad e^{i(p_i x - E_i t)}|\nu_i\rangle \qquad \text{for } i = (1,2). \tag{14}$$

Starting from a flavour eigenstate $|\nu_\alpha\rangle$, the probability for detecting a state $\langle\nu_\beta|$ at a distance L and time t is given by:

$$P(\nu_\alpha \to \nu_\beta) \quad \equiv \quad |\langle\nu_\beta|\nu_\alpha(t,L)\rangle|^2 = \sin^2 2\theta \ \sin^2\left[\frac{(p_1-p_2)L - (E_1-E_2)t}{2}\right] . \tag{15}$$

In the 'same-energy prescription', which is consistent with the wave-packet treatment [2], one assumes that the two neutrino mass eigentstates have the same energy, $E_1 = E_2 = E$, but different momentum:

$$p_1 = \sqrt{E^2 - m_1^2}\,, \qquad p_2 = \sqrt{E^2 - m_1^2 + \Delta m_{12}^2} \qquad (\text{with} \qquad \Delta m_{12}^2 \equiv m_1^2 - m_2^2) \tag{16}$$

which leads to:

$$P(\nu_\alpha \to \nu_\beta) = \sin^2 2\theta \sin^2 \frac{(p_1-p_2)L}{2} \simeq \sin^2 2\theta \sin^2\left(\kappa \frac{\Delta m_{12}^2 L}{E}\right), \tag{17}$$

In (17) κ is 1/4 in natural units ($\hbar = c = 1$) or 1.27 if we consider practical units where the energy is expressed in GeV, the distance in km and the mass difference squared in eV^2.

2.2.2 *Three families in vacuum*

In the three-family scenario, the general relation between the flavour eigenstates ν_α and the mass eigenstates ν_i is given by the 3x3 mixing matrix V:

$$V = UA, \tag{18}$$

where the matrix A contains the Majorana phases

$$A = \begin{pmatrix} e^{i\alpha} & 0 & 0 \\ 0 & e^{i\beta} & 0 \\ 0 & 0 & 1 \end{pmatrix} \tag{19}$$

that are not observable in oscillation experiments, and U is the MNSP matrix [68, 71], which is usually parameterized by [72] [3]:

$$U = \begin{pmatrix} U_{e1} & U_{e2} & U_{e3} \\ U_{\mu 1} & U_{\mu 2} & U_{\mu 3} \\ U_{\tau 1} & U_{\tau 2} & U_{\tau 3} \end{pmatrix} = \begin{pmatrix} c_{12}c_{13} & s_{12}c_{13} & s_{13}e^{-i\delta} \\ -s_{12}c_{23} - c_{12}s_{13}s_{23}e^{i\delta} & c_{12}c_{23} - s_{12}s_{13}s_{23}e^{i\delta} & c_{13}s_{23} \\ s_{12}s_{23} - c_{12}s_{13}c_{23}e^{i\delta} & -c_{12}s_{23} - s_{12}s_{13}c_{23}e^{i\delta} & c_{13}c_{23} \end{pmatrix} \tag{20}$$

[2] For a detailed discussion, see for example [69] and [70].

[3] Notice, though, that our convention for the sign of δ is opposite from that used in this reference. The MNSP matrix is the leptonic analogue to the CKM [73] matrix of the quark sector.

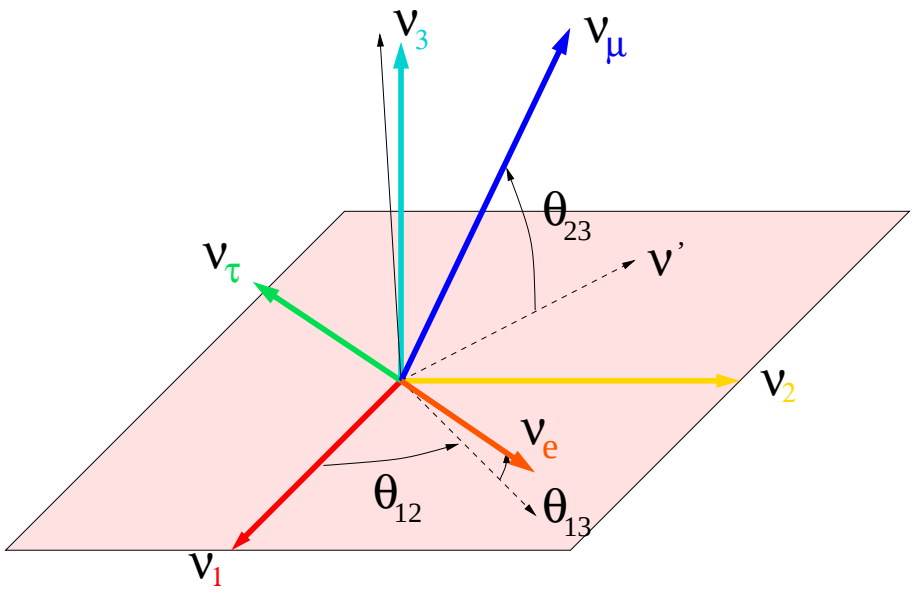

Fig. 5: *Representaion of the 3-dimensional rotation between the flavor and mass neutrino eigenstates.*

where, for the sake of brevity, we write $s_{ij} \equiv \sin\theta_{ij}$, $c_{ij} \equiv \cos\theta_{ij}$. The relevant angles can be derived from the matrix elements via the following relations:

$$\tan^2\theta_{23} \equiv \frac{|U_{\mu 3}|^2}{|U_{\tau 3}|^2}, \tag{21}$$

$$\tan^2\theta_{12} \equiv \frac{|U_{e2}|^2}{|U_{e1}|^2}, \tag{22}$$

$$\sin^2\theta_{13} \equiv |U_{e3}|^2, \tag{23}$$

$$\sin\delta \equiv \frac{8\ Im(U^*_{e2}U_{e3}U_{\mu 2}U^*_{\mu 3})}{\sin 2\theta_{12}\sin 2\theta_{23}\sin 2\theta_{13}\cos\theta_{13}}. \tag{24}$$

The relations between mass and flavor eigenstates can be visualized as rotations in a three-dimensional space, with the angles defined as in Fig. 5.

With a derivation analogous to the two-family case, the oscillation probability for neutrinos reads

$$P(\nu_\alpha \to \nu_\beta) = \sum_{jk} J_{\alpha\beta jk} e^{-i\Delta m^2_{jk}L/2E} \tag{25}$$

where $J_{\alpha\beta jk} = U_{\beta j}U^*_{\beta k}U^*_{\alpha j}U_{\alpha k}$. For antineutrinos, the probability is obtained with the substitution $J_{\alpha\beta jk} \to J^*_{\alpha\beta jk}$. As $J_{\alpha\beta jk}$ is not real in general, due to the phase δ, neutrino and antineutrino oscillation probabilities are different, and therefore CP is violated in the neutrino mixing sector. The CP-even and CP-odd contributions in the oscillation probability can easily be distinguished by separating the real and imaginary parts of $J_{\alpha\beta jk}$:

$$P(\nu_\alpha \to \nu_\beta) = \delta_{\alpha\beta} - 4\sum_{j>k} Re(J_{\alpha\beta jk})\sin^2\frac{\Delta m^2_{jk}L}{4E} + 2\sum_{j>k} Im(J_{\alpha\beta jk})\sin\frac{\Delta m^2_{jk}L}{2E}. \tag{26}$$

The Jarlskog determinant J [74] is defined by:

$$Im(J_{\alpha\beta jk}) = J\sum_{\gamma,l}\epsilon_{\alpha\beta\gamma}\,\epsilon_{jkl} \tag{27}$$

and can be expressed in terms of the mixing parameters, as:

$$J = c_{13} \sin 2\theta_{12} \sin 2\theta_{13} \sin 2\theta_{23} \sin \delta. \tag{28}$$

We define a complex quantity $\tilde{J}$ whose real part is J:

$$\tilde{J} = c_{13} \sin 2\theta_{12} \sin 2\theta_{13} \sin 2\theta_{23} e^{i\delta}. \tag{29}$$

Oscillations in a three-generation scenario are consequently described by six independent parameters: two mass differences (Δm^2_{12} and Δm^2_{23}), three Euler angles (θ_{12}, θ_{23} and θ_{13}) and one CP-violating phase δ. As an example, we give the full oscillation probability for the oscillation $\nu_e \to \nu_\mu$:

$$\begin{aligned} P(\nu_e \to \nu_\mu) = P(\bar{\nu}_\mu \to \bar{\nu}_e) &= \\ 4c^2_{13}[\sin^2 \Delta_{23} s^2_{12} s^2_{13} s^2_{23} &+ c^2_{12}(\sin^2 \Delta_{13} s^2_{13} s^2_{23} + \sin^2 \Delta_{12} s^2_{12}(1 - (1 + s^2_{13}) s^2_{23}))] \\ &- \frac{1}{4}|\tilde{J}| \cos\delta[\cos 2\Delta_{13} - \cos 2\Delta_{23} - 2\cos 2\theta_{12} \sin^2 \Delta_{12}] \\ &+ \frac{1}{4}|\tilde{J}| \sin\delta[\sin 2\Delta_{12} - \sin 2\Delta_{13} + \sin 2\Delta_{23}], \end{aligned} \tag{30}$$

where we have used the contracted notation $\Delta_{jk} \equiv \Delta m^2_{jk} L/4E$ [75]. The second and third lines are the CP-violating terms, and are proportional to the imaginary and real parts of $\tilde{J}$, respectively.

The present experimental knowledge on neutrino oscillation parameters indicates $\Delta m^2_{12} \ll \Delta m^2_{23}$ and small values for θ_{13}. In this situation, a good and simple approximation for the $\nu_e \to \nu_\mu$ transition probability is obtained by expanding to second order in the small parameters, $\theta_{13}, \Delta_{12}/\Delta_{13}$ and Δ_{12} [116]:

$$P_{\nu_e\nu_\mu} = s^2_{23} \sin^2 2\theta_{13} \sin^2 \Delta_{23} + c^2_{23} \sin^2 2\theta_{12} \sin^2 \Delta_{12} + |\tilde{J}| \cos(\delta - \Delta_{23}) \Delta_{12} \sin \Delta_{23}. \tag{31}$$

We refer to the three terms in (31) as the atmospheric $P^{atm}_{\nu(\bar{\nu})}$, solar P^{sol}, and interference $P^{inter}_{\nu(\bar{\nu})}$ terms, respectively [117]. It is easy to show that

$$|P^{inter}_{\nu(\bar{\nu})}| \leq P^{atm}_{\nu(\bar{\nu})} + P^{sol}, \tag{32}$$

implying two very different regimes. When θ_{13} is relatively large or Δm^2_{12} small, the probability is dominated by the atmospheric term, since $P^{atm}_{\nu(\bar{\nu})} \gg P^{sol}$. We will refer to this situation as the atmospheric regime. Conversely, when θ_{13} is very small or Δm^2_{12} large, the solar term dominates: $P^{sol} \gg P^{atm}_{\nu(\bar{\nu})}$. This is the solar regime. The interference term is relevant only if either Δm^2_{12} or θ_{13} are non-negligible. The possibility of observing CP violation in neutrino oscillations is connected to the possibility of separating the interference term from the solar and atmospheric contributions in (31).

If we neglect completely Δm^2_{12}, setting it to zero[4], oscillation probabilities take the simplified form

$$P(\nu_e \to \nu_e) = 1 - \sin^2 2\theta_{13} \sin^2 \Delta_{23} \tag{33}$$

$$P(\nu_e \to \nu_\mu) = \sin^2 2\theta_{13} \sin^2 \theta_{23} \sin^2 \Delta_{23} \tag{34}$$

$$P(\nu_e \to \nu_\tau) = \sin^2 2\theta_{13} \cos^2 \theta_{23} \sin^2 \Delta_{23} \tag{35}$$

$$P(\nu_\mu \to \nu_\mu) = 1 - 4\cos^2 \theta_{13} \sin^2 \theta_{23}(1 - \cos^2 \theta_{13} \sin^2 \theta_{23}) \sin^2 \Delta_{23} \tag{36}$$

$$P(\nu_\mu \to \nu_\tau) = \cos^4 \theta_{13} \sin^2 2\theta_{23} \sin^2 \Delta_{23}. \tag{37}$$

As expected CP-violating effects are absent since they require the interference of oscillations from two mass differences.

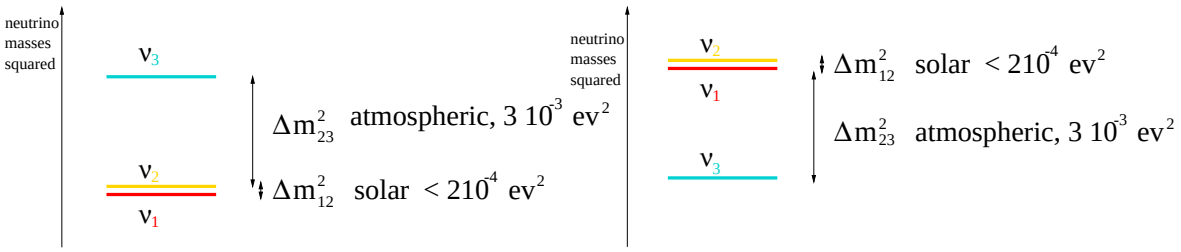

Fig. 6: *Two possible configurations for the neutrino mass texture: direct (left) or inverted (right).*

2.2.3 Oscillations in matter

So far, we have analyzed neutrino oscillations in vacuum. When neutrinos travel through matter (e.g. in the Sun, Earth, or a supernova), their coherent forward scattering from particles they encounter along the way can significantly modify their propagation. As a result, the probability for changing flavor can be rather different from its vacuum value. This is known as the Mikheyev-Smirnov-Wolfenstein (MSW) effect [82].

The reason is simple: matter contains electrons but no muons or taus. Neutrinos of the three flavors interact with the electrons, the protons and the neutrons of the matter via neutral currents (NC). Electron neutrinos in addition interact with electrons via the charged current (CC). Since the W mass is much larger than typical center-of-mass energies for neutrino scattering, the relevant parts of the Lagrangian for electron neutrinos can be written in the Fermi approximation

$$\mathcal{L} = \bar{\nu}_e(i\partial\!\!\!/ - m)\nu_e - 2\sqrt{2}G_F(\bar{\nu}_{eL}\gamma_\mu\nu_{eL})(\bar{e}_L\gamma^\mu e_L). \tag{38}$$

The latter term modifies the effective mass of the ν_e when it goes through matter and, consequently, the transition probability changes. In the electron reference frame only the γ_0 part of the electron current contributes, being just the number operator:

$$< \bar{e}_L\gamma_0 e_L >= n_e/2 \tag{39}$$

with n_e the electron density given by:

$$n_e = N_A \times Y_e \times \rho(r)\ , \tag{40}$$

and $Y_e = Z/A$ and ρ are the electron fraction and the density of the medium. Both of them depend on the physical propierties of the medium traversed by the neutrinos. For the Earth's mantle, $Y_e = 0.494$, and for the Earth's core $Y_e = 0.466$ [76]. The contribution to the ν_e effective Hamiltonian due to the CC interaction with matter is consequently given by:

$$A = \sqrt{2}\,G_F\,n_e\ . \tag{41}$$

For antineutrinos A has to be replaced by $-A$, so the behaviour in matter of neutrinos and antineutrinos is different (matter is not CP invariant). In the treatment of oscillations, the extra potential only appears for electron neutrinos, so the oscillatory terms will no longer be proportional to the mass-squared differences between the three families, but to effective masses-squared that result from the diagonalization of the Hamiltonian:

$$U \begin{pmatrix} m_1^2 & 0 & 0 \\ 0 & m_2^2 & 0 \\ 0 & 0 & m_3^2 \end{pmatrix} U^\dagger + \begin{pmatrix} D & 0 & 0 \\ 0 & 0 & 0 \\ 0 & 0 & 0 \end{pmatrix}, \tag{42}$$

with $D = \pm 2AE_\nu$ (depending if neutrinos or antineutrinos are considered).

[4] This is a good approximation if LOW or VO solutions happen to be the one chosen by nature for the solar oscillation.

The diagonalization of the 3-family Hamiltonian in the presence of the extra matter term modifies the effective mixing angles appearing in oscillation formulae. It has to be noticed that the ordering of the masses in the Hamiltonian is relevant, and the effect of matter is swapped between neutrinos and antineutrinos in the cases of direct and reversed mass hierarchy, as seen in Fig. 6. Thus, the effect of matter in a neutrino oscillation experiment allows the determination of the sign of Δm^2_{23}.

The full formulae for the effective quantities (mass differences and angles) in a three-family scenario are quite complicated, and can be found in [77] and [78]. However, it can be shown that, in the case $|\Delta m^2_{12}| \ll |\Delta m^2_{13}| \approx |\Delta m^2_{23}|$, the three-family mixing decouples into two independent two-family mixing scenarios, even in the presence of matter effects [20]. For energies not too small with respect to that of the oscillation maximum (where $|\Delta m^2_{23} L/E| \approx 1$), the effective oscillation parameters will become (see Fig. 7 [78]):

$$\begin{aligned}
\sin^2\theta^m_{23}(D) &\simeq \sin^2\theta_{23} && (43)\\
\sin^2 2\theta^m_{12}(D) &\simeq \frac{\Delta m^2_{12}}{D}\sin 2\theta_{12} && (44)\\
\sin^2 2\theta^m_{13}(D) &\simeq \frac{\sin^2 2\theta_{13}}{F} && (45)\\
\delta^m &\simeq \delta && (46)\\
\Delta M^2_{12} &\simeq D && (47)\\
\Delta M^2_{23} &\simeq \Delta m^2_{23}\sqrt{F} && (48)\\
& && (49)
\end{aligned}$$

where we have defined

$$F \equiv \sin^2 2\theta_{13} + (\frac{D}{\Delta m^2_{23}} - \cos 2\theta_{13})^2. \tag{50}$$

As expected, we see explicitly that all the angles return to their original values in the limit of small matter density $D \to 0$ (i.e. $F \to 1$) in the limit $\Delta m_{12} \ll \Delta m_{13}$ and $\Delta m_{12} \ll D$.

At the Mikheyev-Smirnov-Wolfenstein (MSW) resonance energy

$$E^{res}_\nu(GeV) = \frac{\cos 2\theta_{13}\Delta m^2_{23}}{2\sqrt{2}G_F n_e} \simeq \frac{1.32\times 10^4 \cos 2\theta_{13}\Delta m^2_{23}(eV^2)}{\rho(g/cm^3)} \tag{51}$$

the value of $\sin^2 2\theta^m_{13}$ becomes equal to 1, independently of the actual value of the angle in vacuum. Also the effective value of Δm^2_{32} is significantly modified. If we take $\Delta m^2_{23} = 2.5\times 10^{-3}$ eV^2, $\theta_{13} \ll 1$ and $\rho = 2.8$ g/cm^3, the energy of this MSW resonance is 11.8 GeV.

To see how this affects the oscillation probability, we can take the simplified formula for the $\nu_e \to \nu_\mu$ oscillation in vacuum, as appears in (31), and neglect the mass difference Δ_{12}. Replacing the vacuum parameters with their effective values, one obtains the approximate $\nu_e \to \nu_\mu$ oscillation probability in matter:

$$P(\nu_e \to \nu_\mu) = \sin^2 2\theta^m_{13}\sin^2\theta^m_{23}\sin^2\Delta^m_{23} = \frac{\sin^2 2\theta_{13}}{F}\sin^2\theta_{23}\sin^2\left(\Delta m^2_{23}\sqrt{F}\frac{L}{4E}\right), \tag{52}$$

and the oscillation probability at the MSW resonance energy becomes

$$P(\nu_e \to \nu_\mu; E^{res}) = \sin^2\theta_{23}\sin^2\left(\Delta m^2_{23}\sin 2\theta_{13}\frac{L}{4E^{res}}\right). \tag{53}$$

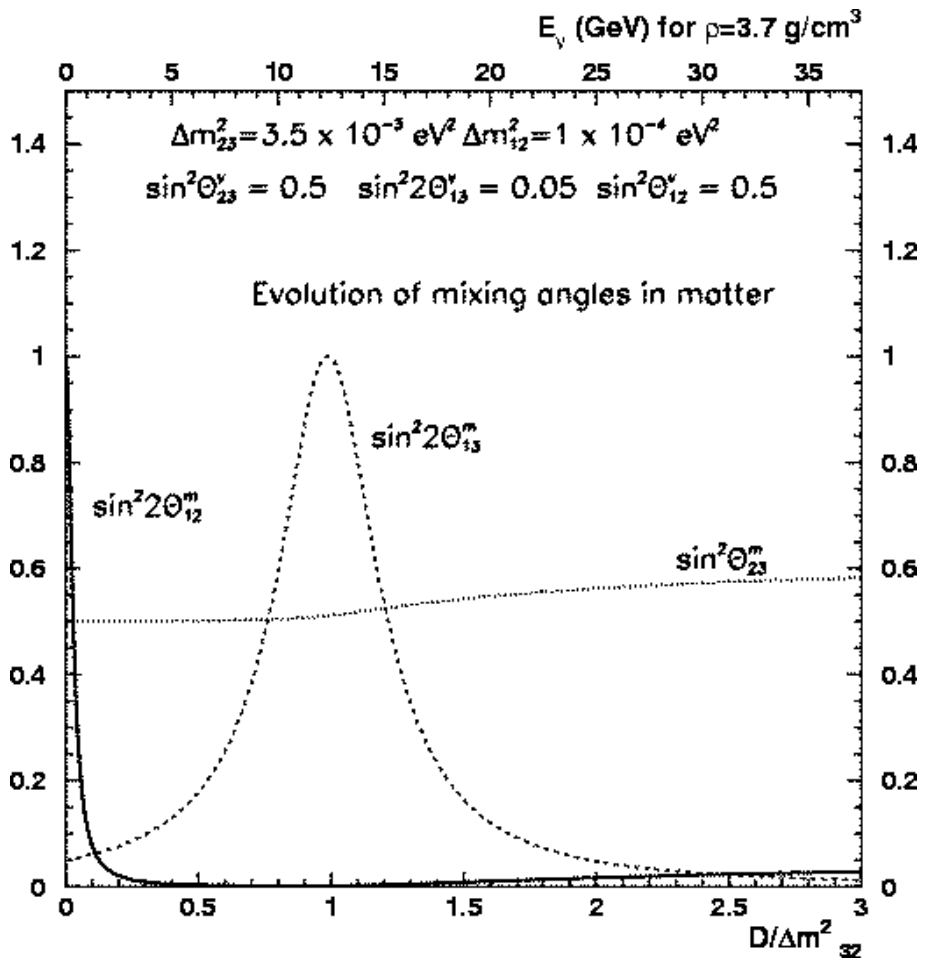

Fig. 7: *Evolution of the effective angles in matter as a function of D.*

If we assume that $\sin 2\theta_{13}$ is small, and if the distance L is not too far away from that of the first maximum, the probability reads:

$$P(\nu_e \to \nu_\mu; E^{res}) \approx s^2_{23} \sin^2 2\theta_{13} \times \left(\Delta m^2_{23} \frac{L}{4E^{res}} \right). \tag{54}$$

In the limit $\Delta m^2_{23} L/4E \ll 1$, this coincides with the vacuum expression of (34). This is why it is not possible to measure the sign of Δm^2_{23} if the baseline is too short. Matter effects become visible at distances where the argument of the $\sin$ function approaches $\pi/4$. The oscillation maximum for the value $E^{res} = 11.8$ GeV and $\Delta m^2_{23} = 2.5 \times 10^{-3}$ eV^2 is $L = 2300$ km, so matter effects start to be visible as an enhancement of the oscillation probability around the MSW resonance energy for baselines longer than about 1000 km. For antineutrinos the effective mixing angle is smaller than the real one. For small baselines, a similar compensation as in (54) takes place, but at distances where matter effects start to play a role the oscillation probability in matter is smaller than that in vacuum.

The above considerations are valid near the resonance energy, in other words for $D \approx \Delta m^2_{23}$. If $D > \Delta m^2_{23}$ i.e., $E_\nu > 2E^{res}$, the effective mixing angle is always smaller than the vacuum one, and the effect of matter is again a suppression of the oscillation probability.

2.2.4 *Current status of neutrino mixing parameters*

We assume that active neutrino oscillations are indeed the solution to the neutrino puzzles, and that there are only three light neutrino species. As discussed above, in this case the Standard Model is augmented by at least 9 new parameters, of which 3 are neutrino masses, 3 are real mixing angles, there is one oscillation phase and two additional Majorana phases, which exist only if the neutrinos are Majorana particles. Neutrino oscillation experiments, however, are not sensitive to the Majorana phases, and we set them to zero henceforth.

The angles θ_{23} and θ_{12} are thought to be mainly responsible for solving, respectively, the atmospheric and solar neutrino puzzles, as long as $|\Delta m^2_{23}| > |\Delta m^2_{12}|$ (normal neutrino mass hierarchy). If the opposite happens to be true ($|\Delta m^2_{23}| < |\Delta m^2_{12}|$, an inverted mass hierarchy), the definitions above can still be related to the appropriate neutrino puzzles, as long as the mass eigenstates are relabelled $3 \to 2 \to 1 \to 3$. We make this assumption henceforth, and refer to $\theta_{23} \equiv \theta_{atm}$, $\theta_{12} \equiv \theta_{sun}$. Thus, the third mass eigenstate is defined as the one whose mass squared is 'further away' from the other two, which are arranged in ascending order of masses-squared, without any loss of generality. Given this choice, the inverted hierarchy differs from the normal hierarchy by the sign of Δm^2_{23}. The entire oscillation parameter space is spanned by varying the three mixing angles from 0 to $\pi/2$, keeping $\Delta m^2_{12} > 0$ [5], Δm^2_{23} (including the sign), and varying δ from $-\pi$ to π.

The current knowledge of the oscillation parameters can be summarized as follows. There is good evidence that $|\Delta m^2_{23}| \gg \Delta m^2_{12}$, and therefore $\Delta m^2_{23} \simeq \Delta m^2_{13}$. This being the case, the current atmospheric data are sensitive to $|\Delta m^2_{23}|$, $\tan^2\theta_{\rm atm}$, and $|U_{e3}|^2$, while the current solar data are sensitive to Δm^2_{12}, $\tan^2\theta_{sun}$, and $|U_{e3}|^2$. The Chooz and Palo Verde reactor experiments, when considered in combination with the solar data, constrain $|U_{e3}|^2$ as a function of $|\Delta m^2_{23}|$. The experimentally allowed range of the parameters depends on a number of assumptions: which experimental data are considered, how many neutrino species participate in the oscillation, what was the statistical recipe used to define allowed regions, etc. We comment briefly later on some of these points. In this Section, we simply quote the current 'standard' results, with some appropriate references.

For the atmospheric and reactor parameters, one obtains [13] at the 99% confidence level (CL),

$$|U_{e3}|^2 < 0.06, \tag{55}$$

$$0.4 < \tan^2\theta_{\rm atm} < 2.5, \tag{56}$$

$$1.2 \times 10^{-3}\ {\rm eV}^2 < |\Delta m^2_{23}| < 6.3 \times 10^{-3}\ {\rm eV}^2. \tag{57}$$

The situation of the solar parameters is less certain, and is best described graphically. Fig. 8 depicts the result of the most recent analysis of all solar neutrino data [81], which uses the current version of the standard solar model [6], but allows the ^{8}B neutrino flux to float in the fit. This particular analysis is performed assuming two-flavour oscillations, a scenario which is realised in the three-flavour case for $|U_{e3}|^2 = 0$. The changes to the allowed regions are not qualitatively significant for values of $|U_{e3}|^2$ up to the upper bound quoted above: in fact, the allowed regions grow, even for $|U_{e3}|^2 = 0$, simply because the confidence level contours are defined for three instead of two degrees of freedom. The right panel of Fig. 8 exhibits the impact of the recent neutral-current measurement from SNO on the preferred solar neutrino oscillation parameters.

There are still several disjoint regions of the parameter space which satisfy the current solar neutrino data at some CL. These include the large mixing angle (LMA) solution, the low Δm^2_{12} MSW solution (LOW), various vacuum (VAC) solutions at very small values of Δm^2_{12}, and (at a lower CL) the small mixing angle (SMA) MSW [82] solution. Of the four regions, two (LMA, and LOW) are very robust, and appear in different types of data analysis. The VAC solutions are rather unstable, and can disappear if the data are analysed in a different fashion. Note that the LOW solution is no longer connected

[5] In two-flavour solar data analyses, it is important also to keep the mixing angle from 0 to $\pi/2$ if $\Delta m^2 > 0$ is fixed, in order to cover the entire parameter space [29, 80].

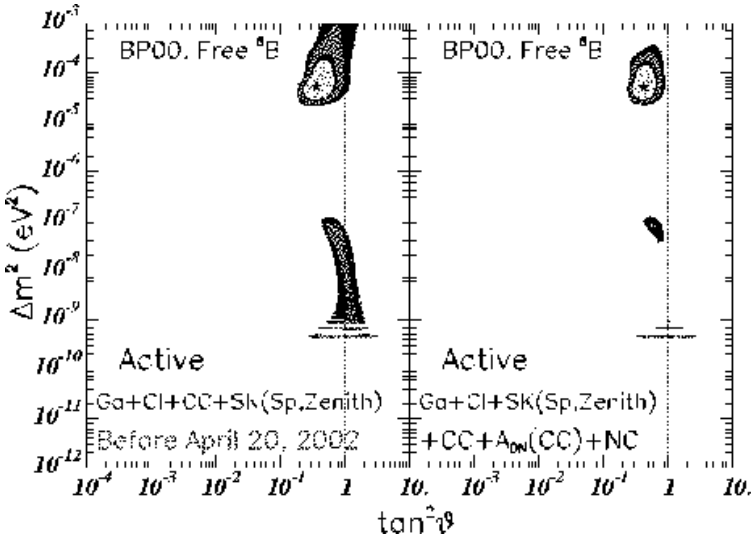

Fig. 8: *Global fits to current solar neutrino data [81], leaving free the ^8B neutrino flux. The best-fit point is marked by the star, while the allowed regions are shown at 90%, 95%, 99%, and 99.73% CL. Here, $\Delta m^2 \equiv \Delta m^2_{12}$ and $\tan^2\theta \equiv \tan^2\theta_{sun}$. This analysis was performed assuming a two-flavour oscillation scenario. In the left panel, only data announced before April 20, 2002 is analyzed, while in the right panel all the current neutrino data is considered, including the recent neutral current measurements from SNO [7].*

to the VAC solutions, as used to be the case [80] before the recent SNO neutral-current data. The SMA solution is currently excluded at more than the three-sigma level, but cannot be completely discarded yet. A word of caution is in order: it has recently been pointed out by several different groups [83] that the standard statistical treatment of the solar neutrino data - which is usually analysed via a χ^2 method, and includes the definition of confidence level contours - is not appropriate. However, a χ^2 method should be perfectly adequate when more data available become available in the near future.

In summary, while some of the oscillation parameters are known with some precision (the atmospheric mass-squared difference is known within a factor of roughly six), the information regarding other parameters is very uncertain. In particular, $\tan^2\theta_{sun}$ can be either very small ($\sim 10^{-4} - 10^{-3}$), or close to unity, while Δm^2_{12} can take many different values, from around 10^{-10} eV^2 to more than 10^{-4} eV^2. Finally, there is absolutely no information on the CP-violating phase δ, nor on the sign of Δm^2_{23}, while for $|U_{e3}|^2$ only a moderate upper bound has been established [6].

2.2.5 Motivations for new physics

So far, we have not discussed the potential implications of the LND data. If the three experimental results from solar, atmospheric and LSND neutrinos are all correct, there must be three different mass-squared differences: $\Delta m^2_{sun} << \Delta m^2_{atm} << \Delta m^2_{lsnd}$, which cannot be accommodated with just three neutrinos. The simplest option for incorporating all the data would be to introduce a fourth light neutrino, which must be *sterile*, i.e., having interactions with Standard Model particles much weaker than the conventional weak interaction, in order not to affect the invisible Z decay width that was measured very precisely at LEP.

In this case, one has to take into account the constraints from cosmological Big Bang Nucleosynthesis: a sterile neutrino that mixes with an active one, and is thus in equilibrium at the time of nucleosynthesis, can change the abundance of primordially produced elements, such as ^{4}He and deuterium. The larger the mixing and the mass differences between the sterile and active neutrinos, the bigger the deviations from the successful standard calculations of the light element abundances. This implies that models where the sterile component contributes to solar rather than atmospheric neutrino oscillations would be accommodated more easily. However, recent data from the two solar neutrino experiments - SNO on charged-current and neutral-current scattering - and Super-Kamiokande - on electron scattering - provide very strong evidence that there are additional active neutrinos coming from the Sun. A large

[6] It is interesting to note that $|U_{e3}|$ can still be as large as the sine of the Cabibbo angle.

mixing between the sterile and active neutrinos is excluded if the SSM calculation of the ^8B flux is correct [178].

Altogether, we conclude that current neutrino data and standard big bang nucleosynthesis disfavour the four-neutrino mixing scheme.

An alternative approach accounts for the LSND results within the three-neutrino framework, by invoking CPT violation [179]. However, this hypothesis involves a dramatic change in the Standard Model that requires more motivation from the data. Another possibility is that small non-standard weak interactions of leptons may instead provide a simultaneous solution to the three neutrino anomalies without introducing a sterile neutrino or invoking CPT violation [180]. According to this hypothesis, $\Delta L = 2$ lepton-number-violating muon decays are invoked to account for the LSND events. These anomalous decays could easily be tested at a Neutrino Factory using a detector capable of charge discrimination [182], as discussed later in this report.

2.2.6 Prospects for the near future

More information will be needed for the detailed planning of neutrino factory experiments, much of which may be provided by near-future experiments, as we now discuss. The precision with which some neutrino oscillation parameters are known will improve significantly in the near future, and it is almost certain that the ambiguity in determining the solution to the solar neutrino puzzle will disappear. In this Section, we review briefly how open questions in the current analysis may be resolved by future experiments, discussing subsequently more details of the experiments.

The values of $|\Delta m^2_{23}|$ and $\tan^2\theta_{\rm atm}$ should be better determined by long-baseline neutrino experiments [16, 21, 23]. In particular, the MINOS experiment [21] aims at 10% uncertainties, while the CNGS programme [23] may achieve slightly better precision. The sensitivity to $|U_{e3}|^2$, on the other hand, is expected to be limited to at most a few %: perhaps $|U_{e3}|^2 = 0.01$ could be obtained at the first-generation long-baseline beams, with JHF doing an order of magnitude better.

In the solar sector, different solutions will be explored by different experiments. We concentrate first on strong 'smoking gun' analyses, and comment later on the prospects for other experiments.

The LMA solution to the solar neutrino puzzle will soon be either established or excluded by the KamLAND reactor experiment [25]. Furthermore, if LMA happens to be the correct solution, KamLAND should be able to measure the oscillation parameters $\tan^2\theta_{sun}$ and Δm^2_{12} with good precision by analysing the $\bar\nu_e$ energy spectrum, as has been recently investigated by different groups [84, 85, 86]. Three years of KamLAND running should allow one to determine, at the three-sigma level, Δm^2_{12} within 5% and $\sin^2 2\theta_{sun}$ within 0.1. A combination of KamLAND reactor data and solar data should start to address the issue whether θ_{sun} is smaller or greater than $\pi/4$ [85].

The LOW solution will be either excluded or unambiguously established by the Borexino experiment [29] (and possibly by an upgrade of the KamLAND experiment such that it can be used to see ^{7}Be solar neutrinos), using the zenith-angle distribution of the ^{7}Be solar neutrino flux. This should allow one to measure, at the three-sigma level, Δm^2_{12} within a factor of three (say, in the range 1 to 3×10^{-7} eV^2) and $\tan^2\theta_{sun}$ within 0.2 [29, 86]. These estimates are very conservative and do not depend, for example, on the solar model prediction for the ^{7}Be neutrino flux [29].

VAC solutions with Δm^2_{12} less than a few $\times10^{-9}$ eV^2 and greater than a few $\times10^{-11}$ eV^2, and $\tan^2\theta_{sun}$ between roughly 0.01 and 100, will also be either excluded or established by experiments capable of measuring the ^{7}Be solar neutrino flux. In this region of parameter space, the flux of ^{7}Be solar neutrinos depends very strongly on the Earth–Sun distance, and anomalous seasonal variations should be readily observed, for example, at GNO or Borexino. Estimates of what will be inferred from the data of these experiments and KamLAND indicate [28] that, even if the ^{7}Be solar neutrino flux is conservatively assumed to be unknown, Δm^2_{12} can be measured at better than the percent level (see also [86]).

The situation with *the SMA solution* is less clear. If SMA is indeed correct, something must be

wrong with part of the current solar neutrino data, or we have been extremely 'unlucky'. Nonetheless, the SMA solution would be favoured if none of the above 'smoking gun' signatures were observed. There are also 'smoking gun' signatures for the SMA solution, but their non-observation would not necessarily exclude the SMA region. One characteristic feature of the SMA solution is a spectrum distortion for ^{8}B neutrinos, which can be measured at Super-Kamiokande and SNO. The current Super-Kamiokande spectrum data are consistent with a constant suppression of the ^{8}B neutrino flux, and an analysis of the Super-Kamiokande data alone excludes the SMA solution at more than 95% CL [87]. Combined analyses of all the solar data render the SMA solution even less likely. The SMA solution also predicts that the ^{7}Be solar neutrino flux should be very suppressed with respect to standard solar model results. Therefore, the measurement of a very small ^{7}Be neutrino flux could be interpreted as a 'smoking gun' signature for the SMA solution. However, background-suppression methods would be needed to measure a very suppressed flux, and some independent checks of the reliability of such techniques are inconclusive [28]. Furthermore, in order to relate a small measured flux to neutrino oscillations, one must rely on predictions from solar physics, which we should prefer to avoid.

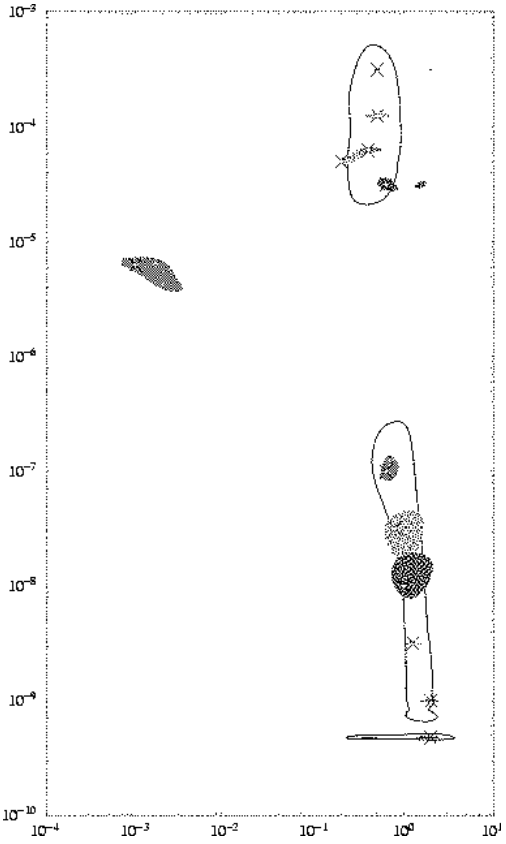

Fig. 9: *The 99% confidence level contours obtained after fitting simulated future solar data (including KamLAND and Borexino), for a few points (marked with an $\times$) in the $(\Delta m^2_{12}/eV^2, \tan^2\theta_{sun})$ plane. The continuous lines indicate the 99% CL contours obtained after analysing the solar data available earlier in 2002. Note that not only is the true solution (SMA, LMA, etc) identified, but the values of $\Delta m^2_{12}/eV^2$ and $\tan^2\theta_{sun}$ are also measured with good accuracy. See [86] for details.*

Fig. 9 depicts the expected 99% CL contours in the $(\Delta m^2_{12}/\mathrm{eV}^2, \tan^2\theta_{sun})$ plane for different candidate solutions to the solar neutrino puzzle, after the advent of KamLAND and Borexino. We see that the large degeneracies in the parameter space will be lifted (with a few exceptions in the LMA region, as pointed out in [85]), and that reasonably precise measurements of the oscillation parameters are to be expected.

Supplementary possibilities are also available. The SNO experiment may also provide sufficient further information to resolve the ambiguities in the solar neutrino sector [88, 89]. Further information may also be obtained if neutrinos from a nearby supernova are detected [90]. Finally, it is important to mention that non-oscillation experiments can also contribute to the understanding of neutrino masses and leptonic mixing angles. In particular, future searches for neutrinoless double beta decay [91] are not only capable of measuring a particular combination of the Majorana neutrino phases, but can also help

piece together the solar neutrino puzzle [92].

We conclude that near-future experiments will provide much of the key information needed for planning neutrino-factory experiments, in particular whether the LMA solar solution is correct.

3 CONVENTIONAL NEUTRINO BEAMS

3.1 First-Generation Long-Baseline Neutrino Projects

The small values of Δm^2 measured in oscillations of atmospheric and solar neutrinos have focused the interest of the community of neutrino physicists on long-baseline projects using neutrinos of artificial origin. As an example, for a value of $\Delta m^2_{23} = 2.5 \times 10^{-3} eV^2$, the maximum of the oscillation probability for 1 GeV neutrinos, a typical energy produced in accelerators, occurs at a distance of about 500 km. The Δm^2 value for solar neutrinos is about two orders of magnitude smaller, so oscillations of reactor neutrinos, whose energy is of the order of 10 MeV, can be observed at the same distance. We describe in this chapter the different approved long-baseline projects.

3.1.1 KamLAND

We have seen that solar neutrino experiments suggest oscillations with parameters in one of four possible regions, usually referred to as the large mixing angle (LMA), small mixing angle (SMA), LOW and vacuum (VAC) solutions. Only the large mixing angle solution would allow the practical possibility of discovering CP violation in neutrino oscillations. This region will be probed over the next few years by the KamLAND reactor neutrino experiment [25], which started taking data in January 2002. After a few years of data taking, KamLAND will be capable of either excluding the entire LMA region or, in the case of a positive signal for oscillations, not only of establishing $\nu_e \leftrightarrow \nu_{\rm other}$ oscillations in the solar parameter region, but also of measuring the oscillation parameters $(\tan^2\theta_{12}, \Delta m^2_{12})$ with unprecedented precision [84, 93, 94].

KamLAND is located in the old Kamiokande site in the Kamioka mine in Japan. Its neutrino source consists of 16 nuclear power plants at distances of a few hundred km. The apparatus consists of approximately 1 kt of liquid scintillator that detects reactor neutrinos through the reaction

$$p + \overline{\nu}_e \rightarrow n + e^+. \tag{58}$$

The positron is then detected via scintillation light and its annihilation with an electron. This annihilation, in delayed coincidence with the γ-ray from neutron capture, represents a very clean signature.

To estimate the precision to which KamLAND could measure the oscillation parameters, the authors of [95] considered a 3 kt-y exposure during which the reactors operated at 78% of their maximum capacity. Backgrounds were neglected and perfect detector efficiency was assumed. Systematic effects, in particular those connected with chemical composition and flux uncertainties, have also been studied.

The measurements that KamLAND could be expected to perform with these assumptions are shown in Fig. 10, taken from [95]. Since the oscillations depend on the mixing angle only through $\sin^2 2\theta_{12}$, there is a two-fold degeneracy in the measurement, hence the reflection symmetry about $\tan^2\theta_{12} = 1$. The LMA solution, which is overlaid, does not possess such a symmetry, so it is necessary to plot against $\tan^2\theta_{12}$ and not $\sin^2 2\theta_{12}$ [97], in order to have a visual combination of the two measurements.

It has been shown in [94] that, combining KamLAND with the solar data, one can solve the two-fold degeneracy, i.e., find out whether $\theta_{12} < \pi/4$ or $\theta_{12} > \pi/4$ at the 95% confidence level (CL) for most of the LMA region. In this reference, a more conservative analysis than in [95] was performed, with comparable results.

3.1.2 Long-baseline accelerator-based experiments

Whilst the KamLAND experiment will help understand oscillations in the solar region, the study of the atmospheric region is best performed with artificial neutrino beams from particle accelerators. Three such beams exist or are planned in three different continents:

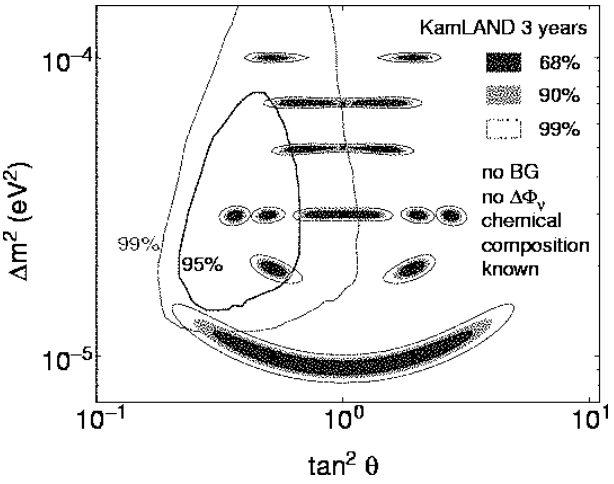

Fig. 10: *The expected measurement of Δm^2 and $\tan^2\theta$ in the KamLAND experiment. Contours for 68%, 90% and 99% CL are shown, and the LMA solution to the solar neutrino problem is overlaid [95].*

- The K2K beam from KEK to Super-Kamiokande,
- The NuMI beam from Fermilab to the Soudan mine,
- The CNGS beam from CERN to the Gran Sasso laboratory.

These three projects are quite different in scope and capabilities, due to the different characteristics of the accelerators that produce the beams, and of the proposed detectors. The K2K beam has lower energy and intensity, and its main aim is to confirm the ν_μ disappearance observed in Super-Kamiokande. The NuMI beam will have more intensity, and the focusing system chosen will produce neutrinos peaked at an energy of about 2 GeV, to achieve a better precision on the measurement of the oscillation parameters. The CNGS beam will have smaller intensity but higher energy than NuMI, and will be used for the τ search, to confirm that the atmospheric deficit is due to $\nu_\mu \rightarrow \nu_\tau$ oscillations. Characteristics of the different beams are shown in Table 1.

Beam	$E_{protons}$(GeV)	Power (MW)	$< E_\nu >$	L (km)
K2K	12	0.005	1.3	250
NuMI (LE)	120	0.41	3.5	734
CNGS	400	0.3	18	732
JHF	50	0.75	0.7	295

Table 1: *Characteristics of long-baseline beams*

A large community is gathering around the possibility of building a beamline for neutrinos at the future Japanese Hadron Facility (JHF), and sending an off-axis beam to Super-Kamiokande, and to a planned future large Čerenkov detector (Hyper-Kamiokande). Details of this second-generation beamline, that will mainly be used to look for a non-zero value of the electron neutrino mixing angle θ_{13}, are given below. A more detailed analysis is present in [96]

3.1.3 K2K

The only long-baseline experiment to have taken data so far is the K2K experiment, which was in the middle of its run when an unfortunate accident in the Super-Kamiokande detector [7] stopped their data taking until January 2003. The goal of K2K is to confirm the evidence of oscillations presented by Super-Kamiokande by looking for the disappearance of ν_μ's. The neutrino beam has a mean energy of about 1 GeV and points toward the Super-Kamiokande detector, which is located some 250 km from the neutrino source. Thus, the $\Delta^2 m$ to which they are sensitive is:

$$\Delta m^2 \sim \frac{1}{250} \sim 4 \times 10^{-3} eV^2$$

near the maximum of the atmospheric oscillation. Before the accident in Super-Kamiokande, K2K had about 5×10^{19} of their planned final 10^{20} protons on target. They had observed 56 events, compared with the 80 ± 6 expected in the case of no oscillations. These numbers and their measured energy spectrum are consistent with the Super-Kamiokande data. However, the K2K data alone could not yet be regarded as an independent confirmation of the atmospheric oscillation effect.

3.1.4 NuMI

The MINOS detector [21] for the NUMI [22] beam between Fermilab and the Soudan mine in Minnesota is currently under construction. Its goal is to make a precision measurement of the parameters governing the atmospheric neutrino oscillation. The experiment has a baseline of 735 km , and can be modified to produce beams of mean energies up to 14 GeV . The low-energy beam, with an average neutrino energy of 3.5 GeV , yields about the same L/E than the K2K experiment, and due to its higher flux is expected to provide a better precision on the atmospheric oscillation angle Δm^2_{23}. The far detector is a 5 kt sandwich of magnetized steel and scintillator planes. The near detector will be located at 1040 m from the proton target, and will be a scaled-down 1 kt version of MINOS. Systematic errors from the difference in the neutrino spectrum between near and far location are expected to be at the level of few %. The run is expected to start in early 2005, and after a two-year run MINOS should be able to perform a 10% measurement of the atmospheric parameters, unless Δ^2_{atm} happens to be too low, as shown in Fig. 11.

3.1.5 CERN-Gran Sasso

Due to the higher energy of the SPS accelerator, the beam from CERN to Gran Sasso is the ideal place to look for τ appearance, and this has been the main objective in designing the detectors at Gran Sasso.

The first approved project aimed at τ identification is the OPERA experiment [98]. The requirement for a large mass and a space resolution of the order of 1 μm has led to the choice of hybrid emulsion as the basic detector component. Lead-emulsion sandwiches are arranged in bricks, walls, modules and supermodules, for a total mass of 1.8 kt. Tracking devices are placed behind each brick to localize where interactions take place, enabling one to remove and develop in real time the interesting brick.

Another detector that will observe neutrinos from the CNGS beam is ICARUS [99]. So far, only a 600 t module is approved, which has already been built and successfully tested in summer 2001 on the surface in Pavia, and a proposal for a five-fold mass increase is pending approval. The detector consists of a large liquid Argon TPC, that allows a three-dimensional reconstruction of neutrino interactions with excellent imaging and energy reconstruction.

The τ identification strategy of the two detectors is complementary. The OPERA approach is topological, the τ being identified by the direct observation of the decay kink, while ICARUS will exploit the different kinematics of τ decays (especially in the golden $\tau \to e$ channel) compared to the backgrounds from charged currents and ν_e in the beam. The τ identification capabilities of the two detectors

[7] See `http://www-sk.icrr.u-tokyo.ac.jp/doc/sk/index.html` for details.

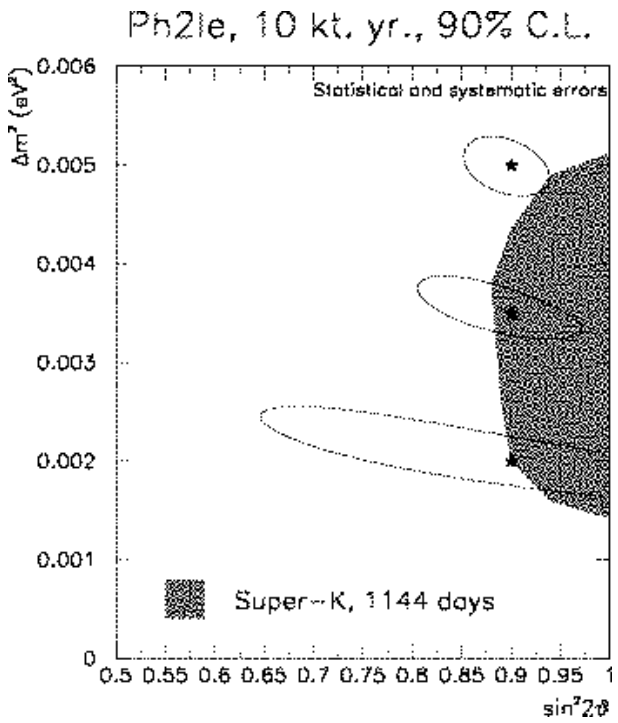

Fig. 11: *Expected 90% C.L. determination of the atmospheric oscillation parameters in a 10 kt-year exposure of MINOS to the low-enegy NuMI beam.*

(assuming the 3 kt option for ICARUS) are quite similar. Each experiment expects to be able to observe about 10 τ events after 5 years of running, with an expected background of 0.7 events, assuming Δm^2_{23} is $2.8 \times 10^{-3} eV^2$.

3.1.6 JHF-Super-Kamiokande

We have seen that the three projects K2K, NuMI and CNGS will give us a better understanding of oscillations in the atmospheric region, measuring precisely the oscillation parameters and establishing the $\nu_\mu \rightarrow \nu_\tau$ nature of such oscillations. Some progress will be also made in the search for a non-zero participation of the electron neutrino in the third flavour eigenstate, namely the element $|U_{e3}|$ of the leptonic mixing matrix. The search for a nonzero value of $\sin\theta_{13}$ is a fundamental step towards defining the future of neutrino physics. A further step in this direction will require high-intensity neutrino beams (super-beams).

The first neutrino super-beam will probably be built from the future Japanese Hadron Facility (JHF) in the JAERI lab at Tokai-mura (60 km NE of KEK) to the Kamioka site [100]. The 50 GeV JHF machine, scheduled to start operation in 2006, is designed to deliver 3.3×10^{14} protons every 3.4 seconds with a high beam power of 0.77 MW, that could later be upgraded to 4 MW [101]. The beam axis will be tilted by 2 degrees with respect to the position of the far location. This off-axis beam will be almost monochromatic around an energy of 800 MeV, and will have a smaller ν_e contamination than the direct beam. The baseline between JHF and Super-Kamiokande is about 295 km.

The first phase of the project could start as early as 2007. Given the great intensity of the beam and the large mass of Super-Kamiokande, in a 5-year run this project would provide the best knowledge of the neutrino mixing matrix parameters before the Neutrino Factory. The authors of [100] claim:

- A precision measurement of the atmospheric oscillation pattern, yielding $\sin^2 2\theta_{23}$ with 1% preci-

sion and Δm^2_{atm} with a precision better than $10^{-4}\ \mathrm{eV}^2$,

- Sensitivity to θ_{13} as small as $3^\circ (\sin^2 2\theta_{13} \sim 0.01)$, by searching for $\nu_\mu \to \nu_e$ appearance (see [100] for details on background reduction, taking advantage of the narrow beam and the good electron discrimination capabilities of Super-Kamiokande). This is illustrated in Fig. 12 (notice that the plotted quantity is $\sin^2 2\theta_{\mu e} \equiv 0.5 \sin^2 2\theta_{13}$). The expected sensitivity is an order of magnitude better than the current limit set by the Chooz experiment, namely $\sin^2 2\theta_{13} < 0.1$.

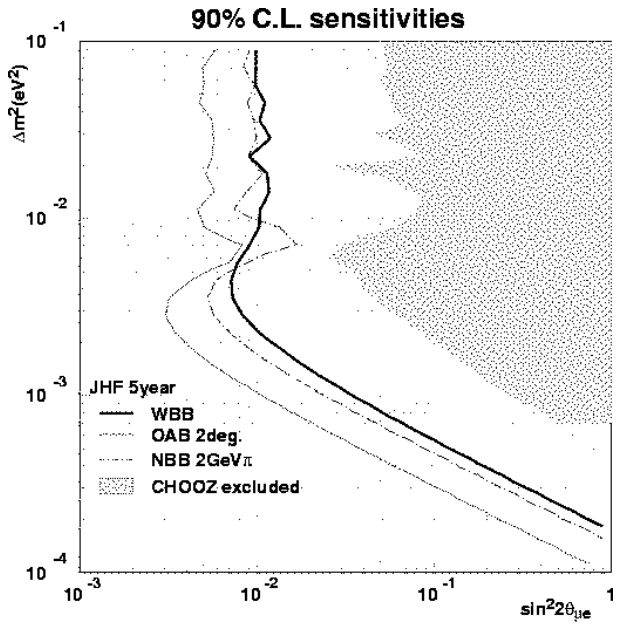

Fig. 12: *The expected 90% CL sensitivity contours for 5-year exposures in various beam configurations for the JHF-Super-Kamiokande project. The 90% CL excluded region of the Chooz experiment is plotted for comparison. Note that the plotted quantity is* $\sin^2 2\theta_{\mu e} \equiv 0.5 \sin^2 2\theta_{13}$.

3.1.7 Possible scenario

After operation of the first-generation neutrino beams and further progress in the JHF project, one could expect the experimental situation to be as follows:

- KamLAND will have established or excluded the LMA solution for the solar oscillations,
- MINOS will have measured the atmospheric oscillation parameters with a few % precision,
- The reality of oscillations will have been proven beyond any doubt by the observation of τ appearance at Gran Sasso,
- The angle θ_{13} will be measured if it is larger than about $2^\circ - 3^\circ$.

3.2 Second-Generation Long-Baseline Neutrino Beams

Extremely intense neutrino beams could have very large discovery potential, in the search for a non-zero value of θ_{13} and possibly CP violation, for a favourable choice of parameters. Several studies have been performed to assess the discovery reach of such machines, also in comparison with Neutrino Factories, since normally the proton driver used to produce such a super-beam would be the first step in the construction of a Neutrino Factory.

We have already seen that the JHF-Super-Kamiokande project can be considered as the first neutrino super-beam. However, it is foreseen to increase the intensity of that beam by almost a factor 5, and to use as a target a next-generation water Čerenkov detector (Hyper-Kamiokande), with an order of magnitude more mass than the present Super-Kamiokande. Such a large water detector would not only be used as a neutrino target, but, due to its large mass, would be able to push the search for nucleon decay into an unexplored region, and also be a unique laboratory for supernova neutrino astronomy. Another possible location for a large water detector is the Fréjus tunnel between France and Italy. This site is located at 130 km from CERN, from where it could be illuminated by a low-energy neutrino beam. Another option has been studied in the United States, in the context of a high-power proton driver for the Fermilab complex. In that case the energy is larger than the previous proposals, and different possible detectors have been studied.

A different way of building a neutrino beam, conceptually similar to that of the Neutrino Factory, is to produce neutrinos from the decays of heavy ions circulating in a storage ring. Compared to storing muons, the quality factor, defined as the ratio of the relativistic γ factor and the free energy E_0 of the reaction is much higher, thus producing narrower beams, and large fluxes even for relatively small beam currents. The resulting β beam would consist of pure ν_e (or $\bar{\nu}_e$, depending on the isotope used for neutrino production), of relatively low energy. The physics capabilities of such a beam are similar to those of the super-beam, but complementary since electron neutrinos are involved instead of muon neutrinos. Very interesting opportunities may instead rise from the possibility of running simultaneously, but with different timing, a super-beam and a radioactive decay beam (beta beam). The possibility of having ν_e and ν_μ in the same beamline, but separated by timing, is extremely interesting since, unlike the Neutrino Factory, oscillated events can be separated from those of the original beam by mean of flavour tagging without the need of lepton charge identification. The most appealing possibility of this option is the direct search for T violation, comparing the $\nu_e \to \nu_\mu$ and $\nu_\mu \to \nu_e$ oscillation probabilities.

3.2.1 JHF-Hyper-Kamiokande

The JHF neutrino project already foresees the possibility of an upgrade to higher neutrino flux (4 MW with respect to the initial 0.77 MW) and the beam will be pointed in a direction intermediate between the present Super-Kamiokande location and the main candidate site for a future Hyper-Kamiokande experiment, in such a way that both locations will be illuminated by a narrow-band beam, off-axis by 2 degrees. The Hyper-Kamiokande far detector would be composed of several almost cubic modules of size $45 \times 45 \times 46$, for a total fiducial volume of 70 kt per module; 16 compartments would make a total fiducial mass of above 1 Mt, read by about 200,000 photomultipliers, if the spacing between them is 1 meter.

A combination of Hyper-Kamiokande and a 4 MW beam would provide the possibility of exploring CP violation in the leptonic sector. For this purpose, it is necessary to compare oscillation probabilities for neutrinos and antineutrinos. The latter can be produced by focusing negative instead of positive pions in the horn system. However, since they are smaller in number, and since antineutrinos have a smaller cross section than neutrinos, the antineutrino run would have to be considerably longer than that with neutrinos, in order to have comparable statistical accuracy. For instance, for an experimental setup with a 4 MW beam, 1 Mt far detector, 2 years of ν_μ and 6.8 years of $\bar{\nu}_\mu$ running, the 3σ sensitivity extends to $\sin\delta > 0.25$ (14 degrees) at large $\sin^2 2\theta_{13}$ and $\sin\delta > 0.55$ for $\sin^2 2\theta_{13} = 0.01$, as seen in Fig. 13.

3.2.2 Possible off-axis experiments in the CNGS beam

Proposals have been made for an off-axis experiment exposed to the CNGS beam, also with the aim of improving the sensitivity to θ_{e3}. One suggestion is to install a water Čerenkov experiment in the Gulf of Taranto, whose distance from CERN could be varied to optimize the sensitivity to the oscillation

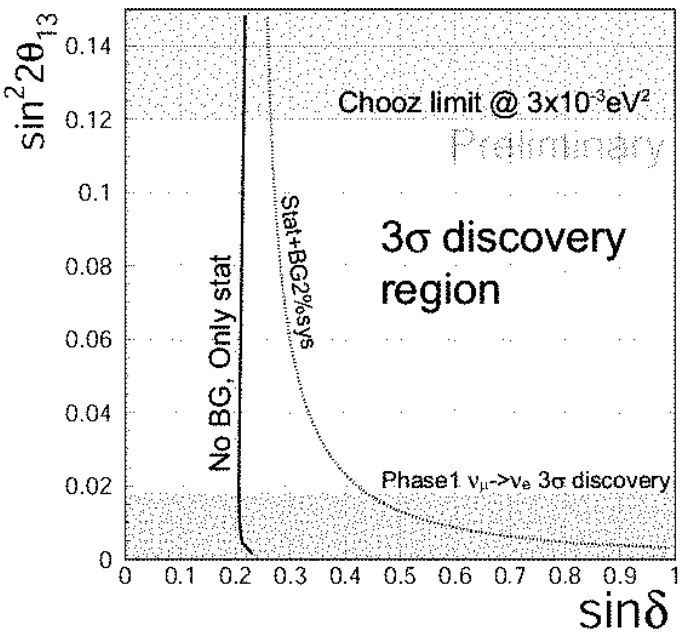

Fig. 13: *The JHF-Hyper-Kamiokande sensitivity for* $\sin^2 2\theta_{13}$ *= 0.01, 0.04 and 0.10.*

pattern [118]. Another suggestion is a surface experiment close to the Gran Sasso laboratory, using the atmosphere as a target [119].

3.2.3 Studies for a high-energy super-beam at FNAL

An efficient way of producing a super-beam at FNAL would be to take advantage of the NuMI [21] investment and make an upgrade of the proton driver [120, 121, 122]. One could then envisage a new generation of experiments to include shooting the intense conventional muon-type neutrino beam, produced with NuMI and the upgraded proton driver, towards a detector located suitably off the main beam direction. These off-axis beams have several advantages with respect to their on-axis counterparts, as discussed earlier. They are more intense, narrower and lower energy beams without a large high-energy tail, and they provide clean access to ν_e appearance, given the existence of a suitable detector with good electron identification capabilities. In order to fully take advantage of such tools, however, two different beams are essential, one predominantly ν_μ and the other predominantly $\bar{\nu}_\mu$. The antineutrino beam, however, provides an extra experimental challenge: as discussed in connection with JHF, the pion production and antineutrino scattering cross sections are suppressed with respect to those for neutrinos. In order to obtain a statistically comparable antineutrino and neutrino data set, the running time ratio between antineutrinos and neutrinos should be 2 or 3 to 1.

Studies show how well experiments in the NuMI beamline with a proton driver upgrade plus an off-axis detector can address these issues [123]. In order to estimate properly the experimental response, e.g., signal efficiency as well as beam and detector-induced backgrounds, a realistic simulation of the NuMI beam was performed, including the response of a 20 kt highly segmented iron detector, followed by a detailed 'data' analysis. A 5 kt Liquid Argon TPC in the same NUMI location would have comparable sensitivity to $|U_{e3}|^2$.

To assess properly the capabilities of such a set up, it is crucial to explore all the different physics scenarios, which we hope will be distinguished by the current KamLAND reactor experiment [25]. For different values of the solar mass-squared difference, we obtain different results for a five-year programme with an upgraded NuMI beam and a 900 km long baseline off-axis experiment. The mean

neutrino energy at this location is 2 GeV, while the ν_e and $\bar{\nu_e}$ fraction in the beam is less then 0.5% in the signal region:

1. If KamLAND does not observe a suppression of the reactor neutrino flux, $|U_{e3}|^2$ can be measured with very good precision and the neutrino mass pattern can be established, as long as $|U_{e3}|^2 \gtrsim \text{few} \times 10^{-3}$.

2. If KamLAND sees a distortion of the reactor neutrino spectrum, one should be capable of measuring $|U_{e3}|^2$ with good precision and obtaining a rather strong hint for CP violation, as long as $|U_{e3}|^2 \gtrsim \text{few} \times 10^{-3}$ and δ is close to either $\pi/2$ or $3\pi/2$, as seen in Fig. 14, assuming that the neutrino mass hierarchy is already known.

3. If KamLAND sees an oscillation signal but is not able to measure Δm^2_{sun}, one should be capable of measuring $|U_{e3}|^2$ with some precision and obtaining a strong hint for CP violation as long as $|U_{e3}|^2 \gtrsim 10^{-2}$ and δ is close to either $\pi/2$ or $3\pi/2$, even if Δm^2_{sun} is poorly known. However, Δm^2_{sun} cannot be measured with any reasonable precision, even assuming that the neutrino mass hierarchy is already known.

Other physics goals of the NuMI off-axis project are to measure with an order of magnitude better precision, compared to MINOS and CNGS estimates, the atmospheric parameters: $\delta(\Delta m^2_{\rm atm}) \lesssim 10^{-4}$ eV^2 and $\delta(\sin^2 2\theta_{\rm atm}) \lesssim 0.01$, confirm $\nu_\mu \leftrightarrow \nu_\tau$ oscillations, or discover sterile neutrinos by measuring the neutral-current event rate, and to improve by a factor of 20 the sensitivity to $\nu_\mu \to \nu_e$ appearance. After a five-year programme using NuMI with a 20 kt off-axis detector, one could establish a two-sigma confidence level on the $\nu_\mu \to \nu_e$ transition of $|U_{e3}|^2 > 0.00085\ (0.0015)$ with (without) an upgrade to the proton driver, assuming $\Delta m^2_{sun} \ll 10^{-4}$ eV^2 and a normal neutrino mass hierarchy.

3.2.4 The SPL super-beam

The planned Super Proton Linac (SPL) would be a 2.2 GeV proton beam of 4 MW power [102], which could be used as a first stage of the Neutrino Factory complex at CERN [103]. It would work with a repetition rate of 75 Hz, delivering $1.5 \cdot 10^{14}$ protons per pulse, corresponding to 10^{23} protons on target (pot) in a conventional year of 10^7 s. These characteristics are also suitable for the production of a super-beam.

Pions would be produced by the interactions of the 2.2 GeV proton beam with a liquid mercury target and focused with a magnetic horn. The target and horn assumed in the following are just those studied for the Neutrino Factory, and no optimization has been attempted for this super-beam. The pions next traverse a cylindrical decay tunnel of 1 meter radius and 20 meters length. These dimensions have been optimized in order to keep the ν_e contribution low and the ν_μ flux as high as possible.

The MARS program[104] has been used to generate and track pions. Polarization effects on μ decays were added, and analytical calculations used to follow the π and μ decays and particle trajectories [105]. The work presented in the following was previously published in somewhat more detail in [106]. The resulting neutrino spectra are shown in Fig. 15 and Table 2. The average energy of the neutrinos is around 250 MeV, and the ν_e contamination $\sim 0.4\%$.

The ν_e in the beam can be produced only by μ decays, since the center-of-mass energy is below the kaon production threshold. The ν_μ and ν_e come from the same decay chain: $\pi^+ \to \nu_\mu \mu^+ \to e^+ \nu_e \overline{\nu}_\mu$, so the ν_e flux can be predicted by a direct measure of the ν_μ themselves. It has been estimated that, combining the measurement of the ν_μ interaction rate at the far detector with the ν_μ and ν_e rates in a nearby detector of 0.5 kt at 1 km from the target, the ν_e contamination can be established with 2% systematic and statistical errors.

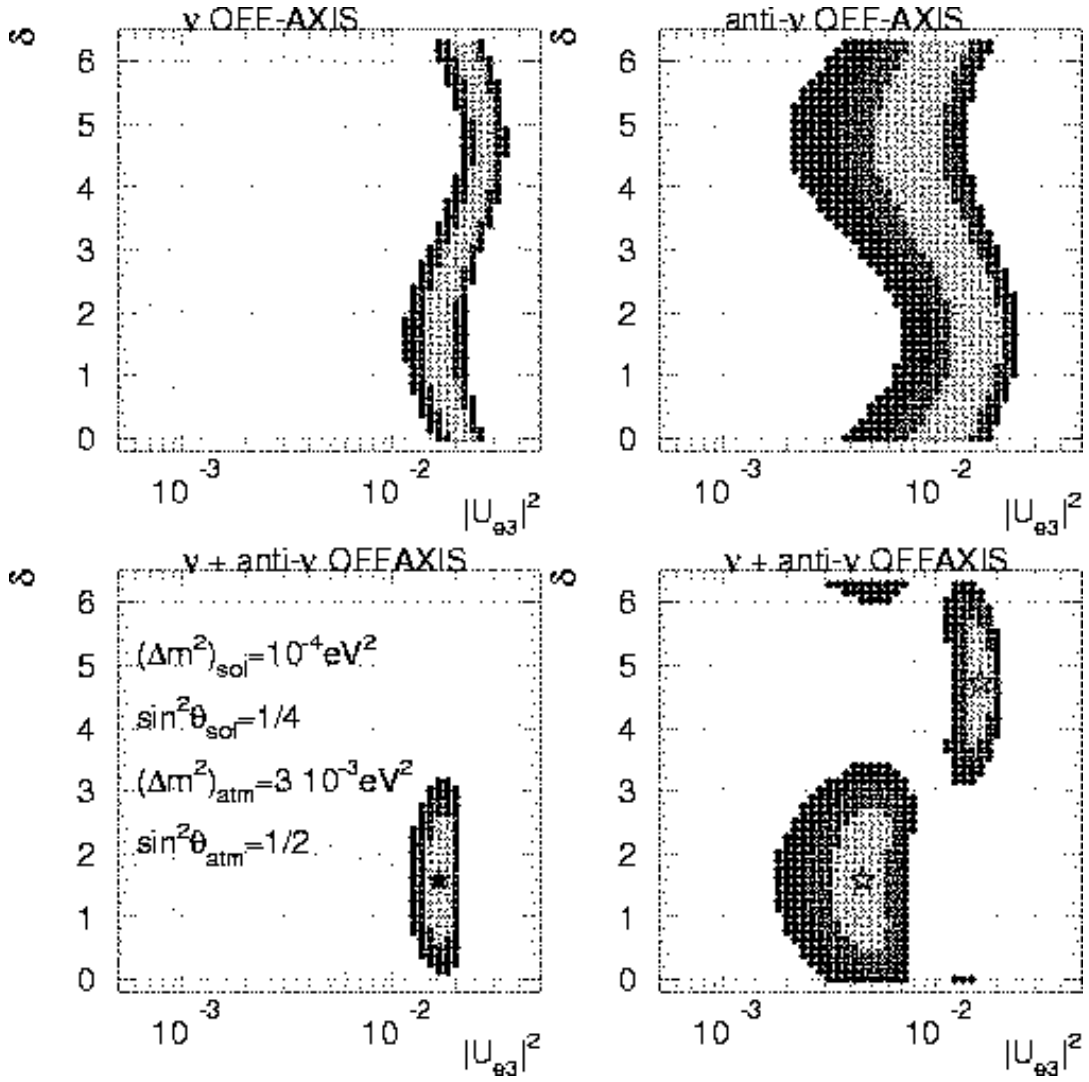

Fig. 14: *Top panel: one-, two-, and three-sigma measurement contours in the* $(|U_{e3}|^2, \delta)$ *plane, after a five-year programme (120 kt-y of neutrino-beam running (left) and 300 kt-y of antineutrino-beam running (right)). The simulated data is consistent with* $|U_{e3}|^2 = 0.017$ *and* $\delta = \pi/2$*. Bottom left panel: same as above, after the two data sets are combined. The solid star indicates the simulated input. Bottom right panel: same as before, for different simulated data points (indicated by the stars):* $\Delta m^2_{13} = +3 \times 10^{-3}$ *eV*^{2}, $\sin^2\theta_{\rm atm} = 1/2$, $\Delta m^2_{12} = 1 \times 10^{-4}$ *eV*^{2}, $\sin^2\theta_{sun} = 1/4$.

Table 2: *The SPL neutrino fluxes, for π^+ (left) and π^- (right) focused in the horn, computed at 50 km from the target.*

π^+ focused beam				π^- focused beam			
Flavor	Absolute Flux ($\nu/10^{23}\mathrm{pot/m^2}$)	Relative (%)	$\langle E_\nu \rangle$ (GeV)	Flavor	Absolute Flux ($\nu/10^{23}\mathrm{pot/m^2}$)	Relative (%)	$\langle E_\nu \rangle$ (GeV)
ν_μ	$1.7 \cdot 10^{12}$	100	0.26	$\overline{\nu}_\mu$	$1.1 \cdot 10^{12}$	100	0.23
$\overline{\nu}_\mu$	$4.1 \cdot 10^{10}$	2.4	0.24	ν_μ	$6.3 \cdot 10^{10}$	5.7	0.25
ν_e	$6.1 \cdot 10^{9}$	0.36	0.24	$\overline{\nu}_e$	$4.3 \cdot 10^{9}$	0.39	0.25
$\overline{\nu}_e$	$1.0 \cdot 10^{8}$	0.006	0.29	ν_e	$1.6 \cdot 10^{8}$	0.15	0.29

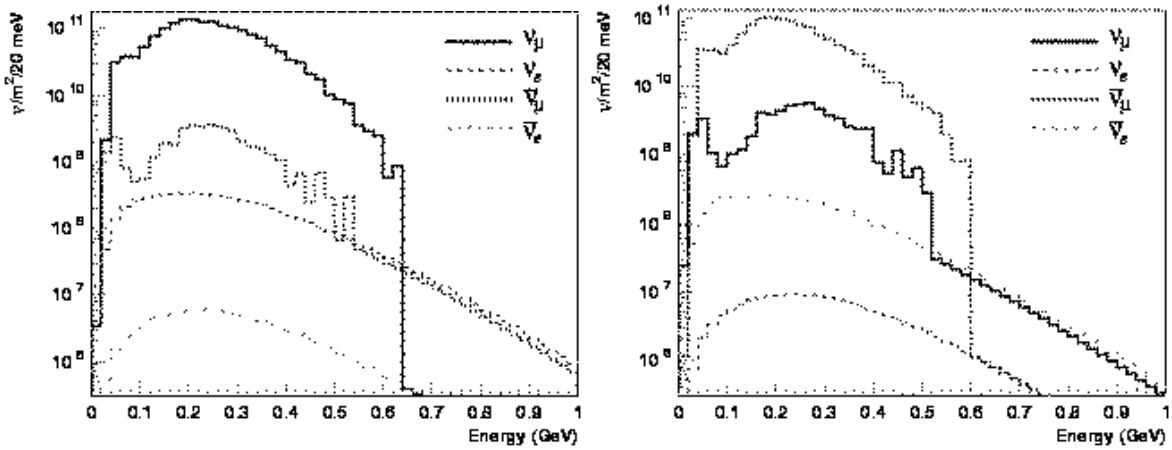

Fig. 15: *The SPL neutrino spectra, for π^+ (left) and π^- (right) focused in the horn, computed at 50 km from the target.*

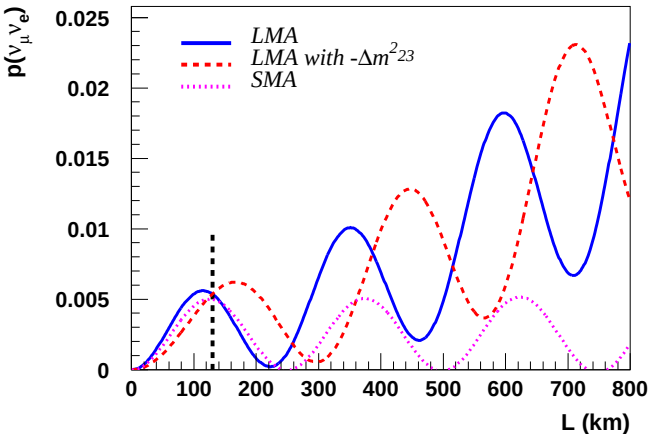

Fig. 16: *The oscillation probability $P(\nu_\mu \to \nu_e)$ computed for the SPL neutrino beam, with $\langle E_{\nu_\mu} \rangle = 0.26$ GeV, $\Delta m^2_{atm} = 2.5 \cdot 10^{-3} eV^2$, $\Delta m^2_{sun} = 5 \cdot 10^{-5}$, $6 \cdot 10^{-6}$ eV^2, $\pm\Delta m^2_{23}$, $\sin^2\theta_{13} = 0.01$, $\delta = 0$.*

3.2.5 Detector scenarios

Fig. 16 shows the oscillation probability $P(\nu_\mu \to \nu_e)$ as a function of the distance. Notice that the first maximum of the oscillation at $L \sim 130$ km matches the distance between CERN and the Modane laboratory in the Fréjus tunnel, where one could locate a large neutrino detector [107]. The detection of low-energy neutrinos at $\mathcal{O}(100)$ km from the source requires a massive target with high efficiency.

Moreover, a search for ν_e appearance demands excellent rejection of physics backgrounds, namely μ misidentification and neutral current π^0 production, which should be controlled to a lower level than the irreducible beam-induced background. Backgrounds from atmospheric neutrinos remain negligible if the accumulator foreseen in the Neutrino Factory complex is used, which provides a duty cycle of 4000.

Here two detector technologies are considered, which have demonstrated excellent performance in the low-energy regime, while being able to provide massive targets. These are water Čerenkov detectors such as Super-Kamiokande[108], and diluted liquid scintillator detectors such as used by the LSND [109] and MiniBOONE experiments [18], where both Čerenkov and scintillation light are measured.

We have considered an apparatus of 40 kt fiducial mass and sensitivity identical to the Super-Kamiokande experiment. The response of the detector to the neutrino beam was studied using the NUANCE [110] neutrino physics generator and detector simulation and reconstruction algorithms developed for the Super-Kamiokande atmospheric neutrino analysis. These algorithms, and their agreement with real neutrino data, have been described elsewhere [108, 111, 112].

The Super-Kamiokande standard algorithms for μ/e separation are very effective in the SPL-super-beam energy regime [h]. Events with a π^0 are easily rejected in events where the two rings are found by a standard π^0 search algorithm, à la Super-Kamiokande. To reject events where only one γ has been initially identified, an algorithm [113] forces the identification of a candidate for a second ring, which, if the primary ring is truly a single electron, is typically either very low energy, or extremely forward. By requiring that the invariant mass formed by the primary and the secondary rings is less than $45\,\mathrm{MeV}/c^2$, almost all remaining π^0 contamination is removed. Since the SPL super-beam would be cleaner and at lower energies than the JHF beam [100], we have not attempted to introduce more aggressive π°rejection algorithms. The data reduction is summarized in Table 3, where we see that contamination by the intrinsic beam ν_e is dominant.

Table 3: *Summary of simulated data samples for π^+ and π^- focused neutrino beams. The numbers in the rightmost column (after all cuts) represent the sample used to estimate the oscillation sensitivity for a 200 kt-y exposure.*

Channel	Initial sample	Visible events	Fit in fid. vol. Single-ring $100-450\,\mathrm{MeV/c^2}$	Tight particle ID	No $\mu \to e$	$m_{\gamma\gamma}$ $\leq 45\,\mathrm{MeV/c^2}$
π^+ focused beam						
ν_μ	3250	887	578.4	5.5	2.5	1.5
ν_e	18	12.	8.2	8.0	8.0	7.8
NC	2887	36.9	8.7	7.7	7.7	1.7
$\nu_\mu \to \nu_e$	100%	82.4%	77.2%	76.5%	70.7%	70.5%
π^- focused beam						
$\bar{\nu}_\mu$	539	186	123	2.3	0.7	0.7
$\bar{\nu}_e$	4	3.3	3	2.7	2.7	2.7
NC	687	11.7	3.3	3	3	0.3
$\overline{\nu}_\mu \to \overline{\nu}_e$	100%	79.3%	74.1%	74.0%	67.1%	67.0%

The energy range (50 MeV-1 GeV) and the rejections against background needed by MiniBOONE

[h] We have only tightened the cut on the particle identification criterion, which is based on a maximum likelihood fit of both the μ-like and e-like hypotheses (P_μ and P_e, respectively.). We use $P_e > P_\mu + 1$ instead of the default $P_e > P_\mu$.

Table 4: *Summary of data samples in a 40 kton liquid scintillator detector at $L = 130$ km for a 200 kt-y exposure.*

π^+ focused beam			π^- focused beam		
Channel	Initial sample	Final sample	Channel	Initial sample	Final sample
${\nu_\mu}^{CC}$	2538	2.5	$\overline{\nu}_\mu^{CC}$	451	0.5
${\nu_e}^{CC}$	12	6	${\overline{\nu}_e}^{CC}$	2.3	1.0
NC (visible)	48	0.5	NC	10	< 0.1
$\nu_\mu \to \nu_e$	100%	50%	$\overline{\nu}_\mu \to \overline{\nu}_e$	100%	50 %

nicely match the requirements of our study. The neutrino-^{12}C cross sections are taken from [114] [i]. Table 4 shows the data reduction assuming no ν_μ-ν_e oscillation, for a 200 kt-y exposure. As before, intrinsic beam ν_e contamination turns out to be the dominant background.

As one can see comparing Tables 3 and 4, the performances of both devices are quite similar. The conclusion is that one would prefer for this experiment a water detector, where truly gargantuan sizes can be afforded more easily.

3.2.6 Physics pote ntial

To illustrate the attainable precision in measuring δm^2_{atm} and θ_{23} , Fig. 17 shows the result of a 200 kt-y exposure ν_μ disappearance experiment using a liquid scintillator detector. The computation is performed defining 4 energy bins in the 0.1-0.7 GeV energy range and including Fermi motion, which is by far the most important limiting factor for energy reconstruction at these energies: see [115] for more details. We find that Δm^2_{23} can be measured with a standard deviation of $1 \cdot 10^{-4}$ eV^2, while $\sin^2 2\theta_{23}$ is measured at the $\sim 1\%$ precision level.

In the case of a water Čerenkov detector, the first energy bin would be lost, since the μ would be below threshold. In this case the resolution on the atmospheric parameters is slightly worsened, especially in the case of low Δm^2. The different solar solutions do not affect $P(\nu_\mu \to \nu_e)$ very much for $L = 130$ km, as can be seen in Fig. 16. Here we use SMA parameters, a hierarchical mass model, and set $\delta = 0$. Given the low statistics and the poor energy resolution, we consider in this case a counting experiment, not exploiting spectral distortions. The right panel of Fig. 17 shows the expected sensitivity for a 5-year run with a 40 kt (400 kt) water target at a distance of 130 km.

The sensitivity of this search turns out to be about 15 (60) times better than the present experimental limit of $\sin^2\theta_{13}$ coming from the Chooz experiment[14]. In the rest of this subsection we assume $\delta m^2_{12} = 10^{-4}$ eV^2 (in the upper part of the LMA region) and $\sin^2 2\theta_{12} = 1$. Since the $\overline{\nu}_\mu + {}^{16}$O cross-section is approximately six times less than that for $\nu + {}^{16}$O at $E_\nu \simeq 0.25$ GeV, we have considered a 10 y run with focused π^- and a 2 y run with focused π^+.

We follow the approach in [116, 117], and fit simultaneously the number of detected electron-like events to the CP phase δ and θ_{13}. Notice that, although we apply a full three-family treatment to our calculations, including matter effects, these are not important at the short distances and low energies considered.

Fig. 18 (left) shows the confidence level contours including statistical and background subtraction errors. A maximal CP-violating phase: $\delta = \pm 90^\circ$ would just be distinguishable from a zero CP-violating phase ($\delta = 0^\circ$). Fig. 18 (right) shows the result of the same fit, now assuming a very large water detector, such as the proposed UNO [33], with a fiducial mass of 400 kt. Clearly, the prospects to observe CP

[i] They come from an upgraded version of the continuous random phase approximation method, and on average they are lower by about $\sim 15\%$ from those quoted by the MiniBOONE experiment.

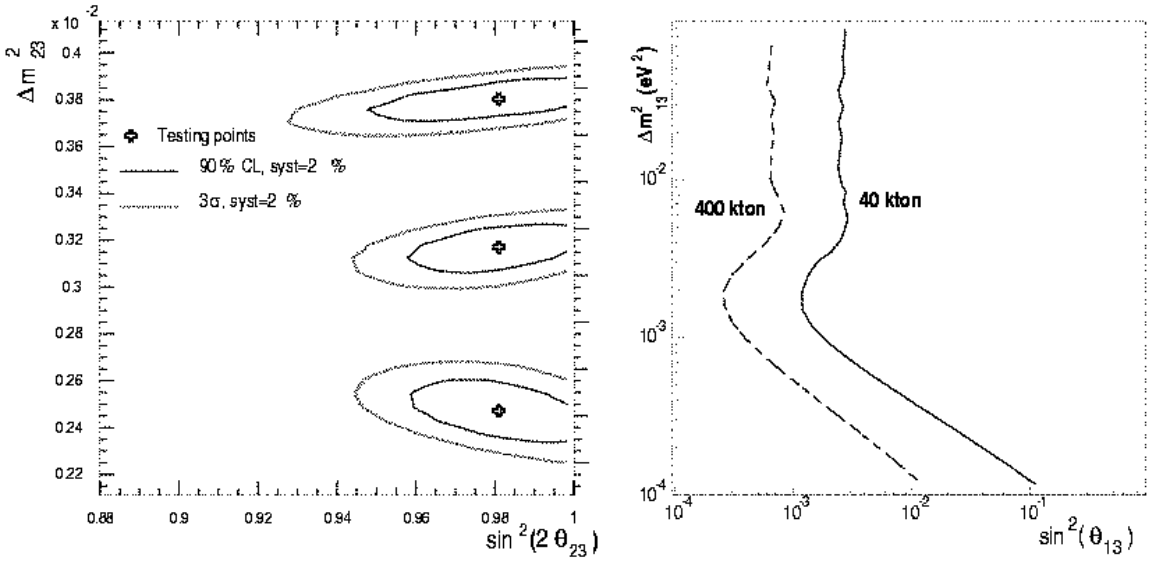

Fig. 17: *Left panel: Fits of δm^2_{atm}(eV^2),$\sin^2(2\theta_{23})$ after a 200 kt-y exposure at $L = 130$km, assuming 2% systematic errors. The crosses mark the initial points $(0.98, 3.8 \cdot 10^{-3})$, $(0.98, 3.2 \cdot 10^{-3})$, $(0.98, 2.5 \cdot 10^{-3})$ in the δm^2_{atm}, $\sin^2(2\theta_{23})$ coordinates. Right panel: The $\nu_\mu \to \nu_e$ oscillation sensitivity for π^+ focused neutrino beams with a 40 (400) kt detector.*

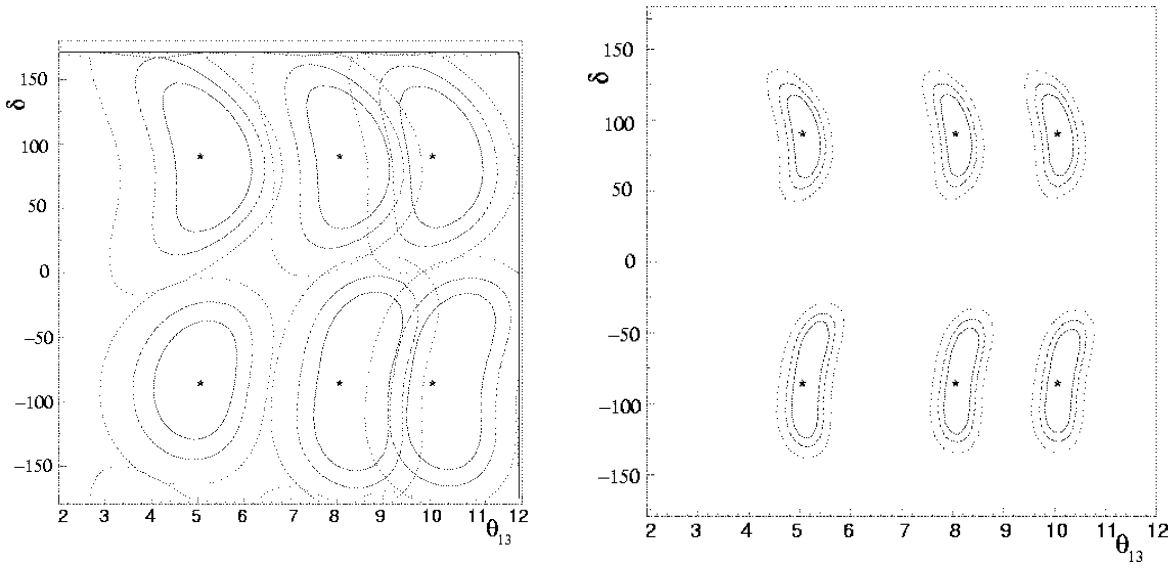

Fig. 18: *The $1\,\sigma$, 90 %CL and 99 %CL intervals resulting from a simultaneous fit to the θ_{13} and δ parameters. The generated values were $\theta_{13} = 5^\circ, 8^\circ, 10^\circ$, $\delta = \pm 90^\circ$. These results were computed for a 10 y anti-neutrino run and a 2-y neutrino run, using a 40 kt detector (left) or a 400 kt detector (right) at 130 km.*

violation are much improved.

Summarizing, we have examined the physics potential of a low-energy super-beam which could be produced by the CERN Super Proton Linac. Water Čerenkov and liquid oil scintillator detectors have been considered.

- The low energy of the beam studied has several advantages. The beam systematics are kept low,

because 2.2 GeV protons are below the kaon production threshold. Furthermore, e/μ and e/π^0 separation in a water (liquid oil) detector is near optimal at these low energies. The drawback is the small anti neutrino cross section, which is more than a factor five smaller than the neutrino cross section. These cross sections are in addition quite uncertain and would certainly need to be measured.

- The peak of the oscillation is at a distance of about 130 km, where an ideal location exists, the Modane laboratory in the Fréjus tunnel.
- A 'moderate-size' detector ('only' twice as big as Super-Kamiokande) at this baseline could, in a five-year run, improve the precision in the determination of the atmospheric parameters by about one order of magnitude with respect to the expected precision of next-generation neutrino experiments such as MINOS. It could also improve by more than one order of magnitude the sensitivity to $\sin^2\theta_{13}$, compared to the present experimental limits.
- Such a detector could also, if the solution to the solar neutrino problem lies in the upper part of the LMA region, detect a maximal CP-violating phase. For CP-violation studies, a very large detector à la UNO (with 400 kt fiducial mass) is mandatory.

3.2.7 Effect of the inclusion of neutrino spectral information

In the previous subsection, the parameters of neutrino oscillations were extracted either by counting the number of events or by fitting smeared generated neutrino energies. Here we describe a reconstruction of the neutrino energy starting from the information available in a water Čerenkov detector, i.e., the lepton energy E_l, its momentum P_l and angle, also considering detector smearing, Fermi motion and Pauli blocking.

In the ideal case, it is possible to reconstruct the neutrino energy from the lepton kinematics in a water Čerenkov detector using

$$E_\nu = \frac{m_n E_l + \frac{m_p^2 - m_n^2 - m_l^2}{2}}{m_n - E_l + P_l\cos(\theta)}, \tag{59}$$

where θ is the angle between the outgoing lepton and the neutrino direction. This angle can be measured via the knowledge of the beam direction, and the reconstructed lepton direction. The simulation used here is the fast Monte Carlo described in [124]. The technique presented in this paragraph aims at unfolding detector and nuclear physics effects, using a Monte Carlo reweighting method. We have used the spectrum calculated for the CERN SPL super-beam. The fast simulation only deals with CC quasi-elastic interactions. To describe nuclear effects, neutrons are generated isotropically in a sphere with Fermi momentum $k_F = 225$ MeV/c. The nuclear potential well is taken to be 50 MeV deep, and the double differential cross section from [125] was used. Pauli blocking was implemented by requiring that the outgoing proton lies outside the Fermi sphere of radius k_F. Based on Super-Kamiokande data [126, 127], the momentum resolution for electrons is set to 2.5%/$\sqrt{E(\mathrm{GeV})}$+0.5%; for muons it is constant and equal to 3% in this energy range; the angular resolution is estimated to be 3 degrees, constant for electrons and muons.

The analysis method is based on the construction, for each data event, of a distribution of all the Monte Carlo events with a visible energy close to that of the data event. It is based on the method described in [128]. For each data event, a box is defined with a small volume around its reconstructed energy. All MC events whose reconstructed energy lie close to that of the data event are considered to be good approximation to the data event, and their value of the generated energy is used in the likelihood function. The total likelihood can be found in [124], and maximizes information from the total number of events and unfolded spectral information. The weight of the each MC event in the box is the ratio

between the number of events for the value of the candidate oscillation parameter set and the number of events for the value of the oscillation parameters at which the MC sample was produced.

The results of a two-dimensional fit of the likelihood for the atmospheric parameters are displayed in Fig. 19. It is clear that the atmospheric parameters are correlated, therefore counting the number of events is not enough to obtain a measurement. The use of the reweighting method dramatically improves the precision, showing the efficiency of the unfolding procedure: Δm^2_{23} can be measured with a standard deviation of $\sim 0.7 \times 10^{-4}$ eV^2, and $\sin^2 2\theta_{23}$ is measured with a precision of $\sim 1.5\%$.

The results are also very promising for CP violation in the neutrino sector: using neutrinos with an exposure of 200 kt-y and antineutrinos with 1000 kt-y to compensate for the lower cross section, we have obtained the results plotted in Fig. 3.2.7. In this case, the number of events (left-hand side plot) contains most of the information, but reconstructing the spectral information reduces the 1σ error on δ by roughly a factor three, from 120° to 35°. We find that $\sin^2 2\theta_{13}$ can be measured with precision $\sim 20\%$.

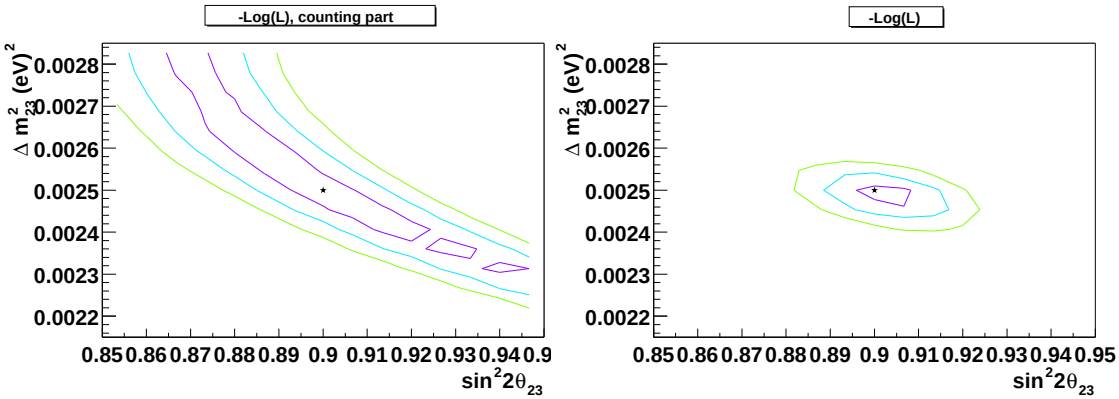

Fig. 19: *Contour plots of the different terms and the total of the log likelihood function. The star indicates the true value of the experimental parameters. The contours are the 1σ, 2σ and 3σ confidence levels.Both plots are made with the (2.5×10^{-3} eV^2, 0.9) sample. In each case, the star indicates the parameters at which the 'experimental' sample was produced. Left panel: contours of the likelihood using counting information only. Right panel: contours of the total likelihood.*

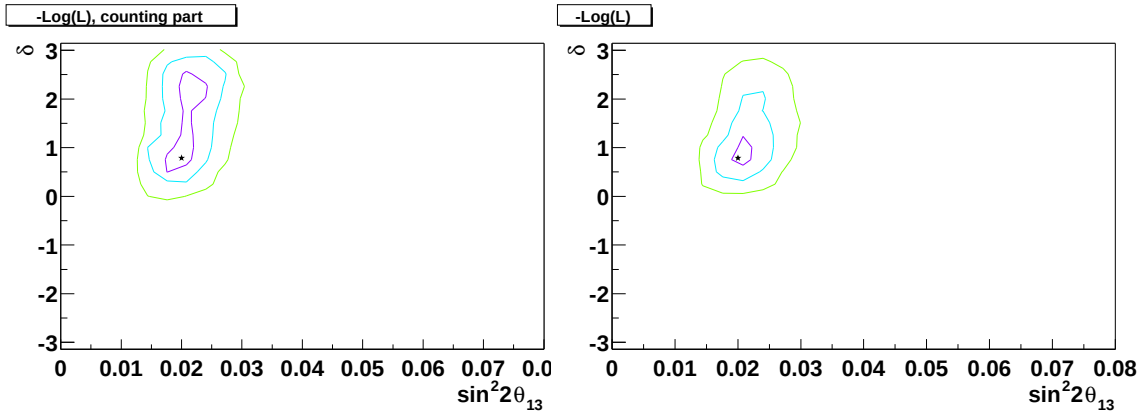

Fig. 20: *Contours of the likelihood, assuming 200 kt-y of electron neutrino data and 1000 kt-y of electron antineutrino data. The star indicates the position at which the 'experimental' sample was produced, and δ is measured in radians. Left panel: contours of the likelihood using counting information only. Right panel: contours of the total likelihood.*

4 BETA BEAMS

4.1 Introduction

The demand for better neutrino beams is correlated with the considerable improvement in neutrino detectors, and to the recent exciting claims of evidence for neutrino oscillations by various experiments. The largest existing detectors are based on the water Čerenkov detection technique, that seems to be scalable to the $\approx$ Mton order of magnitude [129]. Such a detector is motivated independently by the exploration of extra-galactic neutrinos, solar neutrinos, atmospheric neutrinos and proton decay. The additional possibility of a conventional high-intensity beam, called a super-beam would allow one to extend the search for the mixing angle θ_{13}, limited mainly by the beam purity that can be obtained.

A high-intensity neutrino source of a single flavour, with improved backgrounds and known energy spectrum and intensity, could extend further the measurement of the missing lepton mixing parameter, θ_{13}, and allow one to explore the CP-violation phase δ. The beta beam described here could provide such a source.

The beta beam could be exploited well by non-magnetic water Čerenkov detectors, and is very complementary to a super-beam. Combining a super-beam together with a beta beam, the CP-violation phase δ could be measured in complementary ways: by a CP-violation measurement and a T-violation measurement, as is explained below in detail.

4.2 Machine Issues

It is proposed to produce a collimated $\overline{\nu}_{\rm e}$ beam or ν_e beam, by accelerating to high energy radioactive ions that will decay through a beta process [130].

Radioactive ion production and acceleration to low energies of several MeV have already been performed for nuclear studies, and various techniques have been developed, e.g., at the CERN ISOLDE facility [131]. Moroever, the acceleration of positively-charged ions to about 150 GeV/nucleon has already been done in the CERN PS/SPS accelerators for the experimental programme on heavy-ion collisions. Storage of radioactive-ion bunches in a storage ring would be very similar, in principle, to what is being studied for the muon-based neutrino factory scheme [132]. The combination of these capabilities would provide a unique physics opportunity for CERN.

The neutrino beam resulting from radioactive-ion decays has three distinctive and novel features:

- A single neutrino flavour, which is essentially background-free;
- A well-known energy spectrum and intensity;
- Low energy in the ion centre of mass which, when given a large Lorentz boost, results in strong collimation. This feature is particularly important for long-baseline neutrino studies.

4.2.1 Nuclear beta decays

As a guideline, we consider a textbook atomic β^- decay which has well-known characteristics and good features for neutrino production:

$$ {}^6_2\mathrm{He}^{++} \rightarrow \quad {}^6_3\mathrm{Li}^{+++}\, \mathrm{e}^- \overline{\nu}_{\rm e} \quad . $$

The half-life $T_{1/2}$ of ^{6}He is 0.8067 s and the Q value of the decay is 3.5078 MeV [133]. The energy spectrum of the electron produced in ^{6}He beta decay has been measured extensively, and is well described theoretically (without corrections due to the Coulomb attraction between the nucleus and the electron) by the simple analytic formula:

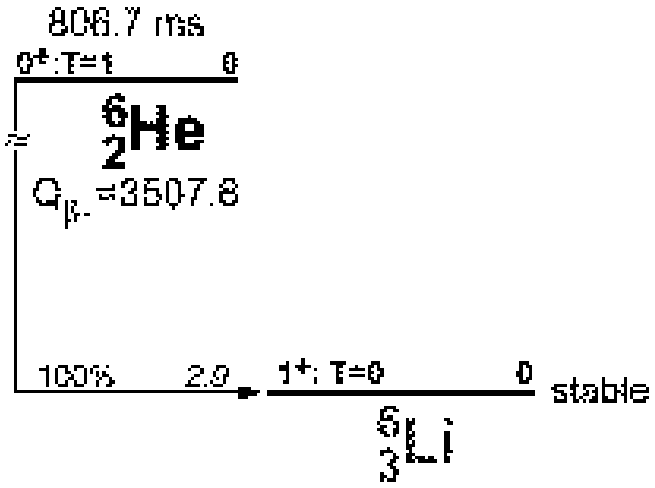

Fig. 21: *Allowed transitions of* $^6\mathrm{He}$ *[133].*

$$N(E)\mathrm{d}E \approx E^2(E-Q)^2\mathrm{d}E \quad ,$$

where E is the electron kinetic energy. The neutrino spectrum may be completely determined by laboratory measurements of the associated electron, without involving a neutrino measurement, since $E_\mathrm{e} + E_\nu \approx Q$ because of the relatively large mass of the nucleus. The average energy of the neutrino from $^6\mathrm{He}$ decay is 1.937 MeV, and the neutrino is emitted isotropically, since the parent ion is spinless. The beta decay of $^6\mathrm{He}$ is an extremely clean process, and in fact is the only allowed nuclear transition, as seen in Fig. 21.

Increasing the atomic number, various potential candidates emerge with different features: lifetime, neutrino energy, and Z/A. A list of possible neutrino and antineutrino emitter candidates is reported in Table 5, as well as the possible neutrino energy if are accelerated to the maximum energy achievable by a 450 GeV proton machine such as the CERN SPS.

4.2.2 The relativistic effect

We suppose that the $^6\mathrm{He}$ ion is accelerated to $\gamma = 150$, corresponding to the typical energy-per-nucleon currently obtained in the heavy-ion runs of the CERN SPS. In the laboratory frame, the neutrino momentum transverse to the beam axis is identical to that observed when the atom is at rest: 1.937 MeV on average. In contrast, the average longitudinal momentum is multiplied by a factor corresponding to γ, and therefore neutrinos have typical decay angles of $1/\gamma$, in our case 7 mrad. In the forward direction, the centre-of-mass neutrino energy is multiplied by the factor 2γ, so that the average neutrino energy at a far detector is 582 MeV, as seen in Fig. 22.

As the lateral dimensions of the far detector are typically much smaller than $1/\gamma$ multiplied by the distance L, the neutrino spectrum has essentially no radial dependence. The neutrino flux per parent decay and unit area is obtained by a Lorentz transformation of the centre-of-mass distribution of neutrino emission into the laboratory system. For the value $\gamma = 150$, the relative neutrino flux computed at distances above ≈ 1 km varies according to the $1/L^2$ scaling law, and at 100 km distance, corresponding to $\langle E \rangle / L = 5.9 \times 10^{-3}$ GeV/km, its value is $\Phi = 7.2 \times 10^{-7}$ m^{-2}. It is important to compare the focusing properties of a beta beam with those of a muon-based neutrino-factory beam. The comparison should be made for identical values of $\langle E \rangle / L$: if we choose arbitrarily the value $\langle E \rangle / L = 5.9 \times 10^{-3}$

Table 5: *Possible characteristics of some beta-beam emitter candidates. The laboratory neutrino energies are computed for emitters accelerated to the maximum energy achievable by a 450 GeV proton accelerator such as the CERN SPS. All energies are in MeV units.*

Nucleus	Z/A	$T_{\frac{1}{2}}$ (s)	Q_β	Q_β^{eff}	E_β	E_ν	E_{LAB}
$\overline{\nu}_{\rm e}$ decay							
$^{6}_{2}$He	3.0	0.807	3.5	3.5	1.57	1.94	582
$^{8}_{2}$He	4.0	0.119	10.7	9.1	4.35	4.80	1079
$^{8}_{3}$Li	2.7	0.838	16.0	13.0	6.24	6.72	2268
$^{9}_{3}$Li	3.0	0.178	13.6	11.9	5.73	6.20	1860
$^{16}_{6}$C	2.7	0.747	8.0	4.5	2.05	2.46	830
$^{18}_{7}$N	2.6	0.624	13.9	8.0	5.33	2.67	933
$^{25}_{10}$Ne	2.5	0.602	7.3	6.9	3.18	3.73	1344
$^{26}_{11}$Na	2.4	1.072	9.3	7.2	3.34	3.81	1450
ν_e decay							
$^{8}_{5}$B	1.6	0.77	17.0	13.9	6.55	7.37	4145
$^{10}_{6}$C	1.7	19.3	2.6	1.9	0.81	1.08	585
$^{18}_{10}$Ne	1.8	1.67	3.4	3.4	1.50	1.86	930
$^{33}_{18}$Ar	1.8	0.173	10.6	8.2	3.97	4.19	2058
$^{34}_{18}$Ar	1.9	0.845	5.0	5.0	2.29	2.67	1270
$^{35}_{18}$Ar	1.9	1.775	4.9	4.9	2.27	2.65	1227
$^{37}_{19}$K	1.9	1.226	5.1	5.1	2.35	2.72	1259
$^{80}_{37}$Rb	2.2	34	4.7	4.5	2.04	2.48	1031

GeV/km previously mentioned, the neutrino-factory detector would be located 5750 km from a 50 GeV muon storage ring [132]. The relative flux of neutrinos reaching the far detector of the muon-based neutrino factory is $5.7 \times 10^{-9}/\mathrm{m}^2$, 128 times less than in a beta beam. It should also be said that the relative neutrino flux comparison is essentially independent of the γ factor, if the comparison is made under identical $\langle E \rangle / L$ conditions, since both fluxes are proportional to $1/L^2$. This is strictly correct if the polarization effects due to the muon spin are neglected. The polarization of the muon affects the energy spectrum and the relative flux of both neutrino flavours produced in the muon decay [135].

Another significant neutrino beam parameter is the number of neutrino interactions when $E/L \approx \Delta m^2$. This is the parameter that determines the overall statistics collected by an oscillation disappearance experiment, and is also indicative of the appearance signal intensity, since

$$I \propto \sin^2(1.27 \frac{\Delta m^2\ [\mathrm{eV}^2] L[\mathrm{km}]}{E[\mathrm{GeV}]}).$$

Assuming the neutrino cross sections to be proportional to the neutrino energy [j], and taking into account the fact that the focusing properties of the neutrino beam depend solely on the γ factor, the neutrino interaction rate $N_{\rm int}$ in the far detector is:

$$N_{\rm int} \propto (\Delta m^2\ )^2 \times \frac{\gamma}{E_{\rm cms}}$$

where $E_{\rm cms}$ is the neutrino energy in the frame where its parent is at rest.

[j] This approximation is good for electron and muon neutrinos at the energies under discussion.

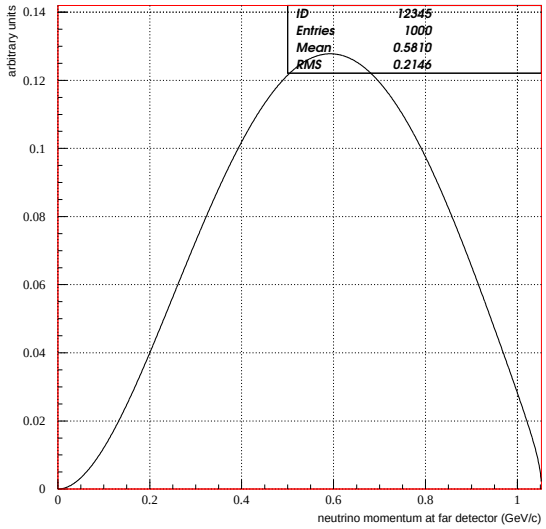

Fig. 22: *The boosted spectrum of* ^{6}He *neutrinos at the far detector.*

The quality factor $\gamma/E_{\rm cms}$ characterizes the neutrino beam and now includes the interaction probability in the approximation previously described. It is straightforward to see that – despite the larger probability that the high-energy neutrinos from muon decay have to interact – a ^{6}He beta beam accelerated to $\gamma = 150$ is more than five times as efficient as a neutrino beam from muons accelerated to $\gamma = 500$.

4.2.3 Baseline, energy and intensity considerations

Order-of-magnitude performances of the acceleration scheme can be estimated from the current efficiencies of existing machines. The acceleration scheme and the target production yields which are assumed are described elsewhere in this report. Table 6 shows the possible neutrino flux of a beta beam, which can be easily scaled to different detector distances as already discussed. This table is estimated for the highest energy possible with ^{6}He acceleration in a facility like the CERN SPS. One may also accelerate other ions, and in particular β^+ emitters that produce a ν_e in the final state. A good candidate is ^{18}Ne, and features of its acceleration scheme are summarized in Table 7.

4.3 Physics Reach of the Beta Beam

4.3.1 Signal

The signal in a beta beam looking for $\nu_e \rightarrow \nu_\mu$ oscillations would be the appearance of ν_μ charged-current events, mainly via quasi-elastic interactions. To select such events the following criteria have been used:

- A single-ring event,
- The track identified as a muon track using the standard Super-Kamiokande identification algorithms,
- The detection of the muon decay into an electron.

Table 6: *Possible characteristics of a beta beam optimized for the $\overline{\nu}_{\rm e}$ interaction rate.*

^{6}He ion production	5×10^{13}/s every 8 s
^{6}He collection efficiency	20%
^{6}He accelerator efficiency	65%
^{6}He maximum final energy	150 GeV/nucleon
$\overline{\nu}_{\rm e}$ average energy	582 MeV
Storage ring total intensity	1×10^{14} ^{6}He ions
Straight section relative length	36%
Running time/year	10^7 s
Detector distance	100 km
$\langle E \rangle / L$	5.9×10^{-3} GeV/km
$\overline{\nu}_{\rm e}$ interaction rate on H_2O	69/kton/year

Table 7: *Possible characteristics of a beta beam optimized for the ν_e interaction rate.*

^{18}Ne ion production	1×10^{12}/s every 4 s
^{18}Ne collection efficiency	50%
^{18}Ne accelerator efficiency	82%
^{18}Ne maximum final energy	75 GeV/nucleon
ν_e average energy	279 MeV
Storage ring total intensity	1.3×10^{13} ^{18}Ne ions
Straight section relative length	36%
Running time/year	10^7 s
Detector distance	130 km
$\langle E \rangle / L$	2.1×10^{-3} GeV/km
ν_e interaction rate on H_2O	3.1/kton/year

The signal efficiency as function of the true neutino energy, in the case of $\overline{\nu}_\mu$ interactions, is shown in Fig. 24(left), with and without the request of the detection of the decay electron. The backgrounds and signal efficiency have been studied in a full simulation, using the NUANCE code [110], reconstructing events in a Super-Kamiokande-like detector.

4.3.2 Backgrounds

The beta beam is intrinsically free from contamination by any different flavour of neutrino. However, background can be generated by imperfections in particle identification or external sources, such as single-pion production in neutral-current ν_e ($\overline{\nu}_e$) interactions, electrons (positrons) mis-identified as muons, and atmospheric neutrino interactions.

Neutral-current (NC) backgrounds come from the resonant processes

$$\nu_e(\overline{\nu}_e\,) + p \rightarrow \nu_e(\overline{\nu}_e\,)\pi^+ n \tag{60}$$

and

$$\nu_e(\overline{\nu}_e\,) + n \rightarrow \nu_e(\overline{\nu}_e\,)\pi^- p \tag{61}$$

In a water Čerenkov detector, pions below 1 GeV can be distinguished from muons only by requiring the decay electron signature to be associated to an identified muon. However, at low neutrino energy this background is intrinsically highly suppressed, since the threshold for these processes is about 400 MeV, and furthermore the outgoing pion must be above the Čerenkov threshold. As a net result, at γ values below 60, NC pion production is suppressed. At higher γ values, single-pion production rises quite fast, as shown in Fig. 23(left). Electrons (positrons) produced by ν_e ($\overline{\nu}_e$) can be mis-identified as

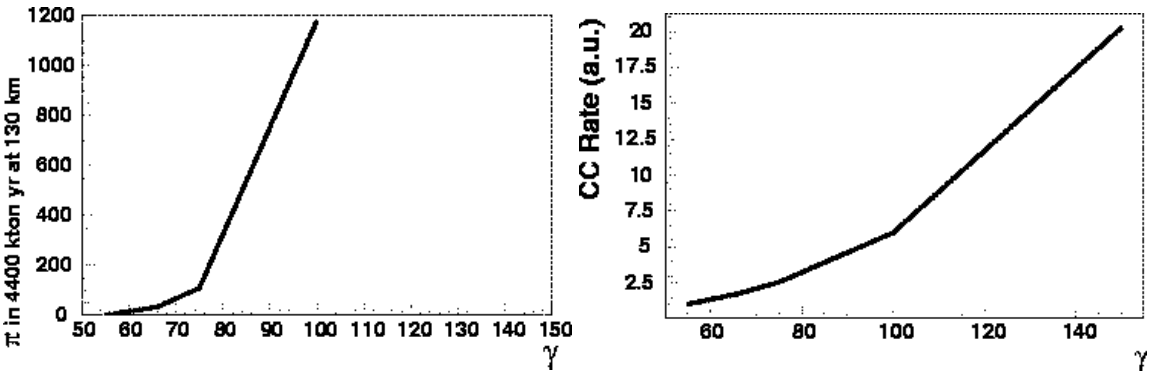

Fig. 23: *Left panel: Backgrounds from single-pion production for a 4400 kt-y exposure, as function of γ. Right panel: The charged-current ν_e interaction rate as function of γ in arbitrary units.*

muons, therefore giving a fake signal. Standard algorithms for particle identification in water Čerenkov detectors are quite effective to suppress such backgrounds. Furthermore, the signal of the decay electron in muon tracks can be used to reinforce the muon identification.

Atmospheric neutrino interactions are extimated to be ~ 50/kton/yr in the energy range of interest for the experiment, a number of interactions that far exceeds the oscillation signal. The atmospheric neutrino backround has to be reduced mainly by timing of the parent ion bunches. The time structure of the interactions in the detector is identical to the time structure of the parent ions in the decay ring. The location of the beta decay does not matter, since the parents have essentially the same speed as the neutrinos. The far-detector duty cycle is therefore given by the ratio of the bunch length to the ring length. For a decay ring of 6.9 km and a bunch length of 10 ns, which seems feasible, this ratio provides a rejection factor of $2 \cdot 10^4$. The directionality of the (anti)neutrinos can be used to suppress further the atmospheric neutrino background by a factor ~ 4. With these rejection factors, the atmospheric neutrino background can be reduced to the order of 1 event/440 kton/yr. Moreover, out-of-spill neutrino interactions can be used to normalize this background to the 1% accuracy level.

4.3.3 Systematic errors

The cross-section estimates for signal and background production at energies below 1 GeV are quite uncertain, the systematic errors being of the order of 20 and 30 % respectively. Systematic errors of this size would seriously reduce the sensitivity of the experiment. On the other hand, a beta beam is ideal for measuring these cross sections, provided that a close detector at the distance of about 1 km from the decay tunnel and of proper size (1 kt at least) can be built:

- The energy and the flux of the neutrino beam is completely defined by the acceleration complex, and can be known with a precision better than 1%, the limiting factor being knowledge of the number of accelerated ions in the machine.
- The near/far residual error is extremely reduced, because in a beta beam the divergence of the beam is completely defined by the decay properties of the parent ion.

- The γ factor of the accelerated ions can be varied, in particular a scan can be initiated below the production threshold of the backgrounds, allowing a precise measure of the cross sections for resonant processes.

It is extimated that a residual systematic error of 2% will be the final precision with which both the signal and the backgrounds can be evaluated.

4.3.4 Beam optimization

The Lorentz boost factor γ of the ion accelerator can be tuned to optimize the sensitivity of the experiment to CP violation in the neutrino sector. We perform the optimization assuming the value $\delta m^2_{atm} = 2.5 \cdot 10^{-3}$ eV^2 for the atmospheric neutrinos, a baseline of 130 km, the CERN-Fréjus distance, and a ^{6}He beam. In principle, baselines in the range 100-250 km are possible, given the characteristics of the acceleration scheme.

There are competitive processes that must be balanced to find the optimal sensitivity:

1. The number of quasi-elastic events in the far detector scales roughly as γ^3, see Fig. 23(right). This factor comes from the beam focussing, which is $\propto \gamma^2$, and the cross section, which is $\propto \gamma$. The number of quasi-elastic events at a given L/E is then proportional to γ.

2. The number of background events from the processes (60, 61) increases with γ, as shown in Fig. 23(left). An excessive background severely limits the sensitivity of the experiment, so background contamination prefers the lowest possible γ.

3. The signal efficiency as function of energy, see in Fig. 24(left), severely disfavours neutrino energies below 300 MeV. We note that the signal efficiency decreases slightly above 0.7 MeV. This is due to the request for single-ring events: at higher values of the ν energy, the fraction of quasi-elastic events decreases.

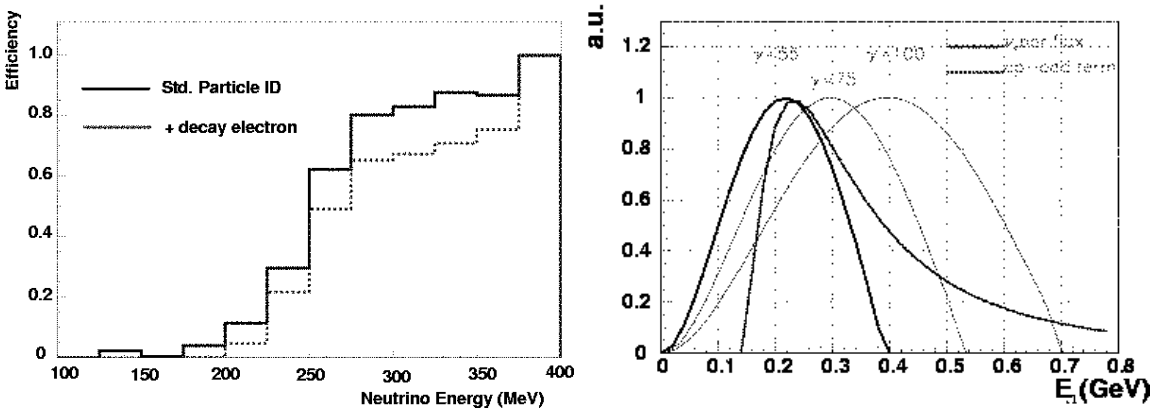

Fig. 24: *The signal efficiency as function of the neutrino energy (left). Energy spectra for different values of γ compared with the probability function for CP-odd oscillations (right).*

4. The true signal of the experiment consists of the observation of those ν_μ produced by the CP-odd term in $p(\nu_e \rightarrow \nu_\mu)$. In Fig. 24(right), this term is compared with the neutrino energy spectrum produced at three different γ values: $\gamma = 50, 75, 100$, all at the baseline of 130 km. It is evident that the neutrino energy is de-tuned with respect to the oscillating term when $\gamma \geq 100$.

Based on these considerations, a γ value of 75 seems to approach the optimal value for CP sensitivity. We report In Table 8 signal and background rates for a 4400 kt-y exposure to ^{6}He and ^{18}Ne beams.

10 years	^6He $\gamma = 75$	^{18}Ne $\gamma = 75$
CC events (no osc, no cut)	40783	18583
Total oscillated	34	63
CP-Odd oscillated	-43	22
Beam background	0	0
Detector bkg.	60	10

Table 8: *Event rates for a 4400 kt-y exposure. The signals are computed for* $\theta_{13} = 3°$, $\delta m^2_{12} = 0.6 \cdot 10^{-4} eV^2$, $\delta = 90°$.

4.3.5 Sensitivity to CP violation

A search for leptonic CP violation can be performed running the beta beam with ^{18}Ne and ^{6}He, and fitting the number of muon-like events to the $p(\nu_e \rightarrow \nu_\mu)$ probability. The fit can provide simultaneus determinations of θ_{13} and the CP phase δ. Uncertainties in the mixing-matrix parameters can affect the precise determination of θ_{13} and δ. These effects have been taken into account, considering as errors in these other parameters the values that can be expected by the near future experiments:

- A 10% error on the solar δm^2 and $\sin^2 2\theta$, as expected from the KamLAND experiment, after 3 years of data taking [25].
- A 2% error on the atmospheric δm^2 and $\sin^2 2\theta$, as expected from the JHF neutrino experiment [100].

Only the diagonal contributions of these errors are considered in the following. They contribute less than 5% of the total error in the final sensitivity. Given the relative interaction rates for quasi-elastic events, a sharing of 3 years of ^{6}He and 7 years of ^{18}Ne has been considered.

The results of this analysis are summarized in Table 8, for an arbitrary choice of the mixing matrix parameters. Since the sensitivity to CP violation is heavily dependent on the true value of δm^2_{12} and θ_{13}, we prefer to express the CP sensitivity for a fixed value of δ in the whole δm^2_{12} , θ_{13}parameter space. The CP sensitivity to separate $\delta = 90°$ from $\delta = 0°$ at the 99%CL as a function of δm^2_{12} and θ_{13}, following the convention of [116], is plotted in Fig. 25.

4.3.6 Synergy between the SPL super-beam and the beta beam

The beta beam needs the SPL as injector, but consumes at most $\sim 3\%$ of the SPL total number of produced protons. The fact that the energies of both the super-beam and the beta beam are below 0.5 GeV, with the beta beam being tunable, offers the fascinating possibility of exposing the same detector to two neutrino beams at the same time.

We recall that the SPL super-beam is a ν_μ ($\overline{\nu}_\mu$) beam, while the beta beam is a ν_e ($\overline{\nu}_e$) beam, so the combination of the two beams offers the possibility of CP, T and CPT searches at the same time:

- Searches for CP violation, running the super-beam with ν_μ and $\overline{\nu}_\mu$, and the beta beam with ^{6}He ($\overline{\nu}_e$) and ^{18}Ne (ν_e).
- Searches for T violation, combining neutrinos from the super-beam ($\nu_\mu \rightarrow \nu_e$) and from the beta beam using ^{18}Ne ($\nu_e \rightarrow \nu_\mu$), or antineutrinos from the super-beam ($\overline{\nu}_\mu \rightarrow \overline{\nu}_e$) and from the beta beam using ^{6}He ($\overline{\nu}_e \rightarrow \overline{\nu}_\mu$).

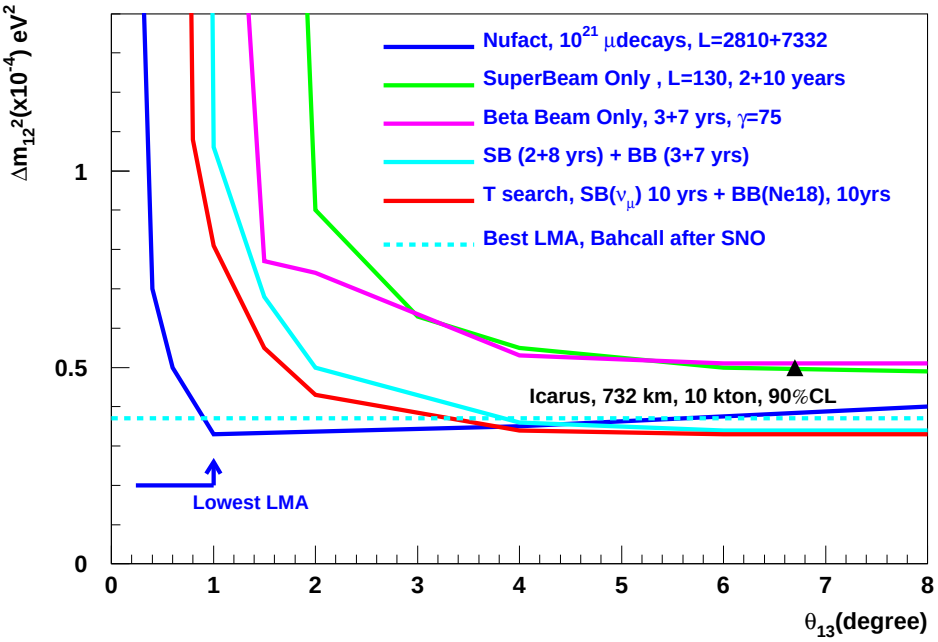

Fig. 25: *The CP sensitivity of the beta beam, of the SPL super-beam, and of their combination. They are compared with a Neutrino Factory experiment with two detectors [116].*

- Searches for CPT violation, comparing $P(\nu_\mu \rightarrow \nu_e)$ to $P(\overline{\nu}_e \rightarrow \overline{\nu}_\mu)$ and $P(\overline{\nu}_\mu \rightarrow \overline{\nu}_e)$ to $P(\nu_e \rightarrow \nu_\mu)$.

It is evident that the combination of the two beams would not result merely in an increase in the statistics of the experiment, but would offer clear advantages in the reduction of systematic errors, and would offer the redundancy needed to establish firmly any CP-violating effect within reach of the experiment.

We should also stress that this combination of beams offers the only known possibility of measuring CPT violation combining signals from the same detector, a crucial issue for the control of systematic errors.

Fig. 25 summarizes the CP sensitivity of different combinations of the super-beam and beta beam compared with the Neutino Factory sensitivity. The combined sensitivity of the super-beam and beta beam complex shown in Fig. 24 is very competitive with that of a Neutrino Factory, offering a truly complementary approach to the search of of leptonic CP violation.

5 THE NEUTRINO FACTORY

5.1 Overview

In a Neutrino Factory, neutrinos are produced by the decays of muons circulating in a storage ring. Most of what is known of muon storage rings is due to the pioneering work of the Muon Collider Collaboration [36]. They were able to formulate and to a large extent simulate the basic concepts of a Muon Collider. The concept of a Neutrino Factory was born from the observation that the beams of neutrinos emitted by the decaying muons along the accelerator chain or in the storage rings could be valuable physics tools [136], the potential of which was emphasised in the ECFA prospective study [137]. Neutrino Factory design is presently being pursued in the United States [138], at CERN [139] and in Japan [140]. It owes much to the earlier Muon Collider studies, and its very similar components are briefly recalled here.

5.1.1 General principles

The design includes a very high-power proton driver, delivering on target typically 4 MW of beam power of protons with energy in excess of a few GeV. A super-conducting linac at 2.2 GeV has been studied at CERN[102], while the US design calls for a rapid cycling proton synchrotron at 16-24 GeV, and an upgrade of JHF is considered in Japan. Designing a target that can withstand the thermal shock and heat load naturally leads to a liquid jet target design, although rotating high temperature solids are also being considered. Pions produced are collected as efficiently as possible by a magnetic channel, which involves a 20 T solenoid or powerful magnetic horns. Pions quickly decay into muons with a similar energy spectrum. At this point the beam is 0.6 m in diameter and has an energy spread of more than 100%.

A momentum interval near the largest particle density, typically 250 ± 100 MeV/c, is monochromatized to within a few MeV by means of phase rotation, using a strong variable electric field to slow down the fastest particles and accelerate the slower ones. This requires low-frequency ($\sim 50 - 100$ MHz) RF cavities or an induction linac. To reduce the transverse emittance, cooling is necessary, and is provided by ionization cooling [141]. This involves energy loss of muons through a low-Z material, e.g., liquid hydrogen, in a strongly focusing magnetic field (solenoids of 5-10 Tesla), which reduces momentum in all three dimensions, followed by accelerating RF cavities, which restore the longitudinal momentum. The net effect is a reduction of emittance, leading to a transverse beam size of a few centimetres.

This leads to a linear configuration, as shown in Fig. 26, for the initial muon beam preparation section, or *muon front-end*. In this concept, each beam element is used only once. It could be interesting, to save hardware, to be able to perform phase rotation and/or transverse cooling in a recirculating configuration. Indeed, a system of large aperture FFAG accelerators with low frequency RF (around 1.5 MHz) is the key to the Japanese Neutrino Factory design. Also, much progress has recently been made on 'ring coolers', which allow both transverse and longitudinal cooling in a circular configuration [142].

Assuming that the delicate questions of optics can be solved, these 'ring' options share the difficulty of injecting or extracting from a ring the very large emittance beam of muons available at the end of the decay channel. The possibility of very large aperture and very fast kickers is the major unknown and will be a key issue for these potentially cost-saving developments.

Last but not least, a linac followed by recirculating linacs - or FFAG accelerators - provide the fast acceleration of muons to an energy of 20 to 50 GeV, the optimal operating energy being presently under discussion. Around 10^{21} muons per year of 10^7 seconds could then be stored in a ring, where they would circulate for a few hundred times during their lifetime. The storage ring can take the shape of a racetrack, triangle or bow-tie. These latter two configurations allow several beams of decay neutrinos to be produced in the direction of short- and long-baseline experiments. Optics have been designed [143] for muon storage rings of either triangular or bow-tie geometry, pointing for instance at distances of 730 km (which would correspond to the CERN-Gran Sasso beam line), and 2800 km (which would

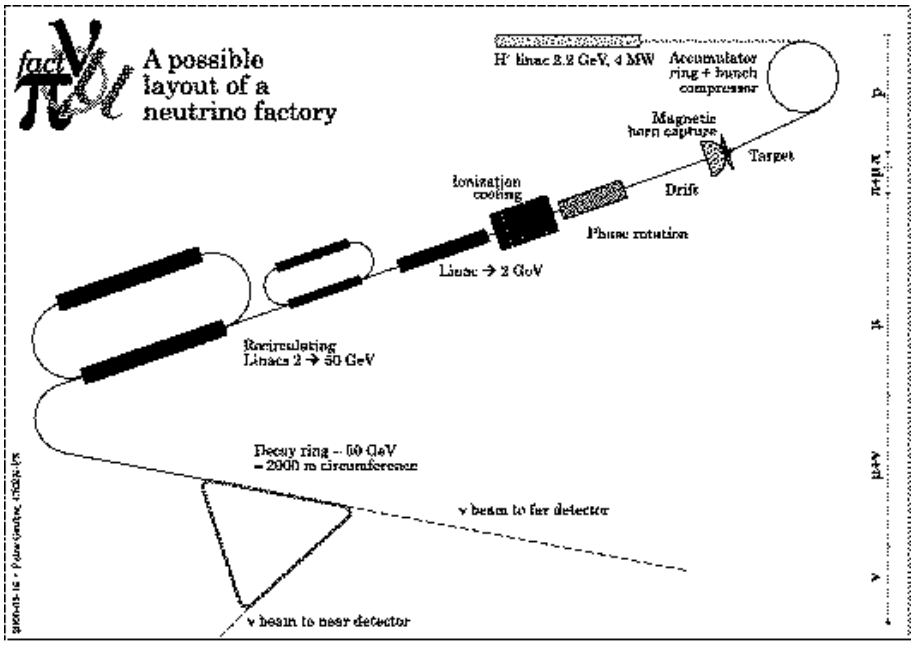

Fig. 26: *Schematic layout of the CERN scenario for a Neutrino Factory.*

correspond to a more distant site in the Canary Islands or the Nordic countries). The geometries of these rings are shown in Fig. 27.

As can be inferred from this brief description, Neutrino Factory design involves many new components and extrapolations beyond state-of-the-art technology. The first design studies [138, 139, 140] have come to the conclusions that, with the present designs and technology, such a machine could indeed be built and reach the desired performance, but that serious work was needed to bring the cost down. Assuming adequate funding, it is considered that about five years of research and development will be necessary to reach a point where a specific, cost-evaluated machine can be proposed.

5.1.2 Rates and backgrounds

The large beam intensities envisaged in the framework of muon collider studies would provide an unprecedented neutrino flux, that would allow one to perform experiments with an unprecedented precision on the oscillation measurements. We now take a closer look at the spectra and event rates produced.

The neutrino energy spectrum in muon decay at rest follows the following distribution:

$$\frac{d^2N_{\nu_\mu}}{dxd\Omega} \propto \frac{2x^2}{4\pi}[(3-2x)+(1-2x)P_\mu\cos\theta] \quad (62)$$

$$\frac{d^2N_{\bar{\nu}_e}}{dxd\Omega} \propto \frac{12x^2}{4\pi}[(1-x)+(1-x)P_\mu\cos\theta] \quad (63)$$

where $x \equiv 2E_\nu/m_\mu$, P_μ is the muon polarisation, and θ is the angle between the muon polarisation vector and the neutrino direction. In the laboratory frame, when considering a detector located on the same axis as the Lorentz boost, as is the case for long-baseline experiments where the detector size can be neglected with respect to the baseline, the shape of the energy distribution is preserved. So, if muons are accelerated to an energy E_μ, the spectral shape will be described by the same formulae as above, this time with $x = E_\nu/E_\mu$. The spectral shape of a Neutrino Factory flux, compared to that of a typical neutrino beam from pion decays, namely the WANF beam at CERN, is shown in Fig. 28.

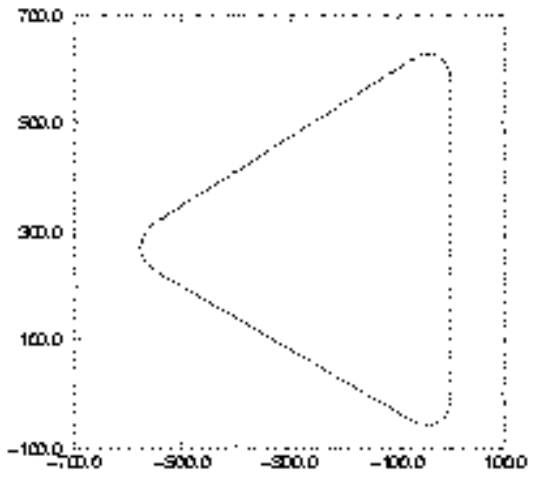

Figure A: Projection of the muon storage ring on a plane tangent to Earth

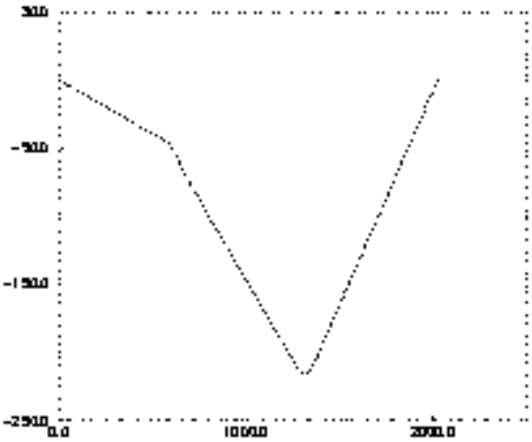

Figure B: Vertical position y along the circumference of the muon storage ring

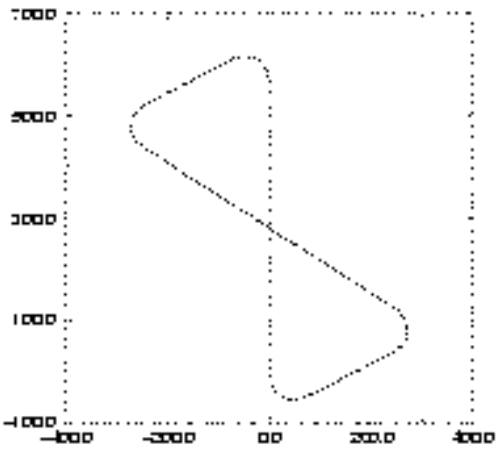

Figure C: Projection of the muon storage ring on a plane tangent to Earth. The orientation is arbitrary.

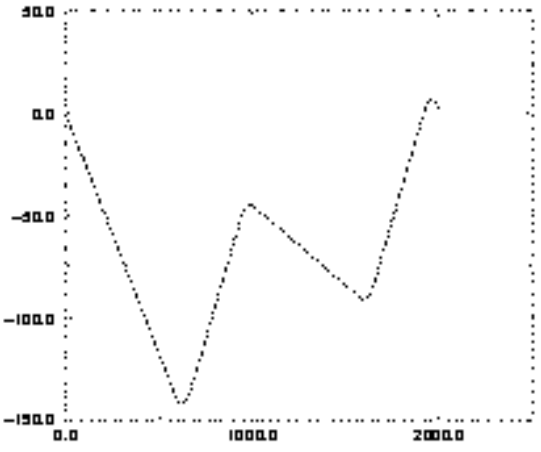

Figure D: Vertical position y along the circumference of the muon storage ring. The origin of y is arbitrary.

Fig. 27: *Description of the decay rings designed in [143]. Top panel: the triangular geometry, bottom panel: the bow-tie geometry.*

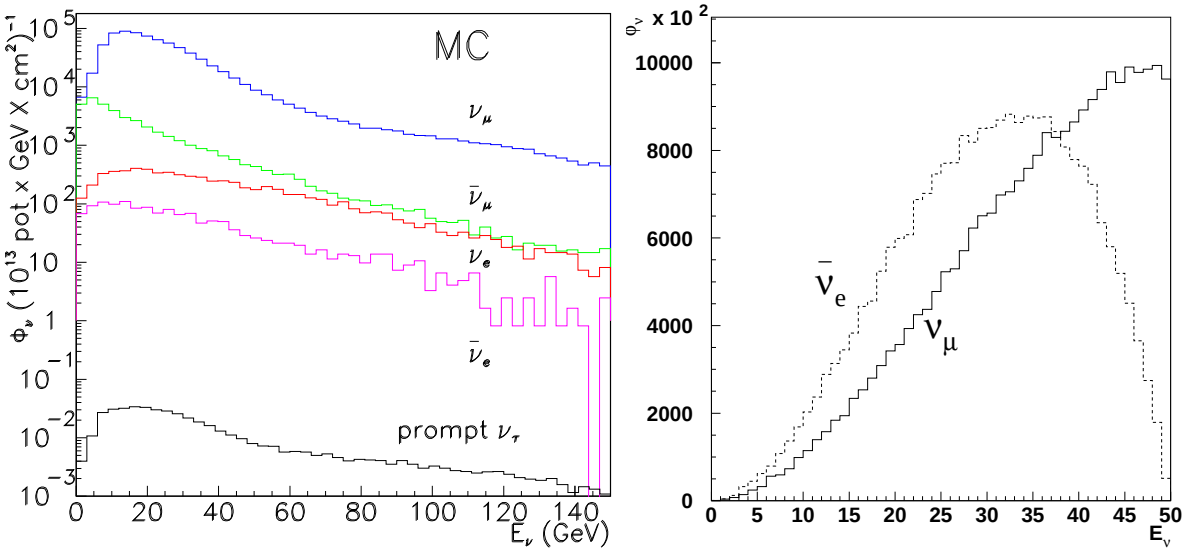

Fig. 28: *Comparison of the neutrino spectra for a traditional neutrino beam (WANF at CERN), on the left, and a neutrino factory, on the right. The vertical axes are not to scale.*

For different values of the muon energy, the total neutrino flux at the far location will increase as E^2, because of the shrinking of the angular opening of the neutrino beam due to the Lorentz boost $\gamma^{-2} = (m_\mu/E_\mu)^2$. Moreover, since the deep-inelastic scattering cross section rises approximately linearly with neutrino energy, and the spectral shape only depends on $x = E_\nu/E_\mu$, the total number of events observed in a far detector will grow as E_μ^3. Geometrical solid-angle considerations suggest that, always assuming negligible detector size with respect to the baseline, the flux goes like $1/L^2$. Neglecting matter effects, the oscillation probabilities will depend on L/E_ν, so keeping the same oscillation probability and maximising the number of events would ideally require very long baselines and large muon energies. The limitation to this logic, apart from the physical size of the Earth's diameter, comes from the matter effect, that depresses oscillation probabilities for baselines above 4000 km. This topic will be discussed later in more quantitative terms.

μ charge	Ev.Class	Events
μ^-	ν_μ CC	134362
	ν_μ NC	39952
	$\bar{\nu}_e$ CC	52000
	$\bar{\nu}_e$ NC	18054
μ^+	$\bar{\nu}_\mu$ CC	60010
	$\bar{\nu}_\mu$ NC	21067
	ν_e CC	117369
	ν_e NC	34558

Table 9: *The number of events detected by a 10 kt detector for 10^{21} muons in the ring, assuming a baseline of 3000 km and a muon energy of 30 GeV.*

The total number of events for the non-oscillation case, observed per kiloton of detector mass at a distance of 3000 km with a 30 GeV muon beam, is shown in Table 9. Rates for different values of the

muon energy, baseline, number of muons or detector mass can be obtained from the relation

$$N_{Events}(E_\mu, L, N^\mu, M) = N^{table}_{Events}(\frac{E_\mu}{30GeV})^3(\frac{3000km}{L})^2(\frac{N^\mu}{10^{21}})(\frac{M}{10kton}).$$

One of the main characteristics of the neutrino factory is that it delivers a well-defined beam free of intrinsic background. For instance, negative muons circulating in the ring will produce ν_μ, that in turn will again produce negative muons in the interaction with the detector. Positive muons are in principle only produced from the oscillation of the $\bar{\nu}_e$ component of the beam. The reversed argument applies for positive muons in the ring. In general, we talk about Right-Sign Muons (RSM) coming from the beam, and Wrong-Sign Muons (WSM) coming from the oscillation. In practice, the picture is not so simple, since other processes can make contributions to the WSM sample. They are quite rare, but they can become important when we want to be sensitive to small oscillation probabilities, for instance if the value of θ_{13} is very small.

The main background contributions to wrong-sign muons, in the case of a beam produced by μ^- decays, are:

- $\bar{\nu}_\mu$ CC events where the right-sign muon is lost, and a wrong-sign muon is produced by the decay of a π, K or D. The most energetic muons are produced by D decays.
- ν_e CC events where the primary electron is not identified. In this case, D decays are not a major problem since, due to the neutrino helicity, they would produce right-sign muons. However, wrong-sing muons can come from pion and kaon decay.
- $\bar{\nu}_\mu$ and ν_e NC events where charm production is suppressed with respect to charged currents, and therefore also the main contributions are given by pion and kaon decays.

These backgrounds can be rejected using the facts that muons coming directly from neutrino interactions are higher in energy and more separated from the hadronic jets than those produced in secondary decays. A cut on momentum and on the transverse momentum Q_t of the muon with respect to the jet can reduce the background to wrong-sign muons by several orders of magnitude.

5.2 Flux Control and Resulting Constraints on the Decay Ring Design

One of the most significant qualities of the Neutrino Factory, and more generally of a system where one stores a beam of decaying particles (such as the beta beam) is the potential for excellent neutrino flux control. The main parameters that govern the systematic uncertainties on the neutrino fluxes are as follows.

- The monitoring of the total number of muons circulating in the ring,
- Theoretical knowledge of the neutrino fluxes from muon decay, including higher-order radiative effects,
- Knowledge of the muon beam polarisation,
- Knowledge of the muon beam energy and energy spread,
- The muon beam angle and angular divergence.

Beam shape parameters are crucial for the measurement of oscillation length, while the absolute normalisation is essential for the measurement of the mixing angle. The relative normalisation of the two muon charges plays a crucial role in the measurement of CP asymmetries.

5.2.1 *Absolute flux monitoring*

Monitoring the total number of muons in the ring can be done in a number of ways. The total beam current can be estimated using a Beam Current Transformer (BCT), the total number of decay electrons can be estimated using an electron spectrometer, the product of the flux and cross section can be inferred from a near-by detector and, finally, the absolute normalisation can be obtained from semi-leptonic neutrino interactions in a nearby detector.

The operation of a BCT in the decay ring could provide fast-response monitoring of the muons in the ring. There are, however, a few potential difficulties that could limit the precision of such a device, which could normally reach the 10^{-3} level. The first one is the presence of decay electrons in the ring, along with the muons. Since all muons decay, the number of accompanying electrons could potentially be much larger than the remaining muons after a few muon lifetimes. A study of such decay electrons has been made [144], with the conclusion that for 50 GeV muon momentum, the decay electrons are lost in the beam elements (or the collimators placed to protect them) after less than half a turn, either because they are momentum-mismatched or because they lose energy in the arcs by synchrotron radiation. Consequently their number should be always less than about 2×10^{-3} of the remaining muons. In addition, most of the losses arise in the straight sections or in the early part of the arcs, so that a BCT situated just at the beginning of a straight section would see an even smaller fraction of them. Another worry could be the existence of a moving electron cloud created by beam-induced multipacting, or by ionization of the residual gas or of the chamber walls. This has been studied by in [145], with the conclusion that the electron cloud will be several orders of magnitude less than the muon flux itself. In the absence of a significant parasitic current, it can be concluded that the BCT readings should be precise to the level of a few 10^{-3}, or better. This seems the most practical way to compare the flux induced from μ^+ and μ^- decays.

The decay electrons will be used to measure the polarisation of the beam with a spectrometer as described below, and in Fig. 29. The same device could in principle be used to monitor the number of electron decays in an absolute way, especially if one selects the momentum bite where the electron spectrum is insensitive to the muon polarisation. Certainly this will be a useful tool, as a cross-check or for monitoring, but a very detailed study of the dependence of the acceptance of this device on the beam parameters must be performed before a conclusion can be reached.

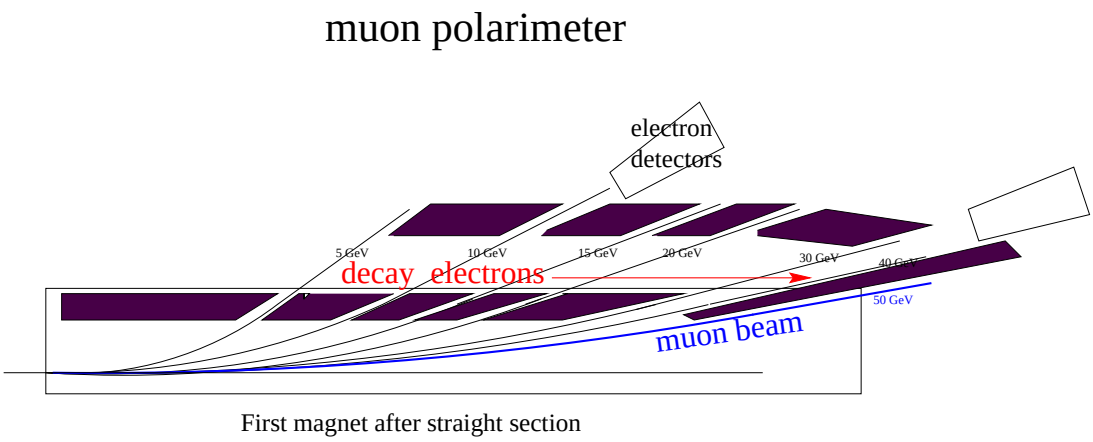

Fig. 29: *A possible muon polarimeter design. The momenta of the decay electrons accumulated in a short straight section are analysed in a bending magnet in the muon decay ring. Slits in the shielding define the acceptance of a number of momentum bins.*

Knowledge of the flux does not provide knowledge of the cross sections folded with the detector acceptance. This task is traditionally delegated to a near detector. The high flux should make things

very easy. The event numbers appearing in Table 9 would be obtained with a detector of 10 kg situated on the neutrino beam axis at a distance of 3 km from the middle of the decay tunnel. Given the high importance of precision measurements in the Neutrino Factory, it is likely that a near detector will be an important tool for beam normalisation. Unlike the situation with conventional pion decay beams, the near detector will in fact be able to measure absolute cross sections for a large number of exclusive and inclusive processes.

It is worthwhile mentioning, finally, the possibility offered by the measurement of purely leptonic interaction processes, which have been discussed in [35]. Of practical interest for normalisation is the measurement of $\nu_\mu + e^- \to \mu^- \nu_e$, which appears as a low-angle forward-going muon with no recoil. Using the standard electroweak theory, this purely leptonic charged-current process can be calculated with high precision, and could be measured with a dedicated detector aimed at measuring also the $\nu_e + e^- \to e^- \nu_e$ and $\bar{\nu_e} + e^- \to e^- \bar{\nu_e}$ processes. The weakness of this method is that it only applies to the μ^- decay beam, but it could be seen as an overall absolute normalisation process for the muon flux.

To conclude, there are many tools to monitor and control the absolute flux normalisation in a neutrino factory, so that the near detectors should be able to provide very accurate measurements of inclusive and exclusive cross sections, within the detector acceptance. A flux normalisation at the level of a few 10^{-3} seems an achievable goal. The relative normalisation of the μ^- and μ^+ decay beams should be known with similar precision.

5.2.2 Theoretical knowledge of the neutrino fluxes from muon decay

The expressions given above for the neutrino flux in muon decay, (63), do not include QED radiative corrections, which have been calculated in [146]. The dominant source of corrections is, as can be expected, related to photon emission from the decay electron. For the electron energy distribution, the corrections are of the order of 1% due to terms proportionanl to $\frac{\alpha}{\pi} \ln(\frac{m_\mu}{m_e})$. It turns out that the neutrino spectrum is insensitive to the electron mass, i.e., the integration over the system of electron and photons cancels mass singularities. It can be seen that, in the forward direction, an overall decrease of the neutrino flux of about 4×10^{-3} is observed, with a larger decrease near the end point. The global decrease can be understood by the overall softening and angular widening of the neutrino decay spectrum due to photon emission.

Since the overall size of the corrections is small, one can certainly trust the calculated spectrum to a precision much better than 10^{-3}.

5.2.3 Muon polarisation

Muons are naturally polarised in pion decay. In the $\pi^+ \to \mu^+ \nu_\mu$ rest frame, both the ν_μ and μ^+ have negative helicity. In the laboratory frame, the resulting average helicity of the muon, or longitudinal polarisation, is reduced from -100% for a pion at rest to $< h >= -18\%$ for pions above 200-300 MeV momentum [147]. For a pion of given momentum, muon polarisation is correlated with muon momentum. It has been argued in [148] that monochromatisation of the pions followed by i) a drift space to separate muons of different momenta, and ii) collection in successive RF buckets, should allow separation in different bunches of muons of different polarisations. This does not change the *average* polarisation, but creates bunches of different polarisation (up to 50%), that can be of use for physics, as long as the times of neutrino interactions are recorded with a precision of a few nanoseconds.

The muon spin precesses in electric and magnetic fields that are present during cooling and acceleration, but the muon spin tune ν – the number of additional spin precessions happening when the muon makes a complete turn – is very low:

$$\nu = a_\mu \gamma = \frac{g_\mu - 2}{2} \frac{\mathrm{E_{beam}}}{m_\mu} = \frac{\mathrm{E_{beam}(GeV)}}{90.6223(6)} \ .$$

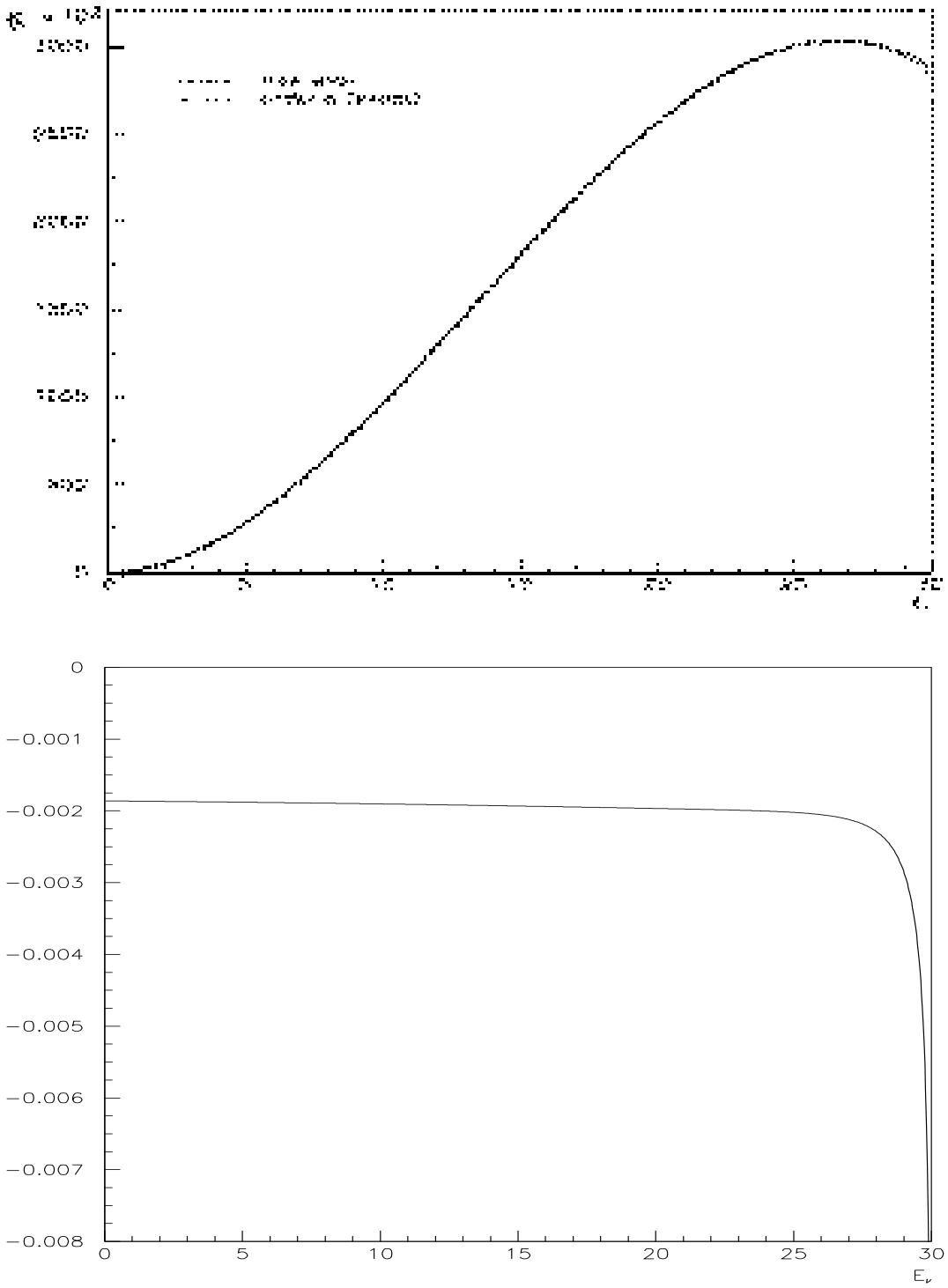

Fig. 30: *Radiative corrections to the muon neutrino flux in μ^- decay. Top panel: the resulting energy distribution at zero angle, bottom panel: the relative change due to the $\mathcal{O}(\alpha)$ correction. The overall reduction of flux is due to the additional energy taken away by photons, which slightly widens the angular distribution of the neutrinos. In order to avoid infinities at the end point, the quantity plotted is $\frac{\Phi(\mathcal{O}(\alpha))-\Phi_0}{\Phi(\mathcal{O}(\alpha))+\Phi_0}$.*

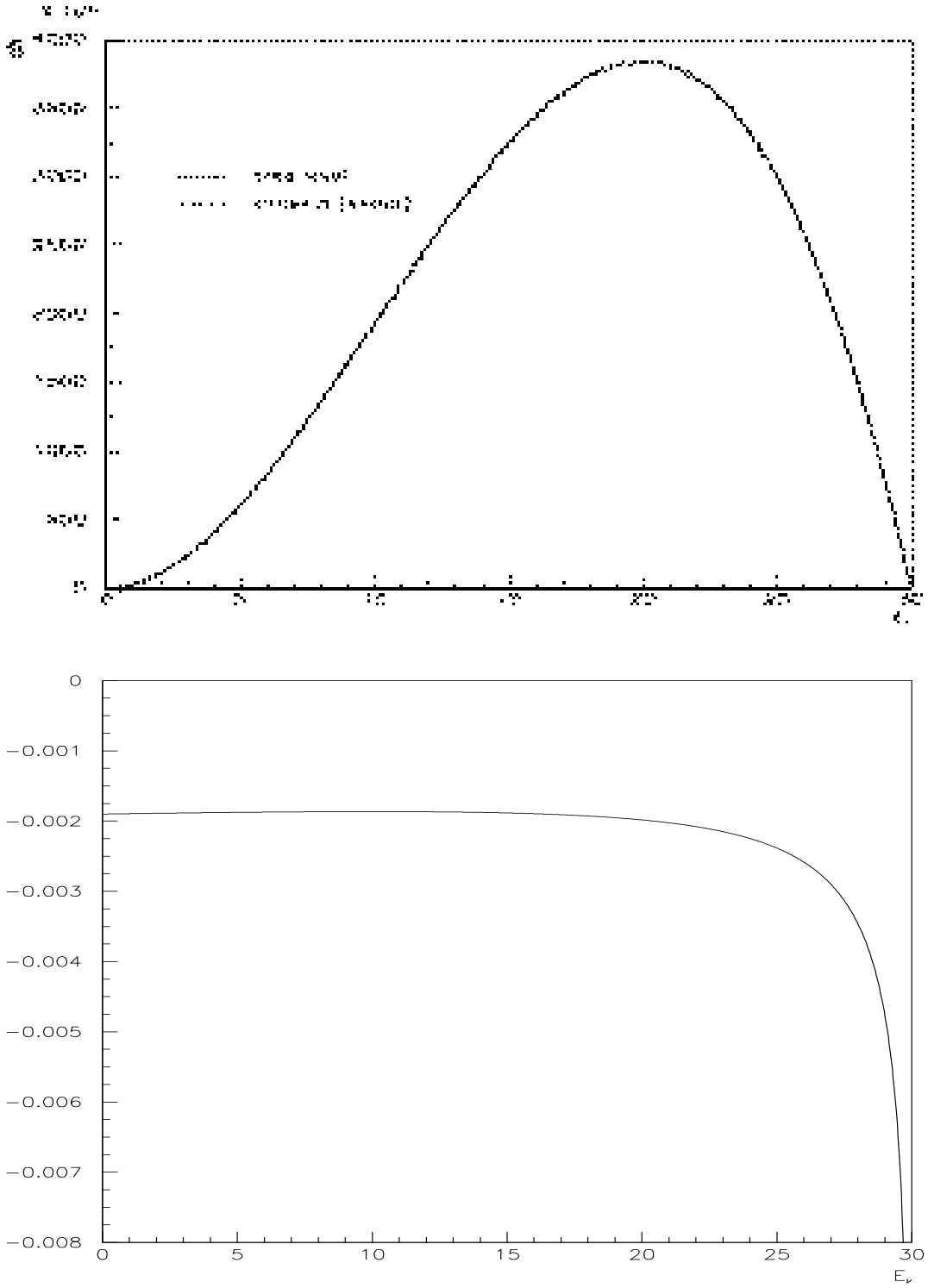

Fig. 31: *Radiative corrections to the electron anti-neutrino flux in μ^- decay. Top panel: the resulting energy distribution at zero angle, bottom panel: the relative change due to the $\mathcal{O}(\alpha)$ correction. The overall reduction of flux is due to the additional energy taken away by photons, which slightly widens the angular distribution of the neutrinos.In order to avoid infinities at the end point, the quantity plotted is $\frac{\Phi(\mathcal{O}(\alpha))-\Phi_0}{\Phi(\mathcal{O}(\alpha))+\Phi_0}$.*

It has been evaluated [147] that 80 to 90% of the original polarisation will survive all muon handling up to the injection into the storage ring. Its orientation will depend on the number of turns that the muons encounter along the accelerator chain, and can be arranged to be longitudinal by an appropriate choice of geometry and of the energies in the recirculating linacs [135]. As we will see, this is not necessarily important.

What will happen to the muon polarisation in the decay ring depends in the first instance on whether its geometry is a ring (race track or triangle) in which the muons undergo one rotation per turn, or a bow-tie, in which the muon undergoes zero net rotation at each turn.

In the case of a ring, the polarisation will precess. The orientation of the polarisation vector will be rotated with respect to the muon direction by an angle which increases each turn by $2\pi\nu$. Unless the energy is chosen very carefully, it will not be aligned, and reduced on average by a factor 2. At a muon energy of precisely $E = 45.311$ GeV, the spin tune is 0.5 and the polarisation flips during each turn. This would allow the most powerful use of the polarisation for physics purposes, but absolutely requires that the orientation is correctly chosen at injection, a condition which is otherwise unnecessary in a ring geometry. If no special measure is taken, however, depolarisation will occur, since particles of different energies will have their spins precess with different spin-tunes.

The muon polarisation can be monitored by momentum analysis of the decay electrons, as discussed in [149], in a polarimeter that could look like that sketched in Fig. 29. One can expect that this measurement will be difficult: the relative normalisation of electron rates in the different energy bins will depend on various muon beam parameters such as its exact angle and divergence, and on a precise modelling of the beam-line geometry. In a ring geometry, the device will be exposed to a succession of negative and positive helicity muon bunches, so it will have to perform relative measurements. These should be sensitive to small effects, with a *relative* precision of a few percent. In a bow-tie geometry, however, there will be no spin precession, and one will be left to measure the polarisation based on the measured electron spectrum. A few % absolute accuracy seems in this case already very challenging.

The spin precession in a storage ring provides a means of high precision (10^{-6} or better) for energy calibration [150]. As shown in [149], the measurement of the depolarisation can be used to measure the energy spread with high precision. In this case, the combined effect of precession and depolarisation ensure that the muon polarisation integrated over a fill averages out to 0 with an excellent precision: simulations show that any residual polarisation is less than 4×10^{-4}.

Depolarisation can be avoided, if the storage ring is equipped with an RF system that ensures that the muons undergo synchrotron oscillations [135]. By doing this, one loses the possibility to measure the energy spread from the depolarisation, but one can maintain the muon polarisation. The average is still essentially zero, but by recording the exact time of neutrino events, one can infer their bunch number and turn number, and deduce the polarisation of the decay muons. In a ring geometry either mode of operation is left open, if one can run with the required RF system on or off.

In a case of a bow-tie, the muons will not depolarise: spin precession is zero no matter what the muon energy is. This configuration is not as convenient as the ring for several reasons.

- It will be impossible to measure the spin precession, so that the energy and energy spread of the muon beam will not be calibrated.
- The polarisation will not average to zero. This, combined with the fact that the polarisation measurement will be more challenging, means that the flux determination will be affected by a sizeable uncertainty, due to the beam polarisation error.
- It will be difficult to change the sign of the muon beam polarisation.
- Unless the geometry is very carefully chosen, the beam polarisation will be different for the two long straight sections.

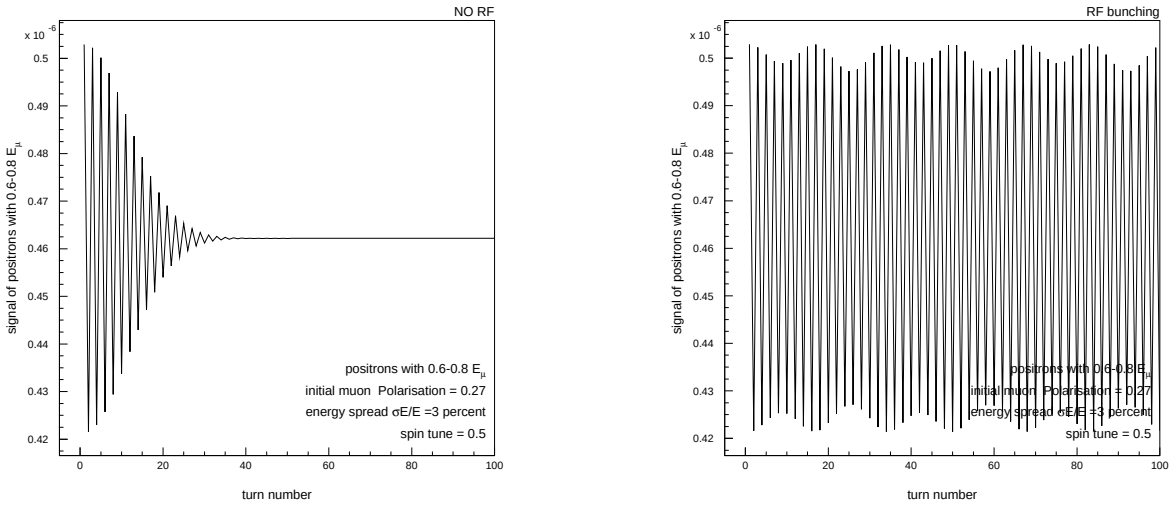

Fig. 32: *Oscillation with turn number in a fill of the number of electrons in the energy range 0.6-0.8 E_μ, normalised to the total number of muon decays during the given turn. The oscillation amplitude is a measure of the beam polarisation, its frequency a measure of the beam energy, and, if there is no RF bunching, its decrease with time is a measure of energy spread. The muon lifetime corresponds here to 300 turns. The beam energy is $E_\mu = 45.311$ GeV and the energy spread is 3×10^{-2}. On the left, there is no bunching RF in the muon storage ring, on the right there is RF bunching with $Q_s = 0.03$.*

For these reasons, and despite the fact that in principle the useful beam polarisation is higher in the bow-tie geometry, *the ring geometry is preferred* from the point of view of beam control.

5.2.4 Neutrino fluxes and muon polarisation

Neutrino spectra with different beam polarisations are given by the following equations valid for μ^+ decays in the muon centre-of-mass (reverse polarisations for μ^-):
– for the ν_μ:

$$\frac{d^2N}{dx\,d\cos\theta} = Nx^2[(3-2x) - \mathcal{P}(1-2x)\cos\theta]$$

– for the ν_e:

$$\frac{d^2N}{dx\,d\cos\theta} = 6Nx^2[(1-x) - \mathcal{P}(1-x)\cos\theta]$$

where θ is the decay angle in the muon centre-of-mass frame, $\mathcal{P}$ is the muon longitudinal polarisation, and $x = 2E_\nu/m_\mu$.

In a long-baseline experiment, one is at extremely small angles, so that $\cos\theta = 1$. In this case, the ν_e component of the beam is completely extinct for $\mathcal{P} = +1$. This is due to spin conservation in the decay: a right-handed muon cannot decay at zero angle into a left-handed ν_e.

Event numbers can readily be obtained by multiplying by the cross section. They are shown in Fig. 33 for a 10 m radius detector 20 m long situated 730 km away. Since the neutrino and anti-neutrino cross sections are in the ratio 1/0.45, negative muons provide enrichment in ν_μ and positive ones in ν_e.

It is clear from Fig. 33 that the combination of muon sign and polarisation allows large variations in the composition of the beam, in a controlled way. Since detector studies show that the muon sign can easily be determined in a charged-current (CC) (anti)neutrino event, but that the electron sign is much

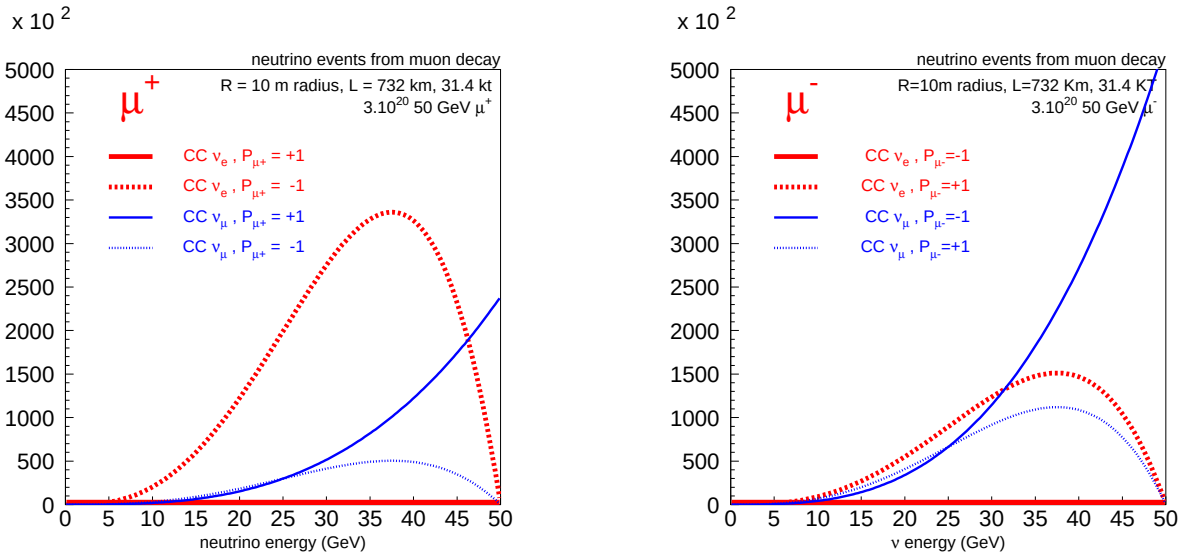

Fig. 33: *Event numbers for a detector of density 5 with 10 m radius that is 20 m long, situated 732 km away from the muon storage ring, for $\mu^+ \to e^+\nu_e\bar{\nu_\mu}$ (left) and $\mu^- \to e^-\bar{\nu}_e\nu_\mu$ (right) beams of 50 GeV. Full lines show the spectra for the 'natural' helicity $\mathcal{P} = +1$ for μ^+, and dashed ones for the opposite case. The CC ν_e for μ^+ with $\mathcal{P} = +1$ and CC ν_e for μ^- with $\mathcal{P} = -1$ are not visible, because the fluxes are almost exactly zero. The vertical axis gives event numbers per bin of 250 MeV. This plot assumes no muon beam angular divergence and no beam energy spread.*

more difficult, we have tried to use the variation of electron neutrino flux with muon polarisation to infer a signal of $\nu_\mu \to \nu_e$ oscillations to be compared (for a T-violation test) with the $\nu_e \to \nu_\mu$ oscillation measured with the wrong-sign muons. Unfortunately, even for 40% beam polarisation, the improvement in the sensitivity to CP/T violation is no more than the equivalent of a factor of 1.5 to 2 in statistics. Certainly, it appears that polarisation is more useful as a tool to measure the beam properties than as a physics tool. Nevertheless, these statements might be parameter-dependent, and should be revisited once the oscillation parameters are better known.

5.2.5 Effect of beam divergence

The opening angle of the neutrino beam is typically $1/\gamma$, where $\gamma = E_\mu/m_\mu$. As soon as the beam divergence is comparable with this natural opening angle, a large fraction of the flux will be lost. This is shown for 45.311 GeV muons in Fig. 34. It is clear that beam divergence results in a loss of events, and in a sizeable distortion of the spectra and of their muon polarisation dependence. A beam divergence not larger than $\sigma\theta_x = \sigma\theta_y = 0.2m_\mu/E_\mu$ seems to be desirable, if one want to avoid a large sensitivity of physics results upon the experimental determination of the muon beam parameters.

This effect has been studied more precisely in [151], where event numbers are calculated for various polarisations and divergences. The impact of the muon beam divergence on the neutrino event rate can be seen in Fig. 35. The first conclusion one can draw from these plots is that, for a given number of muons, the highest flux is obtained for small muon beam divergence. In order to keep the event rate loss due to the muon beam divergence below 5%, the divergence should be close to 0.1 / γ_μ.

From the curves in Fig. 35, one can determine the relative error of the predicted event rate, given the uncertainty in the knowledge of the beam divergence itself. For example, if the beam divergence is 0.1 / γ and is known with a relative precision of 10%, the $\overline{\nu}_\mu$ and ν_e event rates can both be predicted

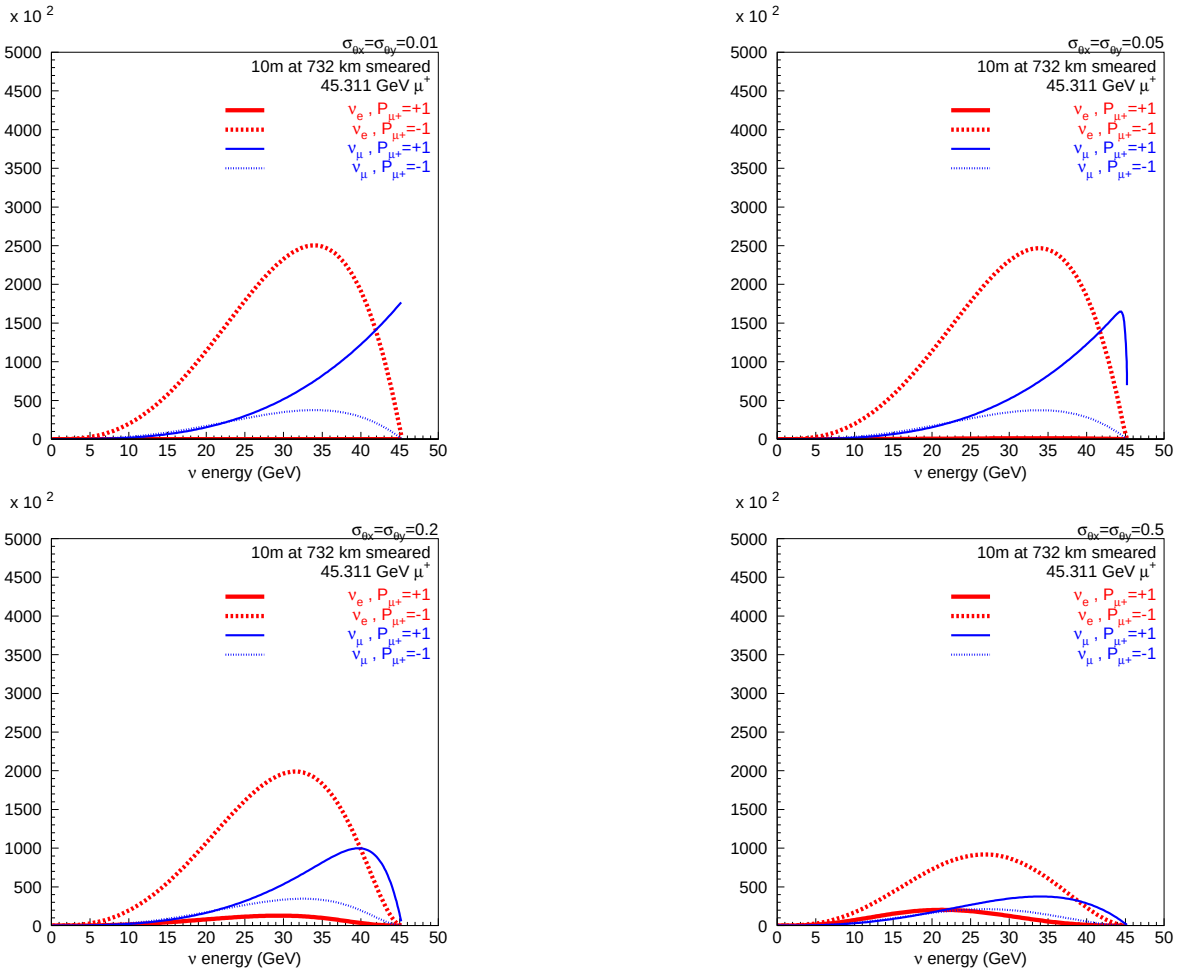

Fig. 34: *Neutrino event spectra for different beam divergences; Upper left: $\sigma\theta_x = \sigma\theta_y = 0.01\ m_\mu/E_\mu$; upper right: $\sigma\theta_x = \sigma\theta_y = 0.05\ m_\mu/E_\mu$; lower left: $\sigma\theta_x = \sigma\theta_y = 0.2\ m_\mu/E_\mu$; lower right: $\sigma\theta_x = \sigma\theta_y = 0.5\ m_\mu/E_\mu$. It is clear that beam divergence results in a loss of events, and in a sizeable distortion of the spectra and of their muon polarisation dependence.*

with an accuracy of about 0.75%. For a divergence of 0.2 / γ, the uncertainty on the flux would be 2.5 %. As we will see, however, the knowledge of the beam divergence is unlikely to be a constant relative fraction.

One can turn the argument around, and request that the beam divergence be 0.1 / γ and known to a relative precision of 1.5%, so that the corresponding uncertainty on flux is only 10^{-3}. It is clear that in this case the muon beam divergence will need to be measured. For a beam of 50 GeV, the beam divergence is 200 micro-radians and the requirement is that it should be known to 3 micro-radians.

As a measurement device, one could imagine a gas Čerenkov detector focusing the Čerenkov radiation in such a way as to make an image of the muon beam direction, as sketched in Fig. 37. This has been studied in [152], with the conclusion that for 200 micro-radians divergence, a precision of a few % can be achieved. The additional multiple scattering introduced by the device leads to a growth of emittance during the muon fill, by a few tens of micro-radians, which is small and will be measured. Since the resolution is dominated by optical imperfections, diffraction effects and heating effects in the gas of the Čerenkov detector, they act as an additional experimental smearing $\sigma_{\rm exp}$ added in quadrature

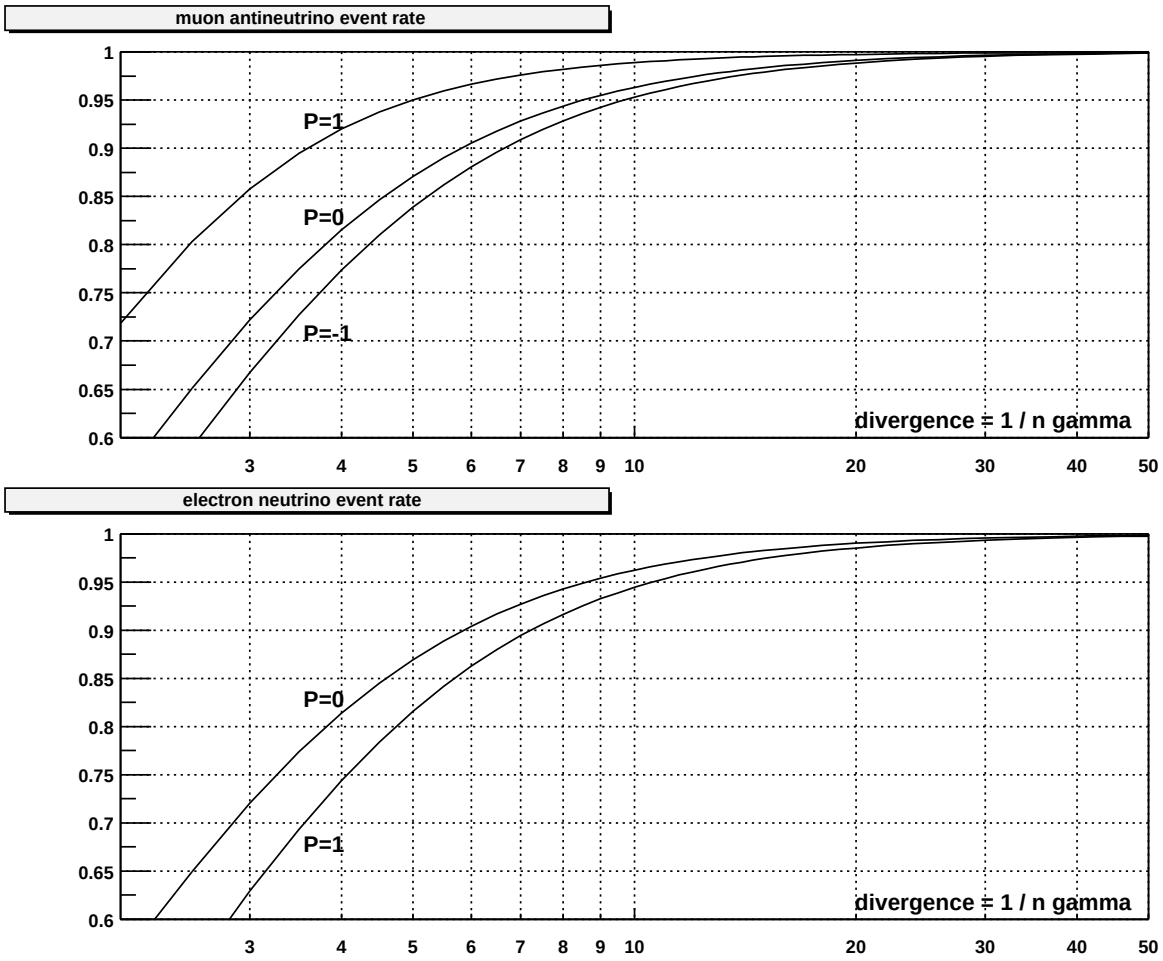

Fig. 35: *The relative event rates for muon anti-neutrinos (top) and electron neutrinos (bottom), for various polarisation values as a function of the beam divergence, parametrised as* $1/n\gamma$.

to the true beam divergence $\sigma_{\rm beam}$. In the scheme of Fig. 37, the largest effect is optical diffraction, which amounts to 30 micro-radians. It is easy to show that the correction for experimental resolution is

$$\frac{\Delta\sigma_{\rm beam}}{\sigma_{\rm beam}} = \frac{\Delta\sigma_{\rm exp}}{\sigma_{\rm exp}} \left(\frac{\sigma_{\rm exp}}{\sigma_{\rm beam}}\right)^2 . \tag{64}$$

This makes the beam divergence progressively harder to measure as it becomes smaller. Assuming that the experimental error is 30 micro-radians and is known with a precision of 30% of its value, the above gives a flux uncertainty of 5×10^{-4}, more or less independent of the beam divergence in the range of 0.05 to 0.2.

In conclusion, the requirement that the beam divergence be no greater than $0.1/\gamma$ ensures that the corrections and uncertainties to the neutrino fluxes remain small (below 1%), even if one should rely on the accelerator properties themselves. In order to achieve a higher precision a direct measurement of the beam divergence will be necessary – and is probably feasible. If relaxing this condition would allow a larger muon flux, a divergence measurement device becomes mandatory, and would ensure that the uncertainty on the neutrino flux remains well below 10^{-3}.

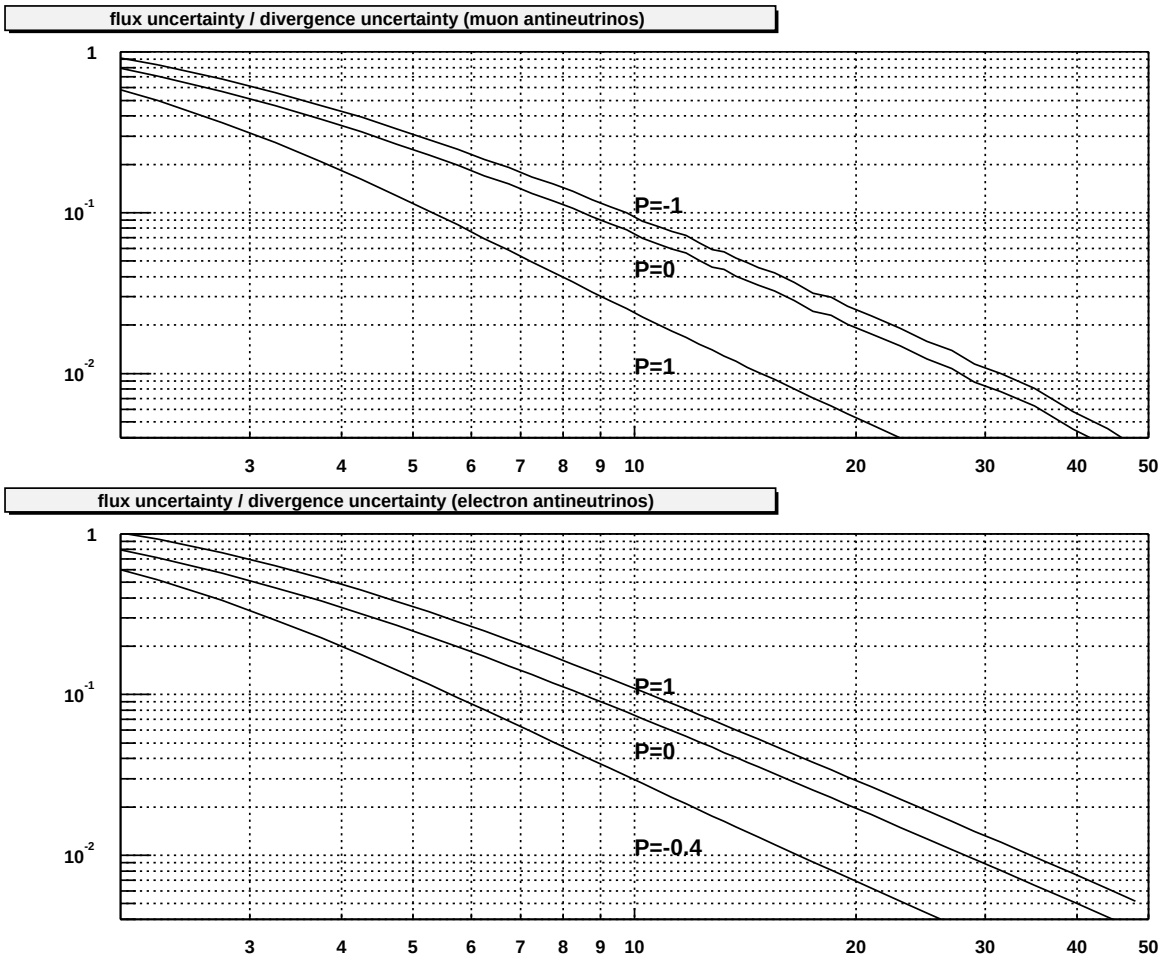

Fig. 36: *The ratio of the uncertainty in the event rate over the uncertainty in the muon beam divergence as a function of the beam divergence, parametrised as* $1/n\gamma$*. The top (bottom) plot corresponds to muon anti-neutrinos (electron neutrinos).*

5.2.6 Summary of uncertainties in the neutrino flux

A first look has been given to the sources of systematic uncertainties in the neutrino fluxes and their possible cures.

- The monitoring of the total number of muons circulating in the ring can be inferred from a Beam Current Transformer with a precision of the order of 10^{-3} or better. The decay electrons vanish quickly and are not a problem.
- The theoretical knowledge of the neutrino fluxes from muon decay is not an issue. Radiative effects have been calculated: they amount to around 4×10^{-3}, with an error that is much smaller.
- The muon beam polarisation determines the flux directly, both in shape and magnitude. Its seems delicate to determine its value with a precision much better than a few %. In a ring geometry, however, polarisation precesses and averages out with high precision (a few $\times 10^{-4}$). This is a strong argument in favour of a ring geometry against a bow-tie geometry.
- The event rate varies like the muon beam energy to the third power, but the muon beam energy can be inferred very precisely from the muon spin precession. A polarimeter idea has been outlined,

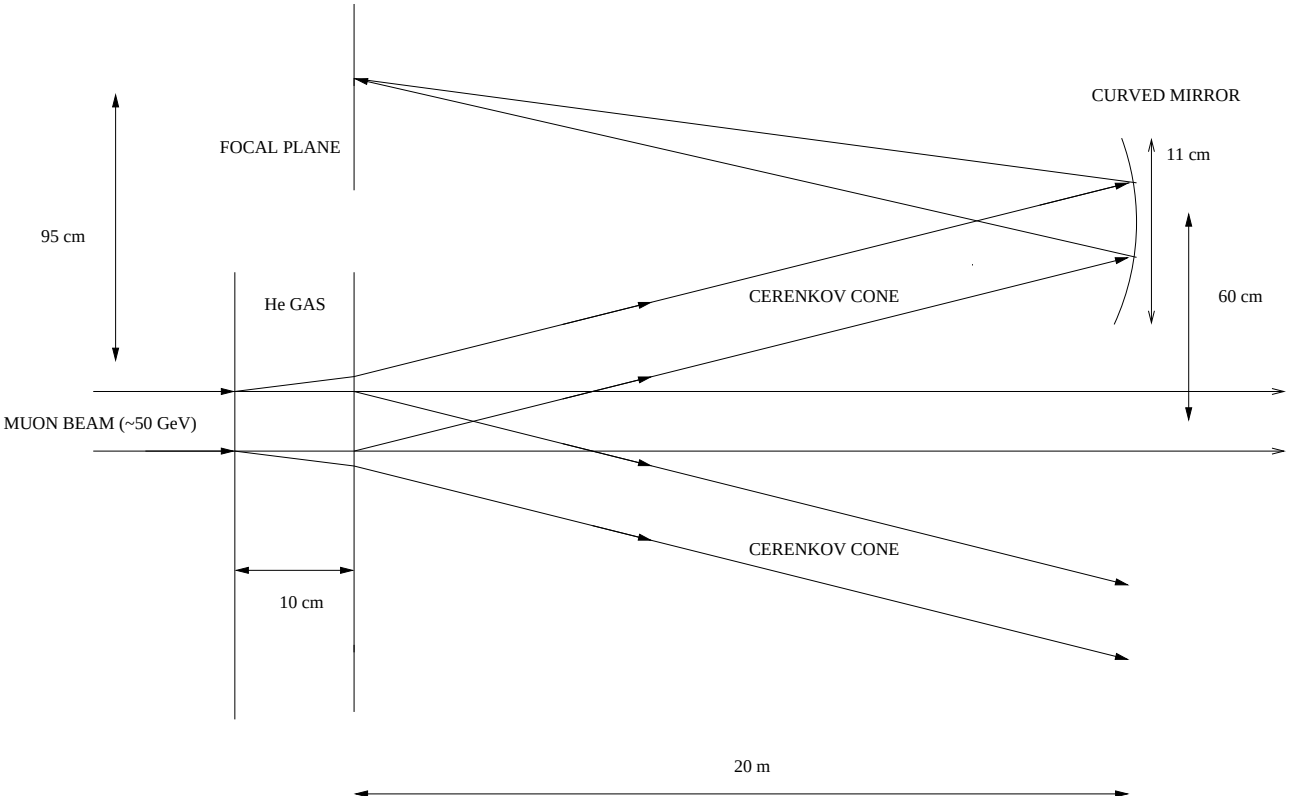

Fig. 37: *Schematic of a muon beam divergence measurement device. A low-pressure He gas volume is contained by windows (one of which must be transparent) within a straight section of the the muon decay ring. The Čerenkov light is collected by a parallel to point optics in the direction of interest, so as to provide an image of the angular distribution of particles in the focal plane.*

and the measurement should cause no difficulty. Beam polarisation can be preserved if an RF system is installed in the decay ring. The energy spread can be derived from the depolarisation pattern, in special runs with no RF if necessary.

- The muon beam angle and angular divergence have an important effect on the neutrino flux. For a given number of muons, the smaller the beam divergence, the higher the flux. Thus the beam divergence in the straight section of the muon decay ring should be made as small as possible, but should not constitute a limit on the number of stored muons.

- Measurement devices for the beam divergence will be necessary, but they can probably be designed and built to ensure a flux uncertainty below 10^{-3}.

In addition, the near detector stations should allow measurements of cross sections with high precision. The inverse muon decay reaction $\nu_\mu + e^- \rightarrow \mu^- \nu_e$ offers the possibility of an absolute normalisation of the flux.

We conclude that, provided the necessary instrumentation is foreseen, the Neutrino Factory flux should be known with a precision of the order of 10^{-3}.

5.3 Detector issues

5.3.1 Magnetic calorimetric iron detectors

The measurement of $\nu_e \rightarrow \nu_\mu$ oscillations through the appearance of wrong-sign muons calls for massive detectors weighing $\mathcal{O}(50)$ Kt, with the capability of μ identification and the measurement of their charge. A large mass magnetized iron calorimeter with active elements based on RPCs or scintillator bars can fulfill both tasks. The particle electric charge can be determined by an external magnetic field $\overline{B}$. A charged particle traversing N steel plates, each of thickness x, will receive a p_t kick of $0.03Nx(cm)B(T)$ GeV. Multiple scattering will introduce a random p_t of $0.014N\sqrt{x/X_0}$ GeV, with $X_0 = 1.76$ cm for the radiation length of steel. After N steel absorbers, the significance of the charge determination will be

$$2\frac{0.003B(T)x(cm)}{0.014\sqrt{x/X_0}}\sqrt{N}.$$

For a typical field $B \sim 1\ T$, a 3 or $4-\sigma$ measurement can easily be obtained for muons.

Based on the MINOS experience [21], proposals have been put forward to use the design of the proposed atmospheric neutrino detector MONOLITH [32], or a novel design of iron-scintillator detector (LMD) [153] as a far detector in a neutrino-factory beam. In the following, we summarize the known experimental results about active read-out elements, and then outline the main aspects of the designs of MONOLITH and LMD.

5.3.2 Summary of the properties of active elements in massive iron calorimetric detectors

Candidate active elements for massive iron calorimetric detectors for ν studies are usually Iarocci proportional tubes, RPCs, or scintillator bars, and each solution has its avantages and disadvantages. Proportional tubes are well studied, and with strip read-out will have good spatial resolution, but do not perform well for calorimetry. RPCs are inexpensive and easy to manufacture, and have good timing properties, but their usual gas is flammable and their operation for long periods of time is still debatable. Scintillators have both good timing properties and very good calorimetric properties. On economic grounds, the use of good-quality scintillator with long attenuation length can be precluded. A relatively cheap solution, pionereed by the MINOS Collaboration, is to use a polystyrene-based scintillator doped with 1% PPO and 0.03% POPOP, extruded into bars of the required dimensions [154]. The bar can be coated with a layer of polystyrene mixed with titanium oxide, which is co-extruded at the same time as the scintillator and provides light-tightness and diffusion of the light back into the scintillator. Because of the poor attenuation length of the scintillator, the light produced in the bar is channelled to the photo-detector via green wavelength-shifting (WLS) fibres of small diameter ~ 1 m. This solution allows the cost of the read-out to be reduced by using multipixel PMTs with pixel dimensions comparable to the fibre size.

Other solutions include the use of liquid scintillator in a vessel with wavelength-shifting fibre read-out, where optical separators can provide a granularity of a few centimeters over a large volume [155]. Individual cells can be formed from extruded rigid PVC, which is made reflective by a layer of titanium dioxide. A WLS fibre along the side of each cell can convert any absorbed blue scintillator light to green, a fraction of which is then trapped inside the fibre and transported to external multipixel PMTs at the very end of the detector. With the extruded scintillator or liquid scintillator option, one can obtain good energy resolutions (both electromagnetic and hadronic), good spatial resolution determined by the cell width d: $\sigma_x \simeq d/\sqrt{12}$, and the possibility of fast timing. Reasonable light yields have been measured. As an example, with extruded scintillator and BCF91A WLS fibers, 8 m long, up to 2 p.e./MIP crossing at the far end have been measured.

5.3.3 The Monolith design

The Monolith concept is based on a massive tracking calorimeter with a modular structure, shown in Fig. 38, where the magnetic field configuration is also shown: iron slabs are magnetized at $B \simeq 1.3$ T.

Each module would be a stack of 120 8 cm thick iron absorber plates (14.5×15 m^2), interleaved with sensitive elements in a 2 cm gap. The detector height is about 13 m, and a mass of 34 kt can be obtained with two such modules. External scintillator counters are foreseen, as a veto, to reduce the background from cosmic-ray muons. As active elements, glass spark counters (RPCs with glass electrodes) were chosen. They provide $x - y$ coordinates with a 3 cm pitch and a time resolution of about 1 ns. The usual bakelite electrodes are substituted by commercially available high-resistivity float-glass electrodes, suitable for operation in streamer mode in a low counting environment. They have stable volume resistivity over long periods and avoid, due to better planarity and homogeneity, surface treatment with linseed oil. The high-voltage supply is applied to the electrodes by means of water-based graphite. Long-term stability of the chambers over several months show a remarkable stability of the efficiency and the time resolution. Test-beam results on a 8 t prototype have shown an hadronic energy resolution $\sigma_E/E \sim 68\%/\sqrt{E} + 2\%$, sufficient for a full reconstruction of energy and direction of interacting neutrinos, a time resolution ~ 1.7 ns and a good tracking capability [157].

On average 95% of the muons induced by atmospheric neutrino interactions inside MONOLITH have their charge correctly assigned, without specific selections on the track quality. This makes it possible to test the neutrino mass hierarchy through the study of earth-induced matter effects with atmospheric neutrinos [158]. In the context of a neutrino factory project, charge discrimination could be significantly improved by selecting only unambigous muon candidates [159]. The efficiency to discover wrong-sign muons was estimated to be around 16%, for a background rejection of order 10^{-6}. The hadron shower direction reconstruction has also been studied in detail.
The sensitivity region in the (Δm^2_{23},$sin2(2\theta_{13})$) parameter space is about two order of magnitude better than the current Chooz limit in the whole Super-Kamiokande 90% $C.L.$ allowed region of Δm^2_{23}, if the baseline is 732 km; better at 3500 km.
This result is achieved also in the simplest version of the detector configuration and of the analysis, i.e. horizontal-8 cm planes and a simple muon momentum cut. Among the possible improvements, the best seems to be the vertical-8 cm planes option, that provides a very good hadronic background rejection. This choice of the detector has also good performances with atmospheric neutrinos.

The results of the analysis of a test beam prototype confirm that the requested hadronic angular resolution is achievable with the massive magnetized calorimeter design.

5.3.4 The Large Magnetic Detector (LMD)

The proposed apparatus, shown in Fig. 39, is a large cylinder of 10 m radius and 20 m length, made of 6 cm thick iron rods interspersed with 2 cm thick scintillator rods built of 2 m long segments. The light read-out on both ends allows the determination of the spatial coordinate along the scintillator rod. The detector mass is 40 kt, and a superconducting coil generates a solenoidal magnetic field of 1 T inside the iron. A neutrino traveling through the detector sees a sandwich of iron and scintillator, with the $x - y$ coordinates being measured from the location of the scintillator rods, and the z coordinate being measured from their longitudinal segmentation.

The performance of the proposed detector would be similar to that of MINOS [21]. The main difference lies in the mass, which is an order of magnitude larger, and in the smaller surface-to-volume ratio which together, we believe, make the large magnetic detector superior for the detection of ν_μ and $\overline{\nu_\mu}$ events at the neutrino factory, and for the simultaneous study of atmospheric neutrino events.

To study the performance of the Large Magnetic Detector, we have performed a fast Monte Carlo simulation based on the GEANT 3 package [156]. The simulation assumes a sequence of 4 cm of iron followed by 1 cm of scientillators. The muon momentum and the hadronic shower are smeared following the parameterizations of the MINOS proposal.

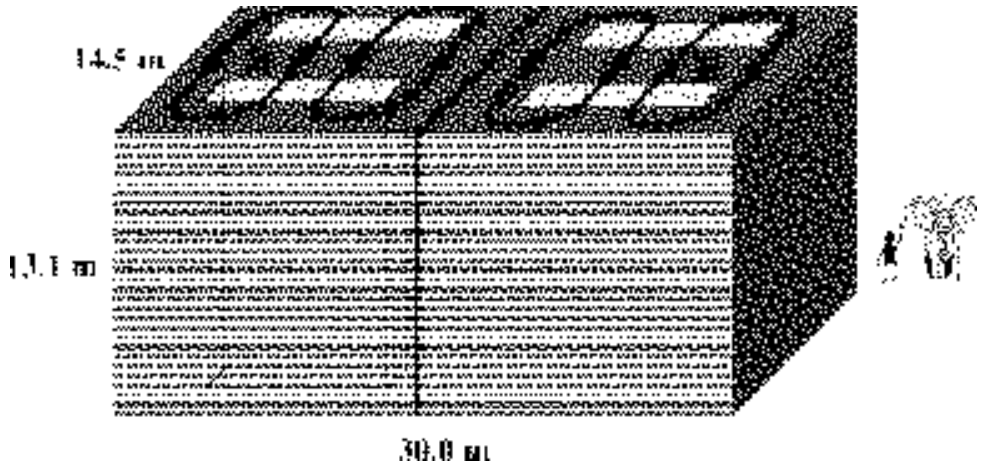

Fig. 38: *Layout of the Monolith detector, showing the magnetic field.*

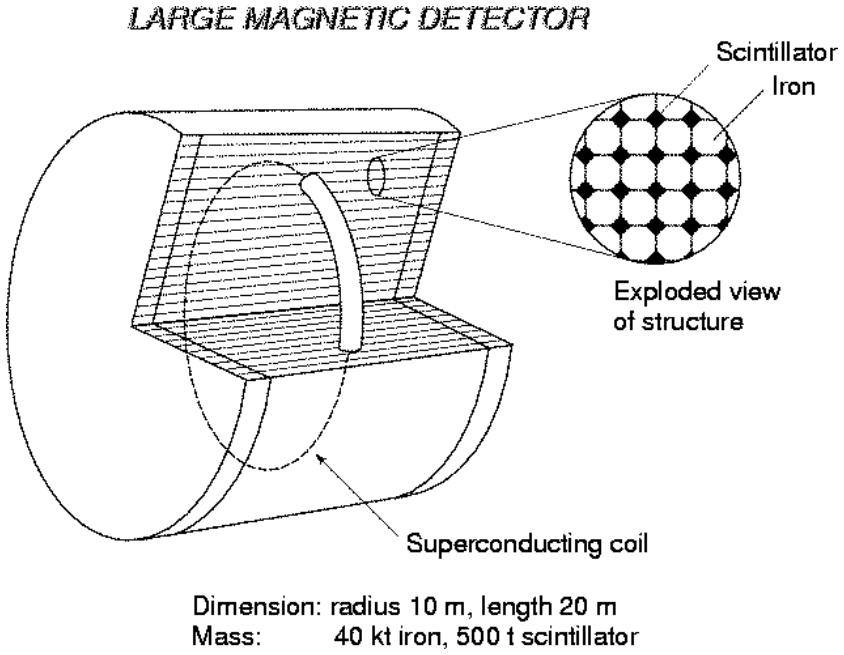

Fig. 39: *Sketch of the Large Magnetic Detector.*

We consider the $\overline{\nu}_\mu + \nu_e$ neutrino beam originating from a μ^+ beam of 50 GeV/*c*. The wrong-sign muon signal is generated assuming the oscillation parameters $\Delta m^2_{23} = 2.8 \times 10^{-3}$, $\theta_{12} = 45^\circ$, and $\theta_{13} = 8^\circ$. We have simulated 25000 ν_μ CC, 10^7 $\overline{\nu}_\mu$ CC, 10^7 $\overline{\nu}_\mu$ NC and 10^7 ν_e CC events.

To study the charge misidentification background, we have considered the 10^7 $\overline{\nu}_\mu$CC events, which have a realistic neutrino spectrum. This simulation includes energy loss and multiple scattering. Finite transverse resolution and loss of hits are simulated *a posteriori*. The momentum and the charge of the μ^+ were computed by means of a Kalman Filter fit to the recorded hits. It was assumed that there would be 2% of lost hits, a transverse resolution of 0.5 cm and a distance between measurement planes of 15 cm. These parameters were varied inside logical limits, and it turned out that even for 20%, 2.0 cm and 25 cm, this background was below 10^{-5} for a momentum cut of 5 GeV.

The discrimination of physical backgrounds from the signal is based on the fact that the μ^- produced in a ν_μ CC signal event is harder and more isolated from the hadron shower axis than in background events ($\overline{\nu}_\mu$CC, ν_e CC, $\overline{\nu}_\mu$NC and ν_e NC). Accordingly, we performed an analysis based on the momentum of the muon, P_μ, and a variable measuring the isolation of the muon from the hadron shower axis, $Q_{\rm t} = P_\mu \sin^2\theta$. Obviously, optimal cuts depend on the baseline. Table 10 gives the signal and background events, after optimal cuts, at three different baselines. The intermediate distance ~ 3500 km turns out to be the best baseline from the point of view of optimizing the S/N ratio and thus the sensitivity to the oscillation parameters.

Table 10: *Signal efficiency and fractional backgrounds for optimal cuts in the LMD detector.*

Baseline(km)	P_μ cut	Q_t cut	ν_μ signal efficiency	$\overline{\nu}_\mu$ CC	ν_e CC	$\overline{\nu}_\mu$+ ν_e NC
732	5.0	1.4	0.24	11×10^{-7}	1.0×10^{-7}	2.0×10^{-7}
3500	5.0	0.7	0.45	54×10^{-7}	1.0×10^{-7}	23×10^{-7}
7332	5.0	0.6	0.52	74×10^{-7}	1.0×10^{-7}	30×10^{-7}

5.3.5 A Liquid Argon detector

A liquid argon time projection chamber (TPC), as developed by the ICARUS Collaboration, is continuously sensitive and self-triggering, with the ability to provide three-dimensional imaging of any ionizing event: see Figure 40. This detector technology combines the characteristics of a bubble chamber with the advantages of electronic read-out. It offers the possibility of performing complementary and simultaneous measurements of neutrinos, including those from cosmic ray events, from the CERN to Gran Sasso beam (CNGS), and even those from the Sun and from supernovae. The same class of liquid argon detector can also be envisaged for high-precision measurements at a neutrino factory, and can be used to perform background-free searches for nucleon decay. Hence, an extremely rich and broad physics programme [99], encompassing both accelerator and non-accelerator physics, will be addressed. This will be able to answer fundamental questions about neutrino properties and about the possible physics of the nucleon decay.

A liquid argon detector is a precise tracking device with geometrical resolution $3\times3\times0.2$ mm^3, that also makes high-resolution dE/dx measurements and has full-sampling electromagnetic and hadronic calorimetry. Imaging provides excellent electron identification and electron/hadron separation. Energy

resolution is excellent ($\sim 3\%/\sqrt{E}$ for electromagnetic showers) and the hadronic energy resolution of contained events is also very good ($\sim 30\%/\sqrt{E_h}$).

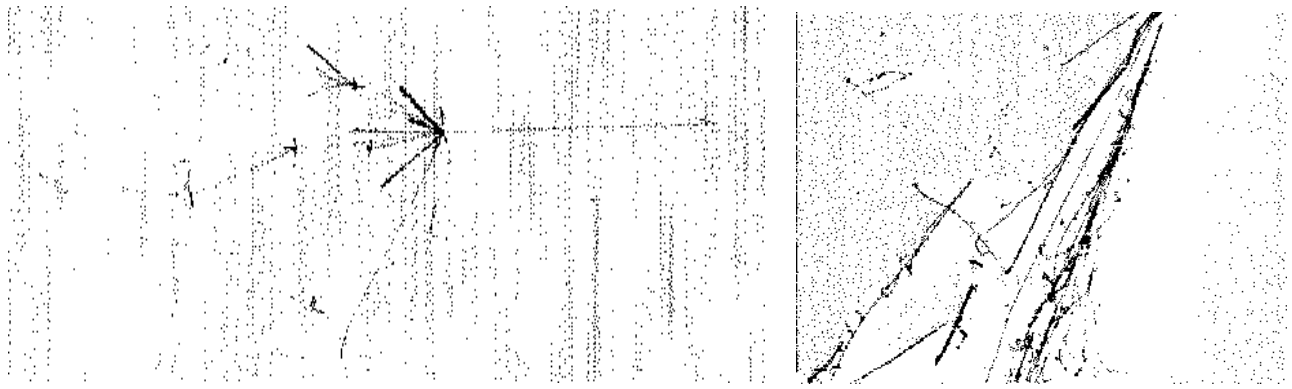

Fig. 40: *Left panel: electronic liquid argon imaging of a hadronic interaction: the collection wire coordinate is represented on the horizontal axis and the drift coordinate on the vertical axis (270×80 cm^2 shown). Right panel: a cosmic ray induced shower (40×40 cm^2 shown).*

The operating principle of the ICARUS liquid argon TPC is rather simple: any ionizing event (from a particle decay or interaction) taking place in the active liquid argon volume, which is maintained at a temperature $T \sim 89$ K, produces ion-electron pairs. In the presence of a strong electric field (~ 0.5 kV/cm), the ions and electrons drift parallel to the field in opposite directions. The motion of the faster electrons induces a current on a number of parallel wire planes located at the end of the sensitive volume. The knowledge of the wire position and the drift time provides the three-dimensional image of the track, while the charge collected on the wire provides information on the deposited energy.

Liquid argon imaging is now a mature technique, that has previously been demonstrated up to the scale of a 15 ton prototype. The latest major milestone has been the successful operation of the ICARUS 600 t prototype (T600), constructed during 2000 with all its various components, which operated during the summer of 2001. The detector is to be transported to the Gran Sasso underground laboratory to continue a long test period that will mainly feature the observation and study of atmospheric and solar neutrinos.

The overall performance of an underground detector is primarily determined by two factors: its total mass and its geometrical granularity, which determines the quality with which signal events can be reconstructed, and hence separated from backgrounds. The final phase of the ICARUS physics program requires a sensitive mass of liquid argon of 5 kt or more. The T600 detector stands today as the first proof that such large detectors can be built, and that liquid argon imaging technology can be implemented on such large scales. The superior bubble-chamber-like features of the ICARUS detector will provide additional and fundamental tools for elucidating in a comprehensive way the pattern of neutrino masses and mixings.

5.3.6 Magnetized liquid argon detectors

The possibility of complementing the excellent dE/dx measurements and energy resolution with those provided by a magnetic field has been studied. Embedding the volume of argon into a magnetic field would not alter the imaging properties of the detector, and measurements of the bending of charged hadrons or penetrating muons would allow a precise determination of the momentum and a determination of the charge: see Fig. 41. Unlike muons or hadrons, the early showering of electrons makes their charge

identification difficult. It is found that the determination of the charge of electrons of energy in the range between 1 and 5 GeV is feasible with good purity, provided the field has a strength in the range of 1 Tesla. Preliminary estimates show that these electrons exhibit an average curvature sufficient to have electron charge discrimination better than 1% with an efficiency of 20%.

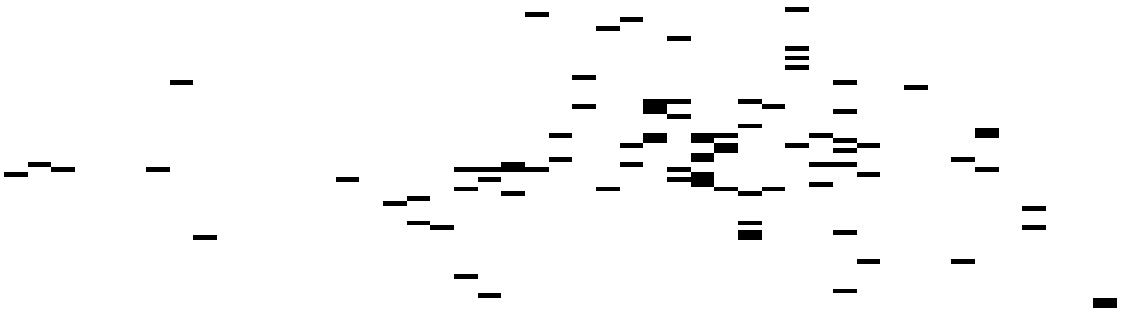

Fig. 41: *Simulation of a 2.5 GeV electron shower in a magnetized liquid argon TPC. The magnetic field has strength $B = 1.5$ T, and is directed perpendicular to the plane of the figure.*

5.3.7 A hybrid emulsion detector

This technology is based on the Emulsion Cloud Chamber (ECC) concept (see references quoted in [160]), which combines the high-precision tracking capabilities of nuclear emulsions and the large mass achievable by employing metal plates as a target. It has already been adopted by the OPERA Collaboration [160, 161] for a long-baseline search for $\nu_\mu \leftrightarrow \nu_\tau$ oscillations in the CNGS beam [162]. The experiment uses nuclear emulsions as high-resolution tracking devices for the direct detection of the τ produced in the ν_τ CC interaction with the target.

The basic element of the ECC is the cell, which is made of a 1 mm thick lead plate followed by a thin emulsion film. The film is made up of a pair of emulsion layers 50 μm thick on either side of a 200 μm plastic base. The number of grain hits in 50 μm (15-20) ensures redundancy in the measurement of particle trajectories and in the measurement of their energy loss in the non-relativistic regime when they are about to stop [160]. This is an important handle to reduce the background coming from ν_μCC charm production with a soft primary muon.

Thanks to the dense ECC structure and the high granularity provided by the nuclear emulsions, the OPERA detector is also suited for electron and γ detection [160]. The resolution in measuring the energy of an electromagnetic shower is about 20%. Furthermore, the nuclear emulsions are able to measure the number of grains associated to each track. This allows an excellent two-track separation: $\mathcal{O}(1)$ μm or even better. Therefore, it is possible to disentangle single-electron tracks from tracks produced by electron pairs coming from γ conversion in the lead.

The outstanding position resolution of nuclear emulsions can also be used to measure the angle of each charged track with an accuracy of about 1 mrad. This allows momentum measurement by using multiple Coulomb scattering with a resolution of about 20%, and the reconstruction of kinematical variables characterizing the event, i.e., the missing transverse momentum at the interaction vertex, p_T^{miss}, and the transverse momentum of a track with respect to hadronic shower direction, Q_T. For details on the event reconstruction, both with the nuclear emulsions and the electronic detector in an OPERA, we refer the interested reader to [160, 161].

Concerning the capability of an emulsion-based detector to handle the high interaction rate expected at a Neutrino Factory, we should stress that only events with a wrong-sign muon (WSM) in the final state are analysed. Therefore, one expects an attainable number of events to be scanned [176]. Hav-

ing in mind that in the past few years the scanning power increased by a factor of 10 every two years, it could be considered as realistic to assume that, by the time the Neutrino Factory will become operational, it will be possible to scan a larger number of events, say by a factor two. Therefore, a lead-emulsion mass a factor two larger than the one proposed for OPERA could be envisaged for a detector operating at a Neutrino Factory [176].

5.4 Oscillation Physics at the Neutrino Factory

The possibility of having intense neutrino beams of well-known composition opens the road to a large variety of physics studies. Having a simultaneous beam of electron and muon neutrinos, distinguished by helicity, allows the study of several oscillation processes. If we consider negative muons in the ring, the following transitions can occur:

- $\nu_\mu \rightarrow \nu_\mu$ disappearance
- $\nu_\mu \rightarrow \nu_e$ appearance
- $\nu_\mu \rightarrow \nu_\tau$ appearance
- $\bar{\nu}_e \rightarrow \bar{\nu}_e$ disappearance
- $\bar{\nu}_e \rightarrow \bar{\nu}_\mu$ appearance
- $\bar{\nu}_e \rightarrow \bar{\nu}_\tau$ appearance

An important feature of the Neutrino Factory is the possibility of having opposite muon charges circulating in the ring, therefore allowing also the study of the charged-conjugated processes of those above.

The simultaneous presence of both neutrino flavours in the beam poses the problem of separating neutrinos due to oscillations from beam background. A simple identification of the lepton produced in charged-current interactions is not sufficient, since muons, for instance, could come from the ν_μ component of the beam, from the oscillation $\bar{\nu}_e \rightarrow \bar{\nu}_\mu$, or even from the oscillation $\bar{\nu}_e \rightarrow \bar{\nu}_\tau$, followed by the decay $\tau \rightarrow \mu$. The obvious way to distinguish neutrinos coming from the beam from those coming from oscillations is to measure the charge of the lepton produced in charged-current events. The ideal case would be to be able to measure the charge for both electrons and muons, and perhaps find a way also to identify taus. Since the last two requirements are quite difficult to match, we consider as a default case that the detector for the neutrino factory will only be able to identify the charge of muons. If also electron identification can be performed, the detected events can be classified in four classes:

- Charged-current electrons,
- Right-sign muons,
- Wrong-sign muons,
- Events with no leptons.

An example of the set of energy spectra for these classes, for positive and negative muons circulating in the ring, is given in Fig. 42. At a later stage, we discuss the physics opportunities that will be opened by a detector able to also identify the charge of the electron, and taus using kinematic criteria.

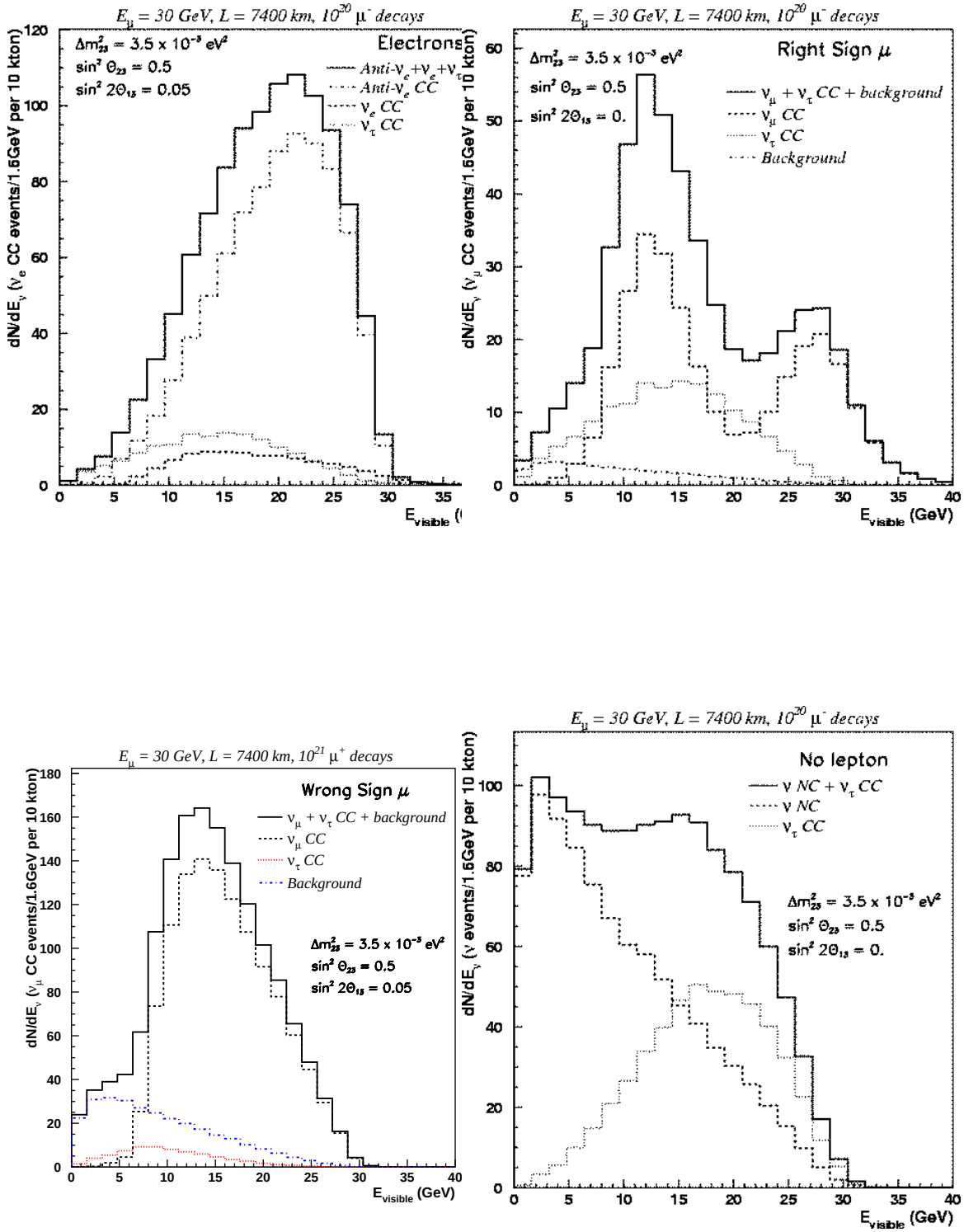

Fig. 42: *The four classes of events that can be studied in a detector with electron and muon charge identification. From the top, left to right: events with high-energy electrons, right-sign muons, wrong-sign muons and no charged leptons [78].*

5.4.1 *Precision measurements of oscillations*

The first parameters to be measured are those governing the leading atmospheric oscillation $\nu_\mu \to \nu_\tau$: θ_{23} and Δm^2_{23}. These parameters are mainly determined from the disappearance of muon neutrinos in the beam, observed using right-sign muon events. The maximum of the oscillation probability will produce a dip in the visible spectrum; the energy position of this dip will be correlated to the value of Δm^2_{23}, and the depth to θ_{23}. It is therefore favourable to choose an energy and baseline such that the maximum of the oscillation probability lies comfortably inside the detectable spectrum.

The precision on the measurement of the oscillation parameters has been addressed by several groups [163, 78, 172], and is normally performed by a fit of the energy spectra of the event classes (as previously said, this fit is largely dominated by right-sign muon events). As shown in Fig. 43, precisions of the order of 1% on Δm^2_{23} and of 10% on $\sin^2\theta_{23}$ are foreseen.

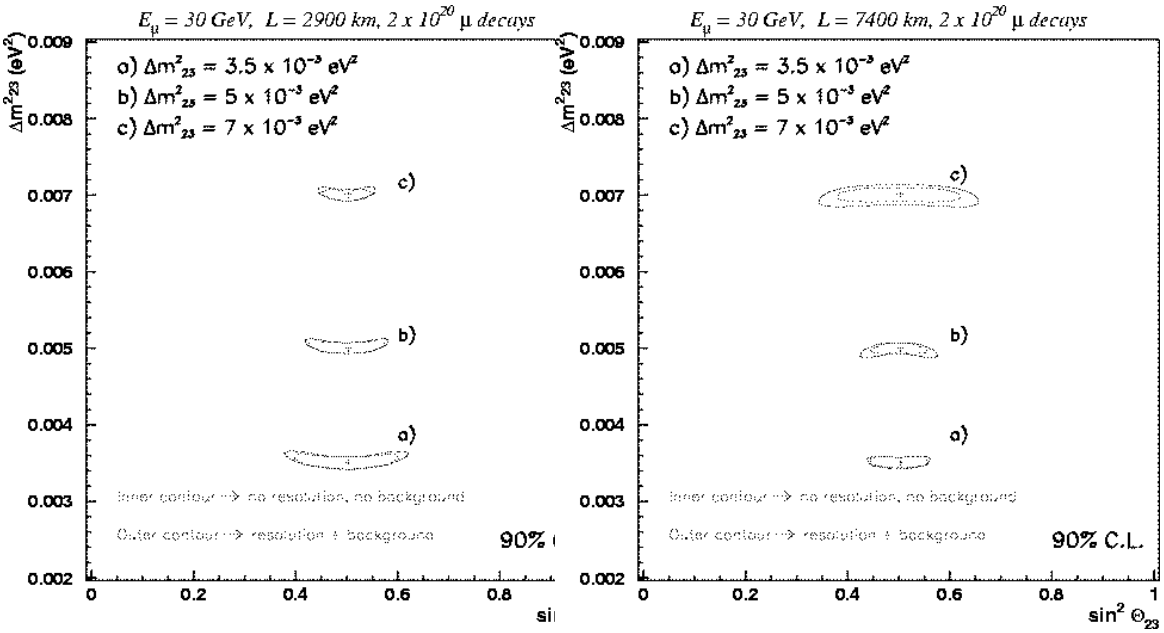

Fig. 43: *Measurement of the parameters of the leading oscillation [78].*

5.4.2 *Sensitivity to* θ_{13}

So far, the most accurate information we have on the angle θ_{13}, i.e., the mixing of electron neutrinos and the other two families (which are maximally mixed among themselves), is that $\sin^2 2\theta_{13} < 0.1$ [14]. In a favourable case, a non-zero value of this parameter could be discovered before the Neutrino Factory by experiments running in first-generation neutrino beams, such as ICARUS, OPERA and MINOS. Much larger sensitivity will however be achieved by super-beams, for instance the JHF-Super-Kamiokande project. Experiments performed in 'conventional' beams from pion decays will, however, always be limited by the presence of a ν_e component in the beam itself, representing an irreducible background to the search for $\nu_\mu \to \nu_e$ oscillations. It was first realized in [20] that the Neutrino Factory would have a significantly improved sensitivity to θ_{13} from the measurement of the wrong-sign muon signal. This measures the oscillation $\nu_e \to \nu_\mu$, where the oscillated muon neutrinos are easily separated from the beam component of opposite helicity by measuring the charge of the produced muon. We have already seen that the decays of charmed particles, kaons and pions can produce a background to the wrong-sign muon sample. Applying strong cuts on muon momentum and isolation, it was reported [116] that the background could be reduced by as much as a factor 10^6, keeping an efficiency of about 40%. An excellent background rejection with good efficiency could also be obtained using a hybrid emulsion detector [176].

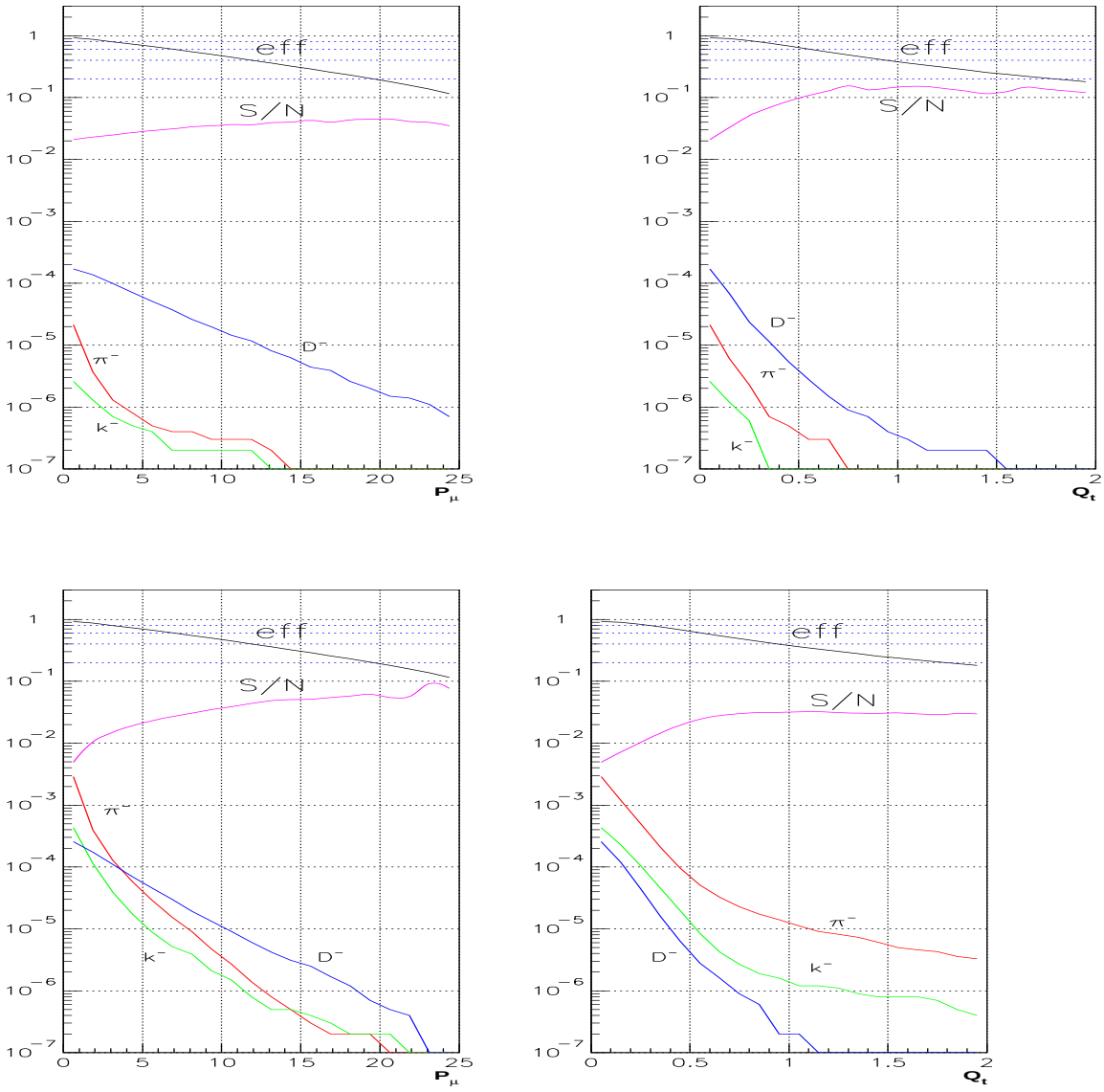

Fig. 44: *Backgrounds and efficiencies for wrong-sign muons, for charged-current (upper plots) and neutral-current (lower plots) events. We display the dependence on the cut on muon momemtum (left plots) and on the Q_t of the muon with respect to the hadronic jet (right plots) [116].*

As in the previous case, the parameter θ_{13} is extracted from a fit to the energy distribution of the various classes, and in this case the fit is largely dominated by the wrong-sign muons. Moreover, from the formula of the oscillation probability we see that the value of θ_{13} has a limited influence on the spectral shape, and even factorizes out from the energy dependence in the approximation $\Delta m^2_{12} = 0$, see (34), so most of the information actually comes from just counting wrong-sign muon events.

The background level is the ultimate limiting factor for this measurement, and pushing background rejection to the high values quoted above allows one to reach sensitivities of the order of $\sin^2\theta_{13} < 10^{-5}$ for the optimal intermediate baseline (see the right plot of Fig. 45). In the ideal case of no background and 100% efficiency for the signal, almost another order of magnitude on the sensitivity could be gained (left plot of Fig. 45).

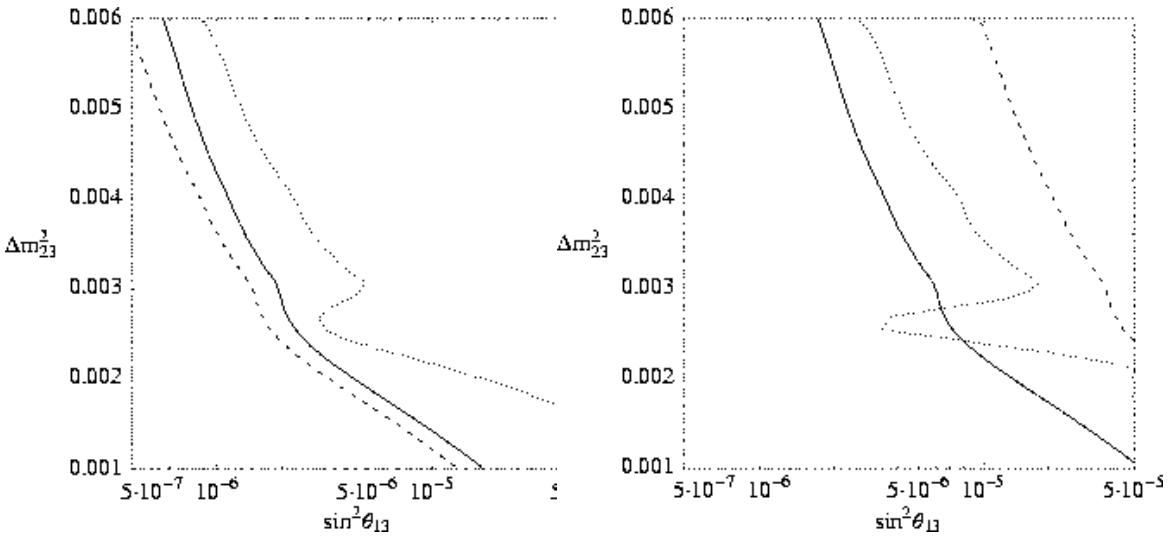

Fig. 45: *Sensitivity to* $\sin^2\theta_{13}$ *for a magnetized iron detector, in the case of no backround (left) and when a realistic background is considered (right). The three lines correspond to baselines of 730 (dashed), 3500 (solid) and 7300 km (dotted). Both plots were made assuming negligible effects of the solar parameters (i.e. for the small angle or small* Δm^2_{12} *solutions of the solar neutrino deficit) [116].*

5.4.3 Matter effects

For practical reasons, long-baseline experiments can only be performed with neutrinos passing through the Earth. We know that electron neutrinos traversing matter interact with the electrons of the material, leading to a modification of the effective mixing matrix, and therefore of the oscillation probability, in a way which is asymmetric between neutrinos and antineutrinos. We have seen in section 2.2.3 that the oscillation probabilities including matter effects in the context of three-family oscillations are rather simple when the solar mass difference, Δm^2_{12}, can be neglected.

According to (52), the oscillation probability $\nu_e \to \nu_\mu$ has the same form as in vacuum (34) if θ_{13} is modified to:

$$\sin^2 2\theta^m_{13}(D) = \frac{\sin^2 2\theta_{13}}{\sin^2 2\theta_{13} + (\frac{D}{\Delta m^2_{23}} - \cos 2\theta_{13})^2} \tag{65}$$

and the effective atmospheric mass splitting is modified to

$$\Delta M^2_{23} \simeq \Delta m^2_{23}\sqrt{\sin^2 2\theta_{13} + (\frac{D}{\Delta m^2_{23}} - \cos 2\theta_{13})^2}. \tag{66}$$

where

$$D = \pm 2\sqrt{2} G_F n_e E = 7.65 \times 10^{-5} eV^2 (\frac{\rho}{gcm^{-3}})(\frac{E}{GeV}),$$

with n_e being the average electron density in the path crossed, ρ the average electron density, and the sign $\pm$ standing for neutrinos and antineutrinos, respectively. The quantity Δm^2_{23} can also be positive in the case of a hierarchical spectrum or negative in the case of the inverted hierarchy. In the first case, the denominator of (65) is always larger than 1 for antineutrinos, and thus the effective angle is always smaller than the vacuum one. For neutrinos, the resonance condition will be met for

$$D \simeq \Delta m^2_{23} \cos 2\theta_{13},$$

for which value the effective angle becomes unity, no matter what the vacuum value was. It is therefore possible to have large enhancements of the oscillation probability, around the resonance energy

$$E^{res} \approx \frac{1.32 \times 10^4 \cos 2\theta \Delta m^2 (eV^2)}{\rho (g/cm^3)}.$$

Note however that the effective mass splitting at resonance decreases linearly with the vacuum value of $\sin 2\theta_{13}$, so, in order to get large probabilities, one needs to go to larger baselines for smaller $\sin 2\theta_{13}$. If the sign of Δm^2_{23} is negative, the same reasoning applies, interchanging neutrinos and antineutrinos.

The asymmetry between neutrinos and antineutrinos due to the matter effect is a very effective way to measure the sign of Δm^2_{23}, and establish the degenerate or hierarchical structure of neutrino masses. It has never been observed, and will be hard to detect with conventional super-beams, since it requires the comparison of runs with neutrinos and antineutrinos, and baselines larger than 1000 km. On the other hand, the crossing of such an MSW resonance is a plausible explanation for reconciling the large disappearance of solar neutrinos from the Sun with the lack of a significant seasonal variation, as would be expected from the eccentricity of the Earth orbit if the oscillation was taking place in the vacuum. Unfortunately, solar neutrino experiments cannot tell us anything about the sign of Δm^2_{23}.

Matter asymmetries on earth are relatively easy to detect at a Neutrino Factory [164, 165]. Although this is good news for the measurement of the sign of Δm^2_{23}, these asymmetries actually interfere with the measurement of leptonic CP violation, which is the most ambitious goal of this machine. The relative amplitudes of the two effects as a function of the baseline can be seen in Fig. 46. It shows, on a logarithmic scale, the ratio of events that have oscillated into muon antineutrinos to events that have oscillated into muon neutrinos, as a function of the baseline. The measurement of such a ratio requires running the machine alternatively with positive and negative muons in the ring. The upper lines correspond to negative values of Δm^2_{23}, and the lower ones to positive values. The three lines are obtained for different values of the CP-violating parameter δ, that will be discussed in more detail in the next section, and the error bars correspond to statistical errors for a 40 kt detector after 10^{21} muon decays in the ring for each muon charge. We see that the asymmetry due to matter effects is quite large, and can easily be detected for baselines larger than about 1000 km. Matter effects and CP violation interfere, and one effect can mask the other, until baselines of about 2000 km. Above that distance matter effects are always larger than CP violation, which is even completely cancelled for one particular distance around 7500 km.

5.4.4 CP violation

Detecting the presence of a complex phase in the leptonic mixing matrix is one of the most ambitious goals of neutrino physics, and would justify the effort of building a neutrino factory [20, 166, 167, 168, 116, 78]. In vacuum, we saw in (30) that the difference between the oscillation probabilities for the transitions $\nu_e \to \nu_\mu$ and $\bar{\nu}_e \to \bar{\nu}_\mu$ can be written as

$$\Delta_{CP} \sim \frac{1}{2} c_{13} \sin 2\theta_{12} \sin 2\theta_{13} \sin 2\theta_{23} \sin \delta [\sin \Delta_{12} \sin \Delta_{13} \sin \Delta_{23}], \quad (67)$$

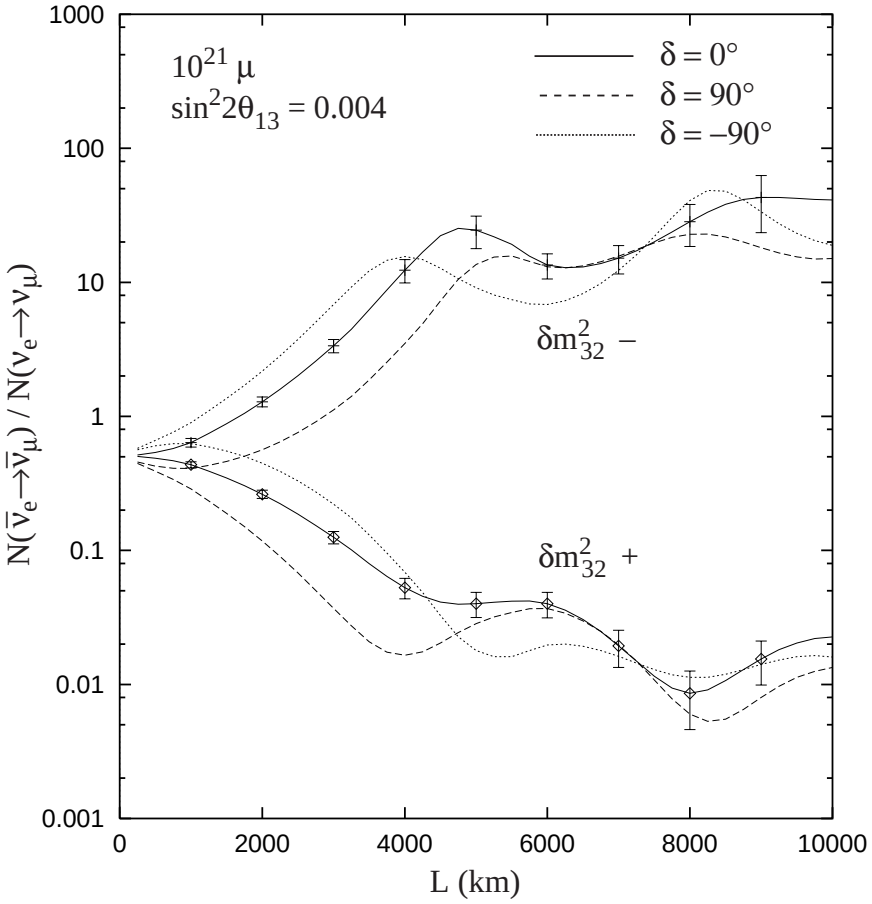

Fig. 46: *Ratio of the oscillation probabilities of neutrinos and antineutrinos as a function of the baseline. The different lines correspond to values of the CP-violating phase δ of $0°$, $90°$ and $-90°$. After about 1000 km, matter effects dominate over CP violation, whose effects even go to zero at a particular baseline around 7500 km [165].*

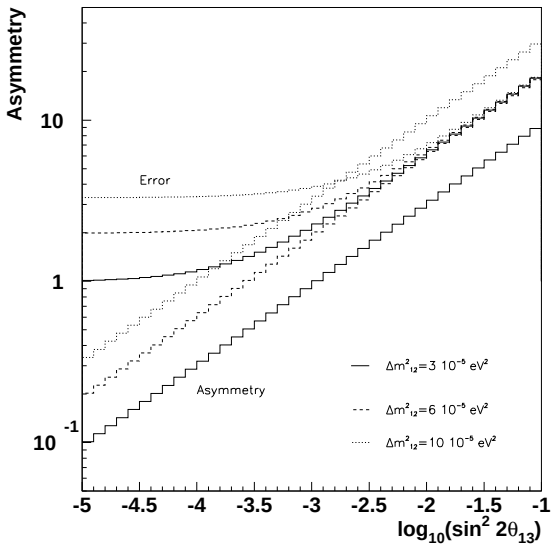

Fig. 47: *The CP-violating asymmetry and its error as a function of θ_{13}, for different values of Δm^2_{12}.*

which shows that, for the large mixing angle solution of the solar deficit, it is suppressed only in the parameters Δ_{12} and θ_{13}. Since the CP-even parts of the probabilities are always larger than the CP-odd parts, they dominate the number of events and thus the error on the measured asymmetry. For small enough Δ_{12}, these terms are approximately proportional to $\sin^2 2\theta_{13}$ and independent of Δ_{12} (they are driven by the atmospheric oscillation, i.e. the first term in (31)). Assuming Gaussian errors, the significance of CP violation will then be proportional to

$$\frac{\Delta_{CP}}{\sqrt{N_{ev}}} \propto \frac{\sin 2\theta_{13}}{\sqrt{\sin^2 2\theta_{13}}}\ \Delta_{12}, \tag{68}$$

and will not depend on θ_{13} [168], while it is linearly proportional to the small mass splitting. The fact that Δ_{12} is actually different from zero means that the subleading oscillation will become important and eventually dominate for small θ_{13}. In this regime the role of $\sin 2\theta_{13}$ and Δ_{12} are interchanged and the significance of the CP asymmetry is suppressed linearly in $\sin 2\theta_{13}$ and approximately independent of the solar mass splitting

$$\frac{\Delta_{CP}}{\sqrt{N_{ev}}} \propto \frac{\Delta_{12}}{\sqrt{(\Delta_{12})^2}}\ \sin 2\theta_{13}. \tag{69}$$

This is shown in Fig. 47, where the CP asymmetry at the maximum of the oscillation probability is compared to its error (computed for a relatively modest neutrino flux) as a function of $\sin^2 2\theta_{13}$. We see that the effect and the error decrease together with $\sin^2 2\theta_{13}$ until a value (that depends on Δ_{12}) where the subleading oscillation becomes dominant, and the number of oscillated events goes to a constant even for very small θ_{13}. In this regime the significance of the asymmetry decreases linearly with $\sin 2\theta_{13}$.

A possible measurement of this asymmetry is given by the integrated asymmetry [20]:

$$A^{CP}_{e\mu} = \frac{\{N[\mu^-]/N_0[e^-]\}_+ - \{N[\mu^+]/N_0[e^+]\}_-}{\{N[\mu^-]/N_0[e^-]\}_+ + \{N[\mu^+]/N_0[e^+]\}_-}, \tag{70}$$

where the suffix defines the sign of the decaying muon, $N[\mu^\pm]$ is the measured number of wrong-sign muons and $N_0[e^\mp]$ the expected number of $\bar{\nu}_e$ and ν_e charged-current interactions in the absence of oscillations. The statistical significance of the asymmetry, i.e., the asymmetry divided by its error, assumed

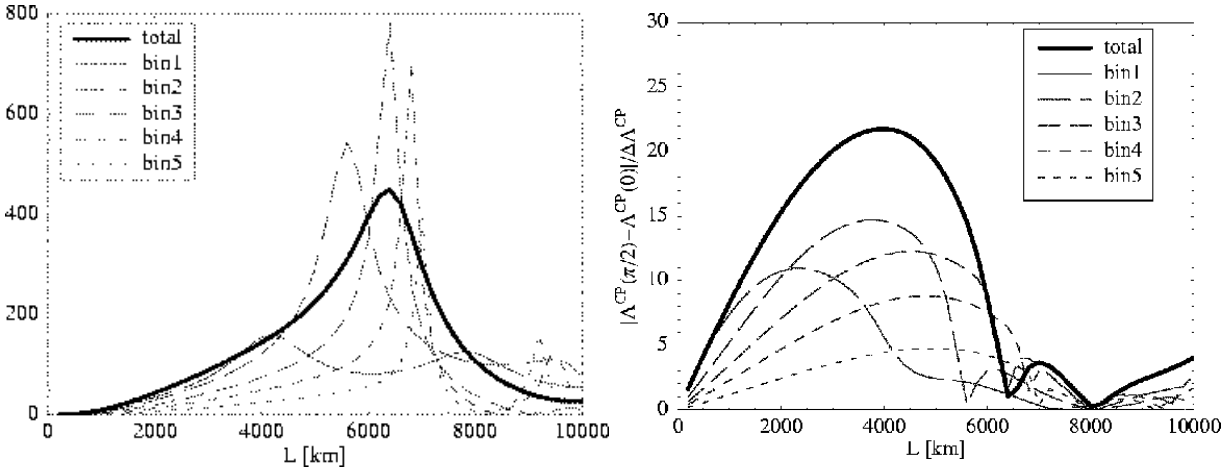

Fig. 48: *The significance of the CP asymmetry as a function of the baseline [116]. On the left, the asymmetry is just the matter-induced asymmetry (SMA solution parameters). On the right we show, for LMA parameters, a subtracted asymmetry directly measuring δ.*

to be Gaussian, in vacuum is proportional to [167]

$$\frac{A^{CP}}{\Delta A^{CP}} \propto \sqrt{E}\left|\sin\left(\frac{\Delta m^2_{23}L}{4E_\nu}\right)\right|. \tag{71}$$

This is maximal at the peak of the atmospheric oscillation.

These considerations, valid in vacuum, get however modified by matter effects, as already seen in Fig. 46. In matter, very large asymmetries are created by the MSW effect. The left plot of Fig. 48 shows the total asymmetry in matter as a function of the baseline, while the one on the right shows the asymmetry obtained after subtracting the matter-induced asymmetry for $\delta = 0$. Clearly the significance of the matter-induced asymmetry and the intrinsic one peak at different baselines.

Although the right plot shows that for the parameters in the LMA range, intrinsic CP violation should be measurable at distances $\mathcal{O}(3000)$ km, this analysis assumes only experimental errors and not 'theoretical' ones. Given that the matter-induced asymmetry depends very sensitively on the oscillation parameters, mainly θ_{13}, θ_{23} and Δm^2_{23} as well as on the Earth matter density, it is very important to clarify whether the expected uncertainties in those 'theoretical' parameters will be small enough not to wash out the effect.

Concerning the atmospheric parameters $|\Delta m^2_{23}|$ and $\sin^2 2\theta_{23}$, we have seen that they can be measured with very good precision using disappearance measurements at the neutrino factory. It was shown [76] that the knowledge of the precise profile of the matter density along the neutrino path is not very relevant, but for a neutrino experiment only the knowledge of the mean value is needed. This average density can probably be known with 5% accuracy [169], or even directly measured with a 10% precision [78].

On the other hand the angle θ_{13} as well as the discrete choices of the sign of Δm^2_{23} and $\cos\theta_{23}$ if $\theta_{23} \neq \pi/4$, will have to be determined simultaneously using the wrong-sign muon signals. The analysis has to be refined to include these unknowns and, as we will see in the next sections, this will reveal the existence of

- Strong parameter correlations: mainly between θ_{13} and δ [116],
- Degenerate solutions [117, 171].

In order to minimize and resolve these, it is important to use all the spectral information available and choose appropiately the baseline. Fig. 49 shows the energy dependence of the intrinsic effect of $\delta \neq 0$.

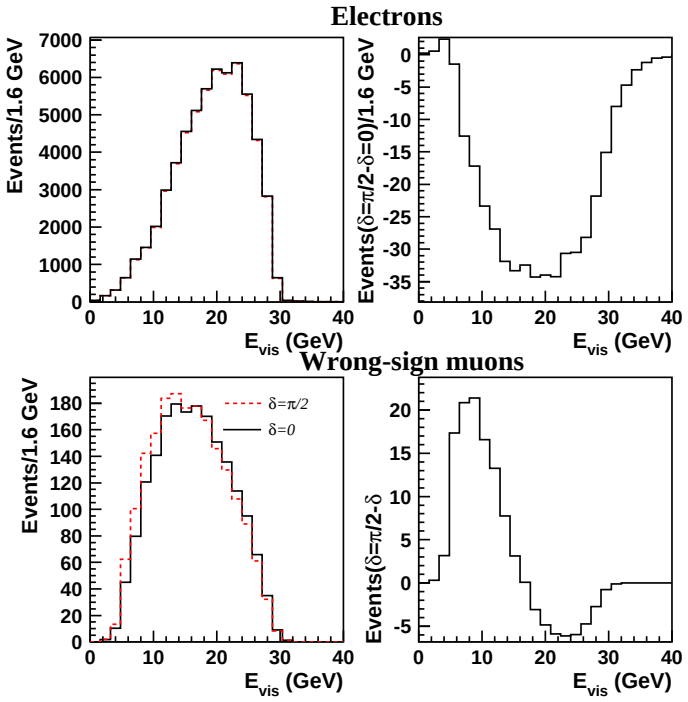

Fig. 49: *Left plots: number of oscillated events for $\delta = 0$ (black histogram) and $\delta = \pi/2$ (red histogram). The right plots represent the difference of the two, for $\nu\mu \to \nu_e$ and $\nu_e \to \nu_\mu$ transitions, respectively. If the difference is similar, the signal in the electron channel is invisible due to the vey large background. In the muon channel, we notice the the shift of the oscillation maximum generated by CP violation [78].*

In the global fit of course we consider the wrong-sign muon signals for both μ^+ and μ^- and not only the CP asymmetries, since also the CP-even parts contain very valuable information on the unknowns.

5.4.5 Correlations and choice of baseline

Due to the small energy dependence induced by CP violation, the use of spectral information to have a simultaneous measurement of δ and θ_{13} is not very effective, and only helps under some conditions. In fact, the first simultaneous fits of θ_{13} and δ perfomed in [116, 78] revealed for most of the cases a strong correlation between the two parameters, which was more important at shorter baselines, see Figs. 50 and 51. The reason for this is easy to understand. The neutrino and antineutrino oscillation probabilities in vacuum (30), have the following dependences on θ_{13} and δ:

$$P(\nu_e \to \nu_\mu)P(\bar{\nu}_\mu \to \bar{\nu}_e) \quad = \quad A \sin^2 2\theta_{13} + B \sin 2\theta_{13} \cos\delta \pm C \sin 2\theta_{13} \sin\delta + D \qquad (72)$$

where the coefficients A, B, C, D depend on the energy, baseline and the remaining oscillation parameters. In matter a similar structure is found, though the coefficients are different for neutrinos and antineutrinos and depend also on the earth matter density. In the limit of large E_ν or small L ($\Delta_{12} < \Delta_{23} \ll 1$), the coefficients A, B and D have the same energy dependence, while C is suppressed by an extra factor Δ_{23} compared to the others. This is so both in vacuum and in matter, because matter effects are irrelevant in this limit. In this situation it is clear that the measurements of the oscillation probabilities for neutrinos

and antineutrinos give information on the same combination of the two unknowns: θ_{13} and δ

$$A \sin^2 2\theta_{13} + B \sin 2\theta_{13} \cos\delta + D, \tag{73}$$

resulting in the strong correlation [116] that can be nicely seen in the left plot of Fig. 57, at a baseline of $L = 732$ km. Even though the spectral information has been used for this baseline, it is only relevant in the low-energy region. The same fit performed with a lower energy threshold in Fig.51 shows that correlations are smaller, but still present. As the baseline is increased the CP-odd term, i.e., the coefficient C, grows and the neutrino and antineutrino probabilities measure two independent combinations of the two parameters. Also the energy dependence in the accessible energy range becomes more important. Indeed, the fits at $L = 3500$ km in Fig. 50 and at $L = 2900$ km in Fig. 51 show that δ and θ_{13} can be disentangled. At even larger baselines, sensitivity to δ is lost.

How much can the neutrino energy threshold actually be lowered in order to reduce correlations, using spectral information in the important low-energy region? The answer to this question depends of course on the detector, but since we want to discriminate the oscillation signal from a constant background, also on the amplitude of the oscillation signal, i.e., on the oscillation parameters. For small values of θ_{13}, the good purity needed to discriminate the wrong-sign muon signal from background requires very hard cuts on the muon momentum, and therefore the loss of the most interesting part of the neutrino spectrum. For instance, a magnetized iron detector can in principle reach background rejection factors of the order of 10^6, but at the price of an effective cutoff on neutrino energies of about 10 GeV.

The conclusion of this study was that in the case of one baseline, the optimal choice to study CP violation was in the intermediate range $L = \mathcal{O}(3000)$ km for a machine of $E_\mu = 30 - 50$ GeV [116].

All the above considerations pointing to the optimal distance of $\mathcal{O}(3000)$km have assumed a constant beam flux. It is possible to argue that a lower-energy machine could profit from savings on the accelerator and provide a larger flux than a high-energy one. If we assume that, for various possible Neutrino Factory designs, the flux can be inversely proportional to the beam energy (in other words, the total beam power is constant), this fact compensates the linear sensitivity growth, and it can be shown [75] that all energy/baseline combinations that keep constant the ratio of these two quantities are equivalent, with a slight preference for the lower energy-baseline combinations, due to the smaller influence of matter effects. This study assumes a neutrino energy threshold of 2 GeV, for which a baseline of 732 km and a maximal neutrino energy of 7.5 GeV are slightly better than a baseline of 2900 km and an energy of 30 GeV, if the flux of the first case is 4 times larger than the second one. However, a coarse detector with larger energy thresholds will always benefit from a longer baseline and higher neutrino energy [172].

Correlations of the phase δ with other oscillation parameters have also been studied in several works [173, 117, 172, 174, 78]. The main conclusions are:

- The parameters of the leading oscillation will be measured independently by the Neutrino Factory itself using the same-sign muon sample, and the precision reached will be much superior than that producing any sizeable systematic effect on the measurement of δ. An exception are sign and octant ambiguities, that can produce degenerate solutions, and will be discussed in the next section.

- Knowledge of the parameters governing solar neutrino oscillations (θ_{12} and Δm_{12}) is essential, but the indications are that KamLand results should be precise enough to reduce to negligible levels the impact of the uncertainties on these measurements to the determination of δ.

- The average earth density can probably be known up to 5% using geophysical techniques [169]; however, a precision at least a factor 2 better would be desirable.

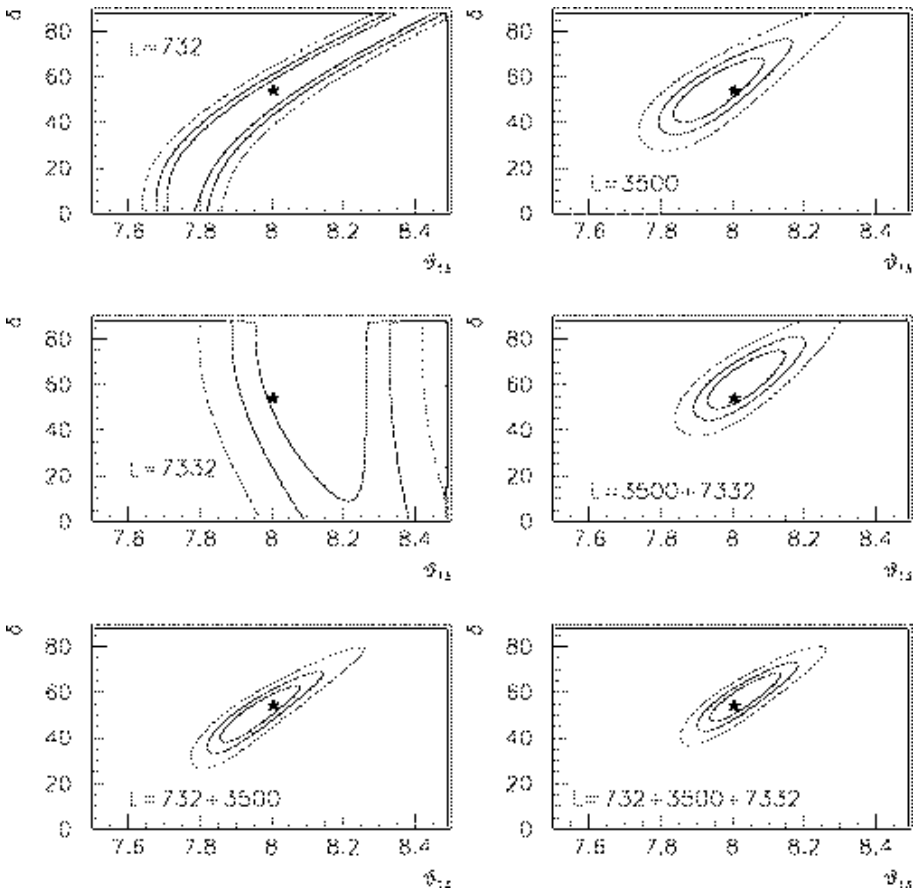

Fig. 50: *Correlations in a simultaneous fit of θ_{13} and δ, using a neutrino energy threshold of about 10 GeV. Using a single baseline correlations are very strong, but can be largely reduced by combining information from different baselines and detector techniques [116].*

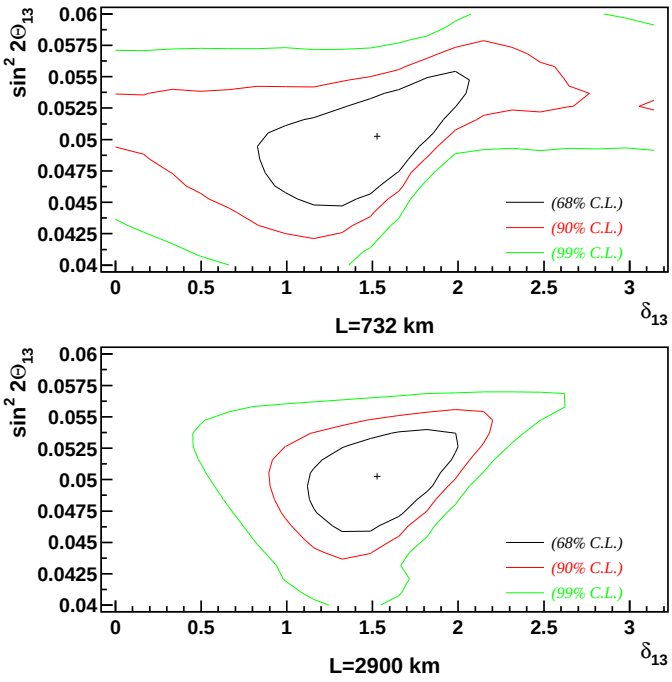

Fig. 51: *Contours in the* $\sin^2 2\theta_{13} - \delta$ *plane assuming very low energy threshold (2 GeV muon energy) at distances of 732 or 2900 km. Even if not as pronounced as in the case of the previous plot, done with much higher neutrino energy thresholds, the short baseline starts to show correlations between the two parameters [78].*

5.4.6 Degeneracies

We have seen in the previous section that it is very hard to disentangle θ_{13} and δ at short baselines of $\mathcal{O}(1000)$ km, because the neutrino and antineutrino probabilities are sensitive to approximately the same combination of the two parameters. At larger baselines the correlation is resolved thanks mainly to the larger $\sin\delta$ term in (73). However, even in this case, the impossibility of measuring precisely the energy dependence of the wrong-sign muon signals can result in the existence of degenerate solutions for the θ_{13} and δ, i.e., disconnected areas of the parameter space that lead to experimentally indistinguishable signatures [117]. The origin of this is that, at fixed neutrino energy and baseline, the equations

$$\begin{aligned} P_{\nu_e\nu_\mu}(\theta'_{13},\delta',\Theta') &\simeq P_{\nu_e\nu_\mu}(\theta_{13},\delta,\Theta) \\ P_{\bar\nu_e\bar\nu_\mu}(\theta'_{13},\delta',\Theta') &\simeq P_{\bar\nu_e\bar\nu_\mu}(\theta_{13},\delta,\Theta) \end{aligned} \tag{74}$$

have more solutions than the true one: $\theta'_{13}=\theta_{13}$ and $\delta'=\delta$. We use the symbols Θ and Θ' to denote the other sets of oscillation parameters. The reason why in general Θ' might be different from Θ is due to the discrete ambiguities of the type sign(Δm^2_{23}) and sign$(\cos\theta_{23})$. The three main types of degeneracies correspond to different choices of Θ':

- Intrinsic, when $\Theta'=\Theta$, so all other parameters are the same, but the conditions (74) are satisfied for sets of θ_{13},δ different from the true one [117].
- The sign of Δm^2_{13} is different in the two sides of the equations (74) [171]. In vacuum, a change of sign of Δm^2_{13} is approximately equivalent to the substitution $\delta\to\pi-\delta$ [170].
- The value of θ_{23} on the left side of (74) is $\pi/2-\theta_{23}$ of that on the right side [171]. The fake solutions obviously collapse to the intrinsic ones for maximal mixing: $\theta_{23}=\pi/2$.

An example of intrinsic degeneracies is shown in Fig. 52, obtained for a simultaneous fit of θ_{13},δ in a large magnetised iron detector. The true values of the parameters are indicated by the stars, while a fit to the observed data would find several disconnected regions. These plots were made for a baseline of 2800 km.

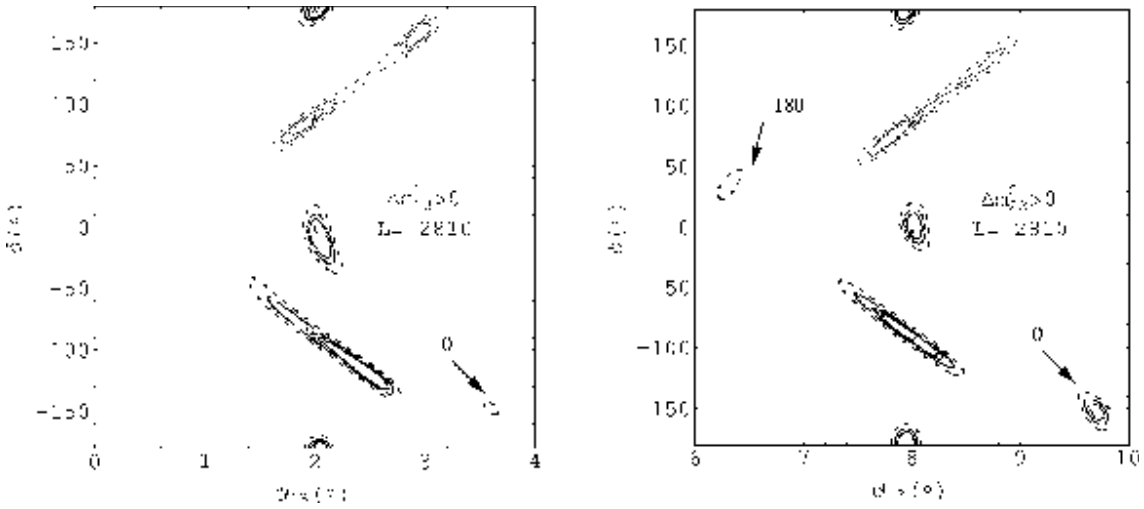

Fig. 52: *Simultaneous fits of δ and θ_{13} at $L=2800$ km, for $\theta_{13}=2^\circ$ (left) and 8° (right). True values are indicated by stars, and many degenerate solutions are present [117].*

Degeneracies can be a very serious source of uncertainties in the determination of the parameters. If, for instance, we define (conservatively) the sensitivity to $\sin^2 2\theta_{13}$ as the largest value of $\sin^2 2\theta_{13}$

which can be fit to $\sin^2 2\theta_{13} = 0$, we will find that the degenerate solution can be interpreted as an additional uncertainty which makes it almost impossible to push the sensitivity to $\sin^2 2\theta_{13}$ much below 10^{-3} [175] (see Fig. 53).

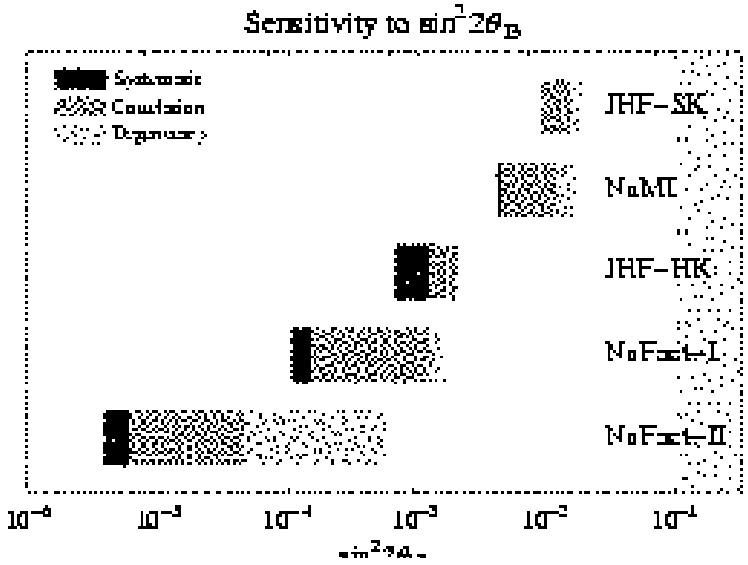

Fig. 53: *Limitations on the achievable sensitivity to* $\sin^2 2\theta_{13}$ *for various assumptions on future experiments, which are described in [175]. The sensitivity to* $\sin^2 2\theta_{13}$ *is defined as the largest value of* $\sin^2 2\theta_{13}$ *which can be fit to* $\sin^2 2\theta_{13} = 0$*, which means that the degenerate solutions enter as an additional source of uncertainties. In this interpretation, the importance of resolving the degeneracies from the combination of various experiments is very clear.*

There are fortunately several handles to deal with these degeneracies. The position of the fake solutions is very sensitive to the value L/E and the presence or not of matter effects. The first possibility is then to have two baselines at the Neutrino Factory, since combining the information of two experiments allows the exploration of a different L/E regime, and matter effects behave differently at two baselines for the disconnected sets of parameters. We see from Fig. 54 that the combination of the intermediate and the very long baseline eliminates all degeneracies. The combination of the intermediate and a short baseline, e.g., 732 km is not so good, because of the strong correlations present in the shorter baseline.

If a baseline of the order of 732 km is used in addition to one around 3000 km, it is more interesting to consider at the shorter baseline a detector with capabilities to detect τ's from $\nu_e \to \nu_\tau$ oscillations. The measurement of this transition would be a great help in resolving degeneracies, since the two processes $\nu_e \to \nu_\mu$ and $\nu_e \to \nu_\tau$ give complementary information[176]. In fact, the formulae for oscillation probabilities in vacuum of these processes are very similar: the $\nu_e \to \nu_\tau$ probability can be obtained from (34) by swapping $s^2_{23} \leftrightarrow c^2_{23}$ and changing the sign of the $\delta-$dependent terms. In Fig. 55, we plot the curves of equal $\nu_e \to \nu_\mu$ and $\nu_e \to \nu_\tau$ probabilities in the ($\Delta\theta_{13} \equiv \theta'_{13} - \theta_{13}$, δ') plane for some fixed values of the true parameters: $\theta_{13} = 5^\circ, \delta = 90^\circ$. The different curves correspond to different energy bins. The curves all meet only at the true values of the parameters: $\delta' = 90^\circ$ and $\Delta\theta = 0$, while all the curves for the wrong-sign muons are approximately degenerate. This illustrates the potential of the combination of golden and silver events to exclude the fake solutions.

In [176] a detailed study of a realistic experimental setup has been presented. The detector considered is an OPERA-like hybrid with lead and emulsion [160]. It has been shown that the τ vertex recognition in the emulsion detector allows one to separate $\nu_e \to \nu_\tau$ from $\nu_e \to \nu_\mu$ muon events, and to reduce strongly the effect of the charm decay background. The outcome of this study is that a 4 kt

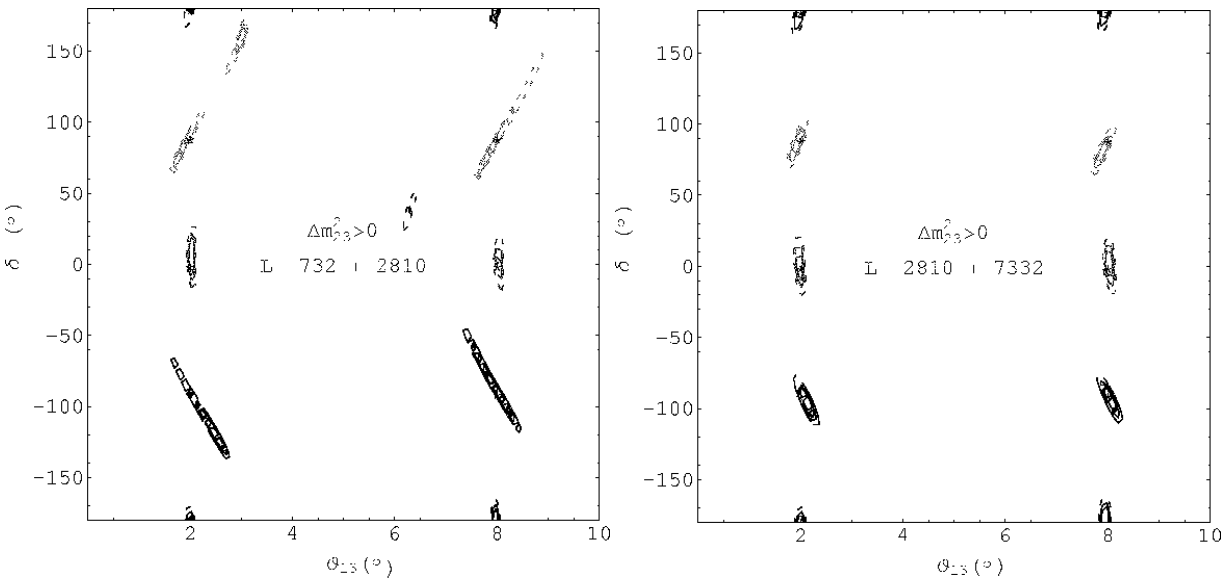

Fig. 54: *For a wide choice of the parameters, in order to reduce correlations in a simultaneous fit to θ_{13} and δ, the combination of the intermediate and the very long baseline is preferred over that of the short and intermediate baselines [117].*

detector at $L = 732$ km in combination with the 40 kt magnetised iron detector at $L = 3000$ km would solve the intrinsic ambiguity for $\theta_{13} \geq 1^\circ$ and any value of δ.

Another interesting approach to resolve degeneracies is the combination of information from the Neutrino Factory and a super-beam [177]. The synergy of the super-beam project with the Neutrino Factory has already been discussed from the point of view of the accelerator infrastructure, since we saw that several components needed for building a super-beam are the same as those for the Neutrino Factory. Most likely, at the time of the operation of this facility, results from the super-beam will already be available, and the synergy between the two projects will emerge in the physics. Due to the very different L/E regime - super-beams are designed to operate around the oscillation maximum - and matter effects - which are much smaller for super-beams due to the shorter baseline, the knowledge of the super-beam results will help resolve the degeneracies.

Sufficiently powerful super-beams can search for CP violation in a favourable corner of the parameter space. It was shown [177] that a combination of the results from the proposed CERN-Fréjus super-beam and a Neutrino Factory with a single baseline could eliminate almost completely all degeneracies. The reason is easy to understand from Fig. 56: the fake solutions, present in both experiments, appear in different areas of the parameter space, and therefore are excluded once the experiments are combined.

Combined with the results of the super-beam, even the baseline of 732 km, normally too short to give definitive results on its own, can provide good measurements of the oscillation parameters. This is shown by the contours in the plane (θ_{13}, δ) in Fig. 57. We already saw that a high-energy Neutrino Factory coupled with a detector with high threshold for neutrino detection reaches its maximal sensitivity for a baseline of about 3000 km. For a shorter baseline, the experiment measures only the combination (73) as we already discussed (left plot in Fig. 57). The addition of the super-beam information, which also is not able to resolve the degeneracies on its own, leads to a very good determination of the two parameters as shown in the right plot of Fig. 57.

This result is extremely important for the definition of the Neutrino Factory design itself. It is common belief that an intermediate baseline of about 3000 km is the best compromise between being long enough to have the maximum of the oscillation at sufficiently high energy, and not too far not to

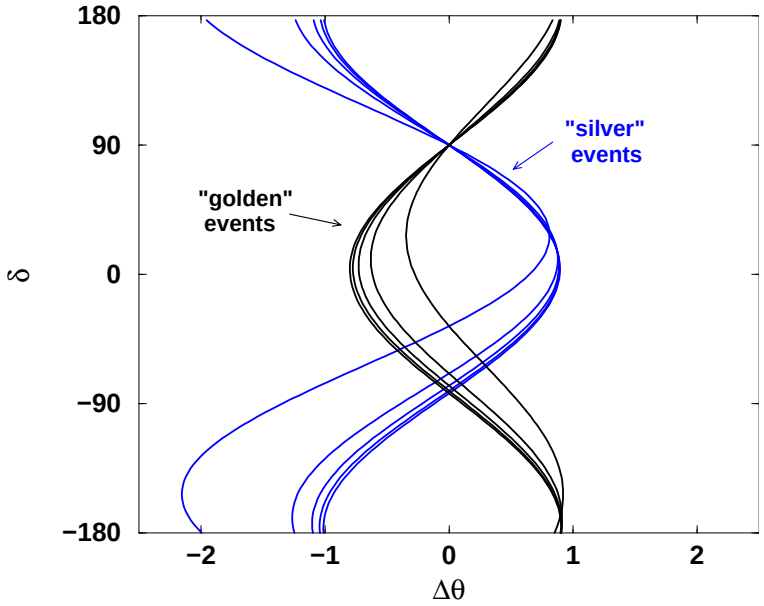

Fig. 55: *Curves of equal oscillation probability in the $\delta, \Delta\theta$ plane (where $\Delta\theta$ is the difference between θ_{13} and its nominal value of 5°), for $\nu_e \to \nu_\mu$ and $\nu_e \to \nu_\tau$. We see that these curves, generated for different energy bins, all meet at the nominal value of the parameters [176].*

have the CP violation suppressed by matter effects. Since a low-energy super-beam will probably be built before the Neutrino Factory, the energy/baseline optimization of the latter will have to take into account the combination with the super-beam results.

5.4.7 T violation

The problem of the neutrino-antineutrino asymmetry generated by matter effects acting as a background to CP violation could be solved if, instead of the CP asymmetry, we could measure the T asymmetry, i.e., the difference in oscillation probability between the processes $\nu_e \to \nu_\mu$ and $\nu_\mu \to \nu_e$. This is in principle possible at the Neutrino Factory, since if the machine is operated with two different beam polarities, both processes (and even their complex conjugates) occur. The problem is that, in order to discriminate oscillated events from the beam component of the same flavour, the charge has to be measured for both leptons. While this is possible in a relatively straightforward way for muon final states, the measurement of the electron charge is much more complicated, due to the early formation of electromagnetic showers. The possibility of measuring the electron charge has been studied [75] for a magnetised liquid argon detector. A charge confusion at the per mille level with an efficiency of about 10% for electrons of less than 5 GeV energy should be reached with values of the magnetic field exceeding 1 Tesla. In that case, it would be possible to measure directly the two T-conjugated oscillation probabilities, and detect the difference between the two (see Fig. 58) with a statistical significance similar to that of the CP violation. Due to the impossibility of detecting the charge of high-energy electrons with realistic values of the magnetic field, an experiment looking for T violation would require a low-energy, high-intensity muon beam.

5.4.8 Search for $\nu_e \to \nu_\tau$

We saw in the previous section that the detection of τ leptons could be useful in resolving the degeneracies in the search for CP violation, due to the different behaviour of the $\delta-$dependent term in the

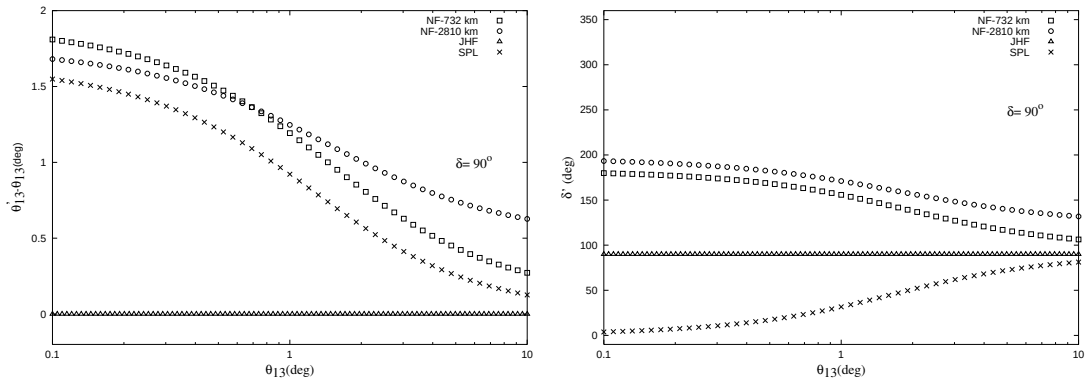

Fig. 56: *Values of $\theta'_{13} - \theta_{13}$ (left) and δ' (right) for the intrinsic fake solution for $\delta = 90°$. We see that fake solutions, albeit present for all kinds of experiments, appear for different values of the parameters, and therefore a combination of experiments allows one to exclude them [177].*

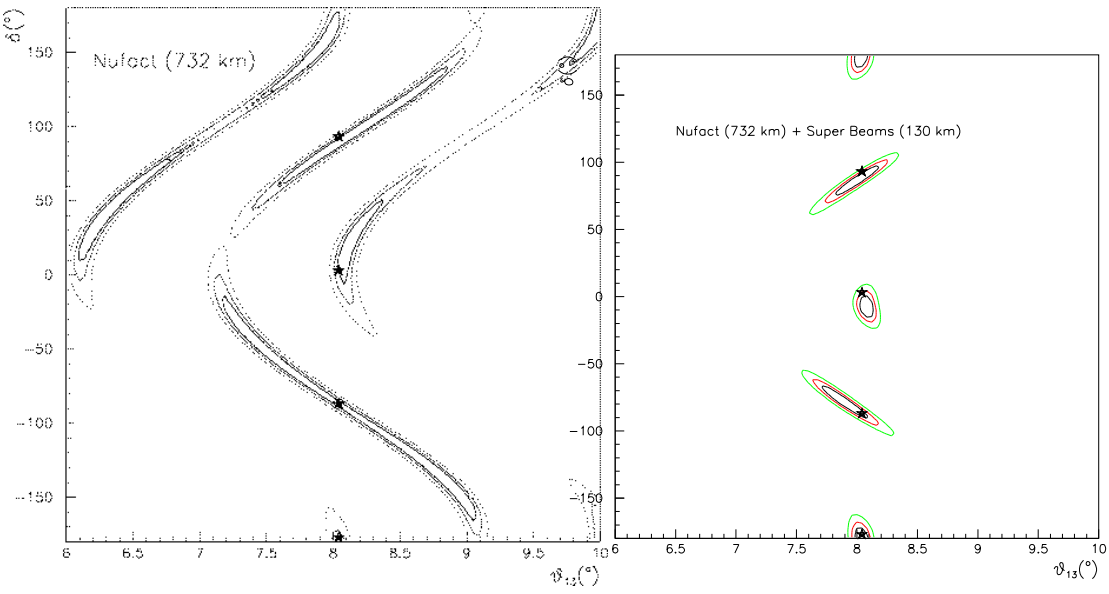

Fig. 57: *Simultaneous measurements of θ_{13} and δ and of the CP-violating phase δ. The left plot is produced using only the information from a Neutrino Factory with an iron magnetised detector placed at 732 km: there are clear correlations between the parameters and degenerate solutions. In the right plot, the Neutrino Factory is combined with the results from the super-beam, and both correlations and degeneracies disappear [177].*

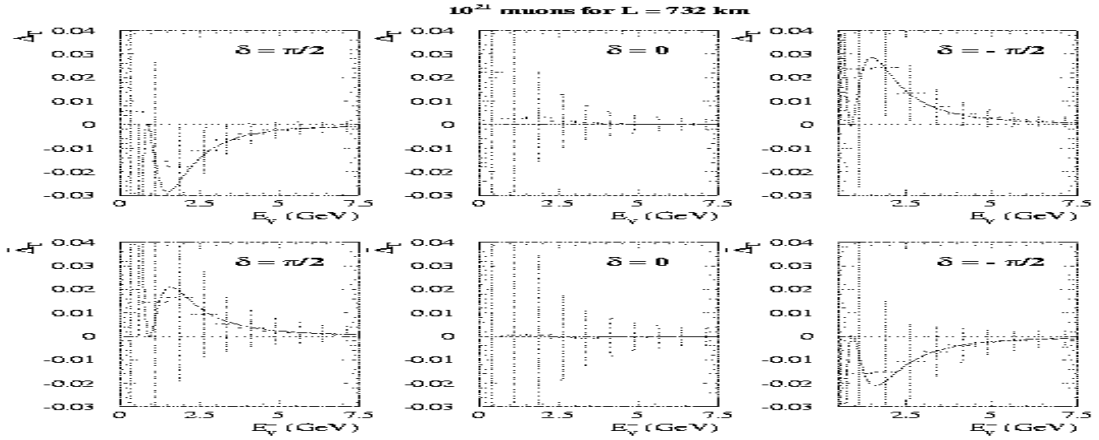

Fig. 58: *Oscillation probabilities for T-conjugate processes measured with a 10 kt detector with electron charge identification capabilities. The error bars correspond to* 10^{21} *muons decays, for an electron charge efficiency of 20% and misidentification of 0.1% [75].*

oscillation probability. The detection of taus, both from $\nu_\mu \to \nu_\tau$ and $\nu_e \to \nu_\tau$ oscillations, is also extremely important as a test of the unitarity of the mixing matrix. Comparing the yields from these channels to those expected from the disappearance, it is possible to put strong limits on the conversion of neutrinos into another species, for instance sterile neutrinos. If we call α and β the ratios of the oscillation probabilities $\nu_\mu \to \nu_\tau$ and $\nu_e \to \nu_\tau$ with respect to their expected value, the precisions on these parameters, with the assumptions made in [78], are shown in Table 11.

Baseline	$\Delta\alpha/\alpha$	$\Delta\beta/\beta$
2900	2%	25%
7400	2%	20%

Table 11: *Precision in the determination of the parameters* α *and* β*, that quantify the amount of* $\nu_\mu \to \nu_\tau$ *and* $\nu_e \to \nu_\tau$ *present in the data [78].*

5.5 *Search for New Physics at the Neutrino Factory*

As discussed earlier, it is not possible to accommodate all the present experimental results within the standard three-family oscillation framework. Up to now, we have assumed that the unconfirmed result from LSND could be explained by some misunderstood experimental effect, rather than by neutrino oscillations. We have already commented that Neutrino Factory physics would be even richer if the LSND result is indeed due to neutrino oscillations.

If the effect is due to some other interactions violating lepton flavour, distinct from neutrino oscillations, again the Neutrino Factory would be the ideal machine to study them. Because of the shape of the produced neutrino spectrum, this machine would also be an ideal place to look for a modification of the MSW potential for matter oscillations, since these effects would mainly be visible in the high-energy

part of the spectrum.

Discussions of these two possibilities are presented in the following two subsections. We note also that a deviation from the standard Lorentz metric due to extra dimensions could be explored by deviations of the neutrino velocity from the speed of light, which could in principle be measurable if one equipped a far detector with RPCs having a time resolution around 200 ps [181].

5.5.1 New physics in short-baseline experiments

The search for lepton-number-violating (LNV) muon decays with $\Delta L = 2$, of the type:

$$\mu^- \to e^- + \nu_e + \nu_\ell \tag{75}$$

where $(\ell = e, \mu, \tau)$, would be possible by looking for wrong-sign electrons, which would produce the following standard charged-current weak interactions in the detector:

$$\nu_e + N \to e^- + X \tag{76}$$

$$\nu_\ell + N \to l^- + X. \tag{77}$$

We assume that μ^- are circulating in the ring, since the signature sought has two neutrinos with negative helicity in the final state, so that one profit from the enhanced cross sections, compared with the positive-helicity case.

The signal for such anomalous muon decays does not depend on the distance between the neutrino source and the detector, unlike the oscillation case, and therefore is better studied with relatively small detectors at short distances, where one benefit from the higher neutrino flux. A 10 ton fiducial mass Liquid Argon detector located at a distance of 100 m from the muon storage ring was considered in [182] as a realistic case.

Because the signal sought consists in the appearance of final-state electrons, while standard events have positrons in the final state, an experiment with electron charge discrimination is mandatory. This is an experimental challenge, given the short radiation length in liquid argon. Realistic efficiencies and experimental backgrounds in a detector with the characteristics of the ICARUS Liquid Argon imaging TPC[183] have been studied. The detector simulated was a medium-sized Liquid Argon vessel surrounded by a dipole magnet.

Table 12 shows the effects of the cuts applied for a normalization of 10^{19} muon decays. To compute the expected number of signal events, a branching probability of 2.5×10^{-3} was considered, compatible with the LSND excess.

Given the low muon energies considered, most of the events will be quasi-elastic. Therefore, a final state configuration containing an electron and a reconstructed proton and no additional hadronic particles is required. These criteria reduce the quas-ielastic background (where we expect a neutron rather than a proton in the final state) by almost three orders of magnitude, while keeping more than 50% of the signal. The neutral-current background, where electron candidates come from π^0 conversion, is in general soft. After a cut on the electron candidate momentum, this kind of background becomes negligible. Preliminary studies indicate that, for a Liquid Argon detector inside a 1 T magnetic field, a fit to the direction of the electromagnetic shower could provide a good determination of the charge of leading electrons. Table 12 shows that applying loose criteria in the determination of the lepton charge is enough to eliminate $\bar{\nu}_e$ charged-current background.

5.5.2 New physics in long-baseline experiments

Exotic physics effects may appear in neutrino production, neutrino interactions or neutrino propagation in matter. Whilst the first two cases are better studied in a near detector, benefiting from the higher flux,

Cuts	ν_e CC	$\bar{\nu}_e$ CC
$E_{\mu^-} = 2$ GeV		
Initial	540	62500
One proton	367	11000
No pions	323	100
$E_e > 1$ GeV	103	17
Candidate charge	21	0.4
$E_{\mu^-} = 5$ GeV		
Initial	5290	802000
One proton	3390	212160
No pions	2112	495
$E_e > 3$ GeV	351	163
Candidate charge	71	4
$E_{\mu^-} = 1$ GeV		
Initial	76	6300
One proton	53	529
No pions	48	8
$E_e > 0.2$ GeV	43	4
Candidate charge	10	0.1

Table 12: *The effects of cuts on background and signal. We assumed a negative muon ring energy E_{μ^-} of 1, 2 and 5 GeV and a total of 10^{19} standard decays. The detector was assumed to be located 100 m from the center of the straight section. The lepton-number-violating decay was assumed to have the branching probability 2.5×10^{-3}. We denote by E_e the energy of the identified electron in the event.*

the effects of new physics on matter propagation are better observed in a long-baseline experiment, and might even interfere in the interpretation of long-baseline oscillation experiments.

We recall that the standard MSW effect gives rise to diagonal contributions to the neutrino squared-mass matrix proportional to the neutrino energy. A flavor-changing neutrino interaction would give rise to a non-diagonal term which, although smaller than the diagonal ones, would also grow with the neutrino energy. The effective neutrino squared-mass matrix M^2_{eff} would become

$$M^2_{eff} = U \begin{pmatrix} 0 & 0 & 0 \\ 0 & \Delta m^2_{21} & 0 \\ 0 & 0 & \Delta m^2_{31} \end{pmatrix} U^\dagger + 2EV \begin{pmatrix} 1+\epsilon_{ee} & \epsilon_{e\mu} & \epsilon_{e\tau} \\ \epsilon_{\mu e} & \epsilon_{\mu\mu} & \epsilon_{\mu\tau} \\ \epsilon_{\tau e} & \epsilon_{\tau\mu} & \epsilon_{\tau\tau} \end{pmatrix} , \tag{78}$$

where E is the neutrino energy, U is the neutrino mixing matrix in the usual parameterization, and $\Delta m^2_{21} > 0$ is the smaller squared-mass difference. In the standard case, all the ϵ parameters are equal to zero.

A model-independent limit on $\epsilon_{\tau\mu}$ can be inferred from atmospheric neutrino data [11]: $\epsilon_{\tau\mu} \lesssim 0.05$. Significant limits on the single $\epsilon^{e,u,d}$ quantities can be obtained if one assumes that the new physics operators originate from SU(2)$_W$-invariant operators. Then experimental bounds on charged-lepton processes imply [184, 185, 186]

$$\epsilon^e_{\mu e} \lesssim 10^{-6} \qquad \epsilon^e_{\tau\mu} \lesssim 3 \cdot 10^{-3} \qquad \epsilon^e_{\tau e} \lesssim 4 \cdot 10^{-3} \tag{79}$$

$$\epsilon^{u,d}_{\mu e} \lesssim 10^{-5} \qquad \epsilon^{u,d}_{\tau\mu} \lesssim 10^{-2} \qquad \epsilon^{u,d}_{\tau e} \lesssim 10^{-2} \ . \tag{80}$$

Since SU(2)$_W$ is broken, the limits above can be evaded. In the case of the exchange of a SU(2)$_W$ multiplet of bosons with SU(2)$_W$ breaking masses [185, 186], the the SU(2)$_W$ breaking masses can relaxed the limits by a factor of about 7, without a conflict with the electroweak precision data.

In general, the interactions involving the third family are far less constrained than those involving the first two. The constraint on $\epsilon_{\mu e}$ is so strong that no neutrino experiment would be able to improve it, since even at the limit the contribution it gives to neutrino oscillation is negligible. On the other hand, a value of $\epsilon_{\tau e}$ close to the experimental bound affects in a significant way both $\nu_e \to \nu_\mu$ and $\nu_e \to \nu_\tau$ oscillations, as seen in Fig. 59.

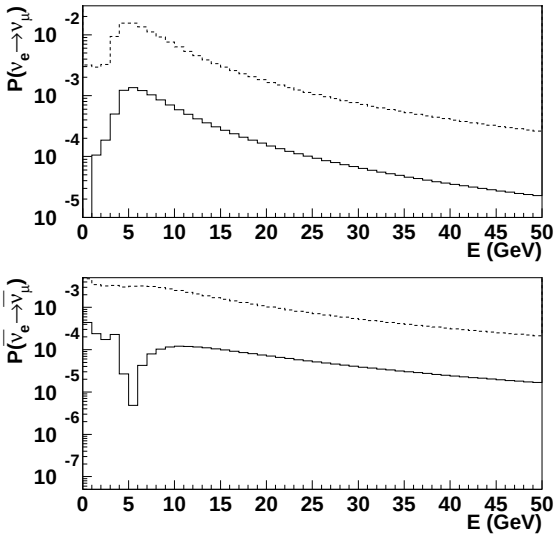

Fig. 59: *The $\nu_e \to \nu_\mu$ oscillation probability in the standard MSW model (full line) and in the presence of flavour-changing interactions (dashed line), for $\sin^2 2\theta_{13} = 0.001$ and $\epsilon_{\tau e} = 0.07$ [188].*

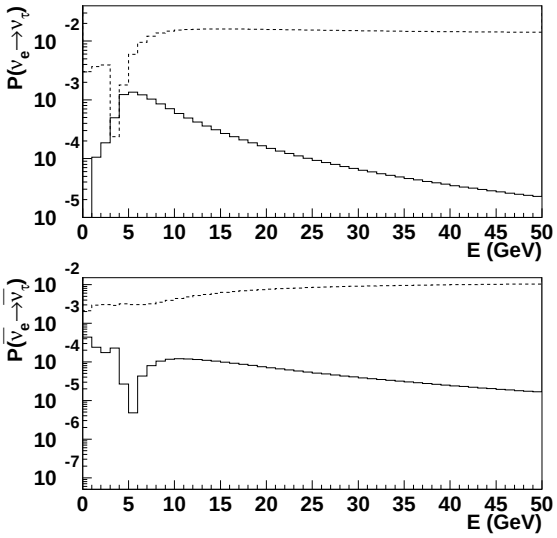

Fig. 60: *The $\nu_e \to \nu_\tau$ oscillation probability in the standard MSW model (full line) and in the presence of flavour-changing interactions (dashed line), for $\sin^2 2\theta_{13} = 0.001$ and $\epsilon_{\tau e} = 0.07$.*

The probability for oscillation into muons gets multiplied by an almost energy-independent factor. The presence of new physics leads to confusion with the case of normal oscillations, and an experiment could be led to infer a value of $\sin^2 2\theta_{13}$ higher than the true quantity [187]. However, the strong rise of the $\nu_e \to \nu_\tau$ probability, a clear indication of the presence of nonstandard interactions, can be seen from the decay $\tau \to \mu$, even with a detector only able to measure the muon momentum. The spectral shape of the muons will be so different that it is possible to distinguish the case of normal oscillation from those of new physics in large region of the parameter space [188], inferring the value of θ_{13} from event counting, and then comparing the observed spectrum with the theoretical one for the estimated θ_{13}. It has been shown that, for $\sin^2 2\theta_{13} \gtrsim 10^{-3}$, or $\epsilon_{13} \gtrsim 10^{-2}$, the spectral differences are such that the two cases can be clearly separated.

6 SUMMARY AND OUTLOOK

Neutrino physics has been making great strides during the past few years. It has provided us with a unique window on physics beyond the Standard Model, and significant progress has recently been made in measuring the parameters of neutrino oscillations. The atmospheric mixing angle θ_{23} seems to be near maximal, and a large value of the solar mixing angle θ_{12} is now also favoured. These notable differences from the small mixings observed previously among quarks whet our appetites for further information on neutrino oscillations. These may cast light on fundamental aspects of physics at the grand unification scale where all the interactions may be unified. Just as the past generation has witnessed the establishment of the Standard Model and quark physics, neutrinos and physics beyond the Standard Model seem destined to be at the forefront of experimental and theoretical physics for the coming generation.

Experiments now underway or being prepared will advance our knowledge of neutrino masses and oscillations in many ways. They will have improved sensitivity to neutrino masses and neutrinoless double-β decay. They will establish whether solar neutrino oscillations occur in the LMA, LOW, SMA or VAC region of parameters. They will clarify whether the LSND anomaly is due to neutrino oscillations. They will presumably confirm the existence of oscillation patterns, and that atmospheric ν_μ oscillate mainly into ν_τ. They will provide more precise measurements of the solar and atmospheric neutrino oscillation parameters, including the mass-squared differences, θ_{12} and θ_{23}. They will have improved sensitivity to θ_{13}.

The neutrino physics communities in Europe, Japan and the United States are all considering actively their options for the following step in oscillation physics. These should be addressed towards the many questions that are unlikely to be resolved in the approved round of experiments. These include pinning down θ_{13}, seeing intrinsically three-generation effects in mixing, searching for CP violation, and fixing the sign of Δm^2_{23} via matter effects. Short-term options include a JHF neutrino beam in Japan and off-axis long-baseline experiments in the United States and Europe. Specific experiments can be devised which address many of the individual open questions, but there is no guarantee that any or all of them will be answered by this next round.

We have presented in this report a set of options for Europe that would provide powerful tools for addressing all the open questions, by providing forefront experimental possibilities.

- A first step could be an intense proton source at CERN, the SPL, that would provide a low-energy neutrino beam of unprecedented power. This study also includes a summary report on the SPL design. The Fréjus tunnel is at just the right distance to observe oscillation effects with an SPL beam, and placing there a megaton-class water Čerenkov detector such as UNO would be an attractive option. The SPL-UNO combination would have a chance of observing CP violation in neutrino oscillations.

- A second possibility that has emerged from this study group is the concept of β beams, coming from the decays of radioactive isotopes produced by the SPL. Many accelerator questions vital for the viability of this concept remain to be investigated, but it may provide an exciting alternative option for studying CP violation in neutrino oscillations, and has interesting synergies with other options considered here.

- The best long-term option for neutrino physics is the neutrino factory based on muon decays in a storage ring. This offers unequalled reach for all the basic open questions: the magnitude of θ_{13}, CP violation and matter effects. Several important questions about the design of a neutrino factory remain to be answered, notably muon cooling. Even without cooling, there is an exciting programme of experiments with slow or stopped muons that complements the neutrino oscillation programme described here. If muon cooling can be perfected beyond the requirements of the neutrino factory, a muon collider may become feasible, offering exciting options in Higgs physics and/or high-energy lepton collisions, as discussed elsewhere.

This report is not the place for detailed studies of the accelerator questions that must be answered before these exciting physics options could become realities. However, we hope that this report communicates sufficient enthusiasm for neutrino physics to provide the motivation needed for research to make these options feasible.

References

[1] The 2002 Nobel Prize for physics was awarded to two pioneers in this field, R. Davis and M. Koshiba, see:
`http:// www.nobel.se/physics/laureates/2002/index.html`.

[2] Super-Kamiokande Coll. (Y. Fukuda *et al.*), Phys. Rev. Lett. **81**, 1562 (1998).

[3] NUSEX Coll. (M. Aglietta *et al.*), Europhys. Lett., **8**, 611 (1989); R. Becker-Szendy *et al.*, Phys. Rev. **D46**, 3720 (1992); Kamiokande Coll. (Y. Hirata *et al.*), Phys. Lett. **B280**, 146 (1992); Kamiokande Coll. (Y. Fukuda *et al.*), Phys. Lett. **B335**, 237 (1994); Frejus Coll. (K. Daum *et al.*), Z. Phys. **C66**, 417 (1995); W.A. Mann, for the Soudan 2 Coll., Nucl. Phys. **B** (Proc. Suppl.) **91**, 134 (2001); B.C. Barish, for the MACRO Coll., Nucl. Phys. **B** (Proc. Suppl.) **91**, 141 (2001).

[4] Homestake Coll. (B.T. Cleveland *et al.*), Astrophys. J. **496**, 505 (1998); GALLEX Coll. (W. Hampel *et al.*), Phys. Lett. **B447**, 127 (1999); Y. Suzuki, for the Super-Kamiokande Coll., Nucl. Phys. **B** (Proc. Suppl.) **91**, 29 (2001); V.N. Gavrin, for the SAGE Coll., Nucl. Phys. **B** (Proc. Suppl.) **91**, 36 (2001); E. Bellotti, for the GNO Coll., Nucl. Phys. **B** (Proc. Suppl.) **91**, 44 (2001); Super-Kamiokande Coll. (S. Fukuda *et al.*), hep-ex/0103032.

[5] SNO Coll. (Q. R. Ahmad *et al.*), Phys. Rev. Lett. **87**, 071301 (2001).

[6] J.N. Bahcall, M.H. Pinsonneault and S. Basu, astro-ph/0010346.

[7] SNO Coll. (Q.R. Ahmad *et al.*), nucl-ex/0204008.

[8] See, for example, J.W.F. Valle, Phys. Lett. **B199**, 432 (1987); E. Akhmedov, Phys. Lett. **B213**, 64 (1988); C.S. Lim and W. Marciano, Phys. Rev. **D37**, 1368 (1988); M. Gasperini, Phys. Rev. **D38**, 2635 (1988); M.M. Guzo, A. Masiero and S.T. Petcov, Phys. Lett. **B260**, 154 (1991); S. Coleman and S.L. Glashow, Phys. Lett. **B405**, 249 (1997); S.L. Glashow *et al.*, Phys. Rev. **D56**, 2433 (1997); G.L. Fogli *et al.*, Phys. Rev. **D59**, 117303 (1999); P. Lipari and M. Lusignoli, Phys. Rev. **D60**, 013003 (1999); M.C. Gonzalez-Garcia *et al.*, Phys. Rev. Lett. **82**, 3202 (1999); V. Barger *et al.*, Phys. Lett. **B462**, 109 (1999) and Phys. Rev. Lett. **82**, 2640 (1999); J. Pulido and E. Akhmedov, Phys. Lett. **B485**, 178 (2000); E. Lisi, A. Marrone, and D. Montanino, Phys. Rev. Lett. **85**, 1166 (2000); S. Bergmann *et al.*, Phys. Rev. **D62**, 073001 (2000); O. Miranda *et al.*, Nucl. Phys. **B595**, 360 (2001); D. Majumdar, A. Raychaudhuri and A. Sil, Phys. Rev. **D63**, 073014 (2001); M.M. Guzzo, H. Nunokawa and R. Tomàs, hep-ph/0104054.

[9] For a review, see G. Altarelli and F. Feruglio, Phys. Rept. **320**, 295 (1999), and references therein.

[10] P.I. Krastev and A.Yu. Smirnov, Phys. Rev. **D65**, 073022 (2002); J.N. Bahcall, M.C. Gonzalez-Garcia and C. Peña-Garay, JHEP **0108**, 014 (2001); A. Bandyopadhyay *et al.*, Phys. Lett. **B519**, 83 (2001); G. L. Fogli *et al.*, Phys. Rev. **D64**, 093007 (2001); P. Creminelli, G. Signorelli, and A. Strumia, JHEP **0105**, 052 (2001) [see hep-ph/0102234 for an update including the SNO data]; and many references therein.

[11] N. Fornengo, M.C. Gonzalez-Garcia and J.W.F. Valle, Nucl. Phys. **B580**, 58 (2000) and references therein.

[12] G.L. Fogli *et al.*, Nucl. Phys. **B** (Proc. Suppl.) **91**, 167 (2001); A. De Rújula, M.B. Gavela and P. Hernández, Phys. Rev. **D63**, 033001 (2001); G. L. Fogli, E. Lisi and A. Marrone, Phys. Rev. D **64**, 093005 (2001).

[13] M.C. Gonzalez-Garcia *et al.*, Phys. Rev. **D63**, 033005 (2001).

[14] B. Achkar *et al.*, Nucl. Phys. **B434**, 503 (1995); Chooz Coll. (M. Apollonio *et al.*), Phys. Lett. **B466**, 415 (1999); Palo Verde Coll. (F. Boehm *et al.*), Nucl. Phys. (Proc. Suppl.) **77**, 166 (1999).

[15] CCFR Coll. (A. Romosan *et al.*), Phys. Rev. Lett. **78**, 2912 (1997); L. Ludovici for the CHORUS Coll., Nucl. Phys. **B** (Proc. Suppl.) **91**, 177 (2001); M. Mezzetto, for the NOMAD Coll., Nucl. Phys. **B** (Proc. Suppl.) **91**, 184 (2001); K. Eitel, for the KARMEN Coll., Nucl. Phys. **B** (Proc. Suppl.) **91**, 191 (2001).

[16] K2K Coll. (S.H. Ahn *et al.*), Phys. Lett. **B511**, 178 (2001); K. Nakamura, for the K2K Coll., Nucl. Phys. **B** (Proc. Suppl.) **91**, 203 (2001); J.E. Hill, for the K2K Coll., hep-ex/0110034. Y. Oyama, for the K2K Coll.,Cairo International Conference on High Energy Physics, Cairo, Egypt, January 9-14, 2001, hep-ex/010401; S. Boyd, for the K2K Coll., Sixth International Workshop on Tau Lepton Physics, Victoria, BC, Canada, September 19, 2000. hep-ex/0011039.
See `http://neutrino.kek.jp/publications/` for further references.

[17] LSND Coll. (C. Athanassopoulos *et al.*), Phys. Rev. Lett. **75**, 2650 (1995); **77**, 3082 (1996); **81**, 1774 (1998); W.C. Louis, for the LSND Coll., Nucl. Phys. **B** (Proc. Suppl.) **91**, 198 (2001); LSND Coll. (A. Aguilar *et al.*), hep-ex/0104049.

[18] A.O. Bazarko, for the MiniBooNE Coll., Nucl. Phys. **B** (Proc. Suppl.) **91**, 210 (2001).

[19] C. Giunti, M.C. Gonzalez-Garcia and C. Peña-Garay, Phys. Rev. **D62**, 013005 (2000); G.L. Fogli, E. Lisi and A. Marrone, Phys. Rev. **D63**, 053008 (2001); O. Yasuda, hep-ph/0006319; and references therein.

[20] A. De Rújula, M.B. Gavela and P. Hernandez, Nucl. Phys. **B547** (1999) 21, hep-ph/9811390.

[21] MINOS Technical Design Report NuMI-L-337 TDR,
`http://www-numi.fnal.gov:8875/minwork/info/tdr/`,
`http://www-numi.fnal.gov:8875/forscientists.html`;
V. Paolone, Nucl. Phys. Proc. Suppl. **100** (2001) 197; S. G. Wojcicki, Nucl. Phys. Proc. Suppl. **91** (2001) 216.

[22] J. Hylen *et al.*, Fermilab-TM-2018, Sept. 1997.

[23] A. Rubbia, Nucl. Phys. **B** (Proc. Suppl.) **91**, 223 (2001).

[24] A.B. McDonald, for the SNO Coll., Nucl. Phys. **B** (Proc. Suppl.) **91**, 21 (2001).

[25] A. Piepke, for the KamLAND Coll., Nucl. Phys. **B** (Proc. Suppl.) **91**, 99 (2001).

[26] GNO Coll. in [4], and references therein.

[27] G. Ranucci *et al.*, Nucl. Phys. **B** (Proc. Suppl.) **91**, 50 (2001).

[28] A. de Gouvêa, A. Friedland and H. Murayama, Phys. Rev. **D60**, 093011 (1999).

[29] A. de Gouvêa, A. Friedland and H. Murayama, JHEP **0103**, 009 (2001).

[30] HELLAZ Coll. (A. de Bellefon *et al.*), Nucl. Phys. (Proc. Suppl.) **77**, 55 (1999).

[31] A. de Gouvêa and H. Murayama, Phys. Rev. Lett. **82**, 3392 (1999); JHEP **0008**, 025 (2000).

[32] P. Antonioli, for the MONOLITH Coll., Nucl. Phys. (Proc. Suppl.) **100**, 142 (2001).

[33] A. Geiser, Nucl. Phys. **B** (Proc. Suppl.) **91**, 147 (2001).

[34] J. Äystö *et al.*, CERN-TH/2001-231, hep-ph/0109217.

[35] M. Mangano *et al.*, CERN-TH/2001-131, hep-ph/0105155.

[36] C.M. Ankenbrandt *et al.*, Phys. Rev. ST Accel. Beams **2**, 081001 (1999).

[37] For a review, see Particle Data Group, `http://pdg.lbl.gov`; V.M. Lobashev *et al.*, Phys. Lett. **B460**, 227 (1999); C. Weinheimer *et al.*, Phys. Lett. **B460**,219 (1999) and Phys. Lett. **B464**, 352 (1999).

[38] KATRIN Coll., hep-ex/0109033.

[39] K.A. Assamagan *et al.*, Phys. Rev. **D53**, 6065 (1996).

[40] R. Barate *et al.*, Eur. Phys. J. **C1**, 395 (1998).

[41] W.H. Furry, Phys. Rev. **56**, 1184 (1939); for reviews, see M. Doi, T. Kotani and E. Takasugi, Prog. of Theor. Phys. Suppl. **83**,1 (1985); H.V. Klapdor-Kleingrothaus, World Scientific, Singapore (2001).

[42] E. Majorana, Nuovo Cimento **14**, 171 (1937).

[43] L. Baudis *et al.*, Phys. Rev. Lett. **83**, 41 (1999).

[44] H.V. Klapdor-Kleingrothaus, A. Dietz, H. Harney and I. Krivosheina, Mod. Phys. Lett. **A 16**, 2069 (2001).

[45] For a recent review, see A. Dolgov, hep-ph/0202122.

[46] S.S. Gerstein and Y.B. Zeldovich, JETP Letters **4**, 120 (1966).

[47] M. Fukugita, G.C. Liu and N. Sugiyama, Phys. Rev. Lett. **84**, 1082 (2000).

[48] S. Sarkar, Rept. Prog. Phys. **59**, 1493 (1996).

[49] For recent analyses of the perspectives in supernova neutrino physics, see for instance G.G. Raffelt, hep-ph/0201099, F. Cei, hep-ex/0202043, and references therein.

[50] S.P. Mikheev and A.Y. Smirnov, Sov. J. Nucl. Phys. **42**, 913 (1985) and Nuovo Cim. **C9**, 17 (1986); J. Frieman, H. Haber and K. Freese, Phys. Lett. **B200**, 15 (1988); Y.Z. Qian *et al.*, Phys. Rev. Lett **71**, 1965 (1993); A. Yu. Smirnov, D. N. Spergel and J. N. Bahcall, Phys. Rev. **D49**, 1389 (1994); B. Jegerlehner, F. Neubig and G. Raffelt, Phys. Rev. **D54**, 1194 (1996); H. Nunokawa, J.T. Peltoniemi, A. Rossi and J.W.F. Valle, Phys. Rev. **D56**, 1704 (1997); M. Kachelriess *et al.*, Phys. Rev. **D65**, 073016 (2002).

[51] M. Fukugita and T. Yanagida, Phys. Lett. **B174**, 45 (1986).

[52] M. Gell-Mann, P. Ramond and R. Slansky, Proceedings of the Supergravity Stony Brook Workshop, New York, 1979, eds. P. Van Nieuwenhuizen and D. Freedman (North-Holland, Amsterdam); T. Yanagida, Proceedings of the Workshop on Unified Theories and Baryon Number in the Universe, Tsukuba, Japan 1979 (edited by A. Sawada and A. Sugamoto, KEK Report No. 79-18, Tsukuba); R. Mohapatra and G. Senjanovic, Phys. Rev. Lett. **44**, 912 (1980).

[53] Z. Maki, M. Nakagawa and S. Sakata, Prog. Theor. Phys. **28**, 247 (1962).

[54] J. Ellis, J. Hisano, S. Lola and M. Raidal, Nucl. Phys. **B621**, 208 (2002); J. Ellis, J. Hisano, M. Raidal and Y. Shimizu, hep-ph/0206110 and Phys. Lett. **B528**, 86 (2002).

[55] C. D. Froggatt and H. B. Nielsen, Nucl. Phys. **B147**, 277 (1979).

[56] For reviews of GUT models, see:
G. Altarelli and F. Feruglio, Phys. Rept. **320**, 295 (1999) and hep-ph/0206077; S. Lola and G.G. Ross, Nucl. Phys. **B553**, 81 (1999).

[57] See, for instance, S.F. King and G.G. Ross, Phys. Lett. **B520**, 243 (2001), and references therein.

[58] K. Babu, C.N. Leung and J. Pantaleone, Phys. Lett. **B319**, 191 (1993); P.H. Chankowski and Z. Pluciennik, Phys. Lett. **B316**, 312 (1993).

[59] J. Ellis and S. Lola, Phys. Lett. **B458**, 310 (1999).

[60] Y. Kuno and Y. Okada, Rev. Mod. Phys. **73**, 151 (2001).

[61] J. Hisano, T. Moroi, K. Tobe and M. Yamaguchi, Phys. Rev. **D53**, 2442 (1996); J. Hisano, D. Nomura and T. Yanagida, Phys. Lett. **B437**, 351 (1998); J. Hisano and D. Nomura, Phys. Rev. **D59**, 116005 (1999); W. Buchmüller, D. Delepine and F. Vissani, Phys. Lett. **B459**, 171 (1999); M. E. Gómez, G. K. Leontaris, S. Lola and J. D. Vergados, Phys. Rev. **D59**, 11609 (1999); J. R. Ellis, M. E. Gómez, G. K. Leontaris, S. Lola and D. V. Nanopoulos, Eur. Phys. J. **C14**, 319 (2000); W. Buchmüller, D. Delepine and L. T. Handoko, Nucl. Phys. **B576**, 445 (2000); J. L. Feng, Y. Nir and Y. Shadmi, Phys. Rev. **D61**, 113005 (2000); J. Sato and K. Tobe, Phys. Rev. **D63**, 116010 (2001); J. Hisano and K. Tobe, Phys. Lett. **B510**, 197 (2001); S. Baek, T. Goto, Y. Okada and K. Okumura, hep-ph/0104146; T. Blazek and S. F. King, hep-ph/0105005; S. Lavignac, I. Masina and C.A. Savoy, hep-ph/0106245.

[62] F. Borzumati and A. Masiero, Phys. Rev. Lett. **57**, 961 (1986).

[63] MEGA Coll. (M.L. Brooks *et al.*), Phys. Rev. Lett. **83**, 1521 (1999).

[64] P. Wintz, *Proceedings of the First International Symposium on Lepton and Baryon Number Violation*, p. 534.

[65] L.M. Barkov *et al.*, Research Proposal for experiment at PSI (1999).

[66] BNL E940 (MECO) M. Bachman *et al.*, proposal Brookhaven P940.

[67] M. Furusaka *et al.*, JAERI/KEK Joint Project Proposal KEK-REPORT-99-4, JAERI-TECH-99-01.

[68] B. Pontecorvo, Sov. Phys. JETP **7**, 172 (1958) [Zh. Eksp. Teor. Fiz. **34**, 247 (1957)].

[69] H. J. Lipkin, Phys. Lett. B **348**, 604 (1995).

[70] Y. Takeuchi, Y. Tazaki, S. Y. Tsai and T. Yamazaki, hep-ph/9809558.

[71] Z. Maki, M. Nakagawa and S. Sakata, Prog. Theor. Phys. **28** 870 (1962).

[72] K,Hagiwara *et al., Particle Data Group* Phys. Rev. D **66** 010001 (2002)

[73] M. Kobayashi and T. Maskawa, Prog. Theor. Phys. **49** (1973) 652.

[74] C. Jarlskog, Adv. Ser. Direct. High Energy Phys. **3** (1989) 3.

[75] A. Bueno, M. Campanelli, S. Navas-Concha and A. Rubbia, Nucl. Phys. **B631**, 239 (2002).

[76] I. Mocioiu and R. Shrock, AIP Conf. Proc. **533**, (2000) 74.

[77] H. W. Zaglauer y K. H. Schwarzer, Z.Phys. **C40**, 273 (1998).

[78] A. Bueno, M. Campanelli and A. Rubbia, Nucl. Phys. **B589**, 577 (2000).

[79] P.F. Harrison and W.G. Scott, Phys. Lett. **B476**, 349 (2000), hep-ph/9912435

[80] A. de Gouvêa, A. Friedland and H. Murayama, Phys. Lett. **B490**, 125 (2000).

[81] P.I. Krastev and A.Yu. Smirnov, in [10].

[82] L. Wolfenstein, Phys. Rev. **D17**, 2369 (1978); S.P. Mikheev and A.Yu. Smirnov, Sov. J. Nucl. Phys. **42**, 913 (1985) [Yad. Fiz. **42**, 1441 (1985)].

[83] M.V. Garzelli and C. Giunti, Phys. Lett. **B488**, 339 (2000), hep-ph/0007155; P. Creminelli, G. Signorelli, and A. Strumia, hep-ph/0102234.

[84] R. Barbieri and A. Strumia [10]; V. Barger, D. Marfatia and B. Wood, Phys. Lett. **B498**, 53 (2001); H. Murayama and A. Pierce, hep-ph/0012075.

[85] A. de Gouvêa and C. Peña-Garay, hep-ph/0107186.

[86] A. Strumia and F. Vissani, hep-ph/0109172.

[87] Super-Kamiokande Coll. (S. Fukuda *et al.*), hep-ex/0103033.

[88] See, for example, M.C. Gonzalez-Garcia, C. Peña-Garay, and A.Yu. Smirnov, Phys. Rev. **D63**, 113004 (2001); V. Barger, D. Marfatia and K. Whisnant, hep-ph/0104095.

[89] See, for example, G.L. Fogli, E. Lisi, and D. Montanino, Phys. Lett. **B434**, 333 (1998); D. Majumdar and A. Raychaudhuri, Pramana **52**, L529 (1999); F.L. Villante, G. Fiorentini and E. Lisi, Phys. Rev. **D59**, 013006 (1999); J.N. Bahcall, P.I. Krastev, and A.Yu. Smirnov, Phys. Lett. **B477**, 401 (2000); Phys. Rev. **D62**, 093004 (2000); **D63**, 053012 (2001); M. Maris and S.T. Petcov, Phys. Rev. **D62**, 093006 (2000); G.L. Fogli *et al.*, hep-ph/0102288; V. Barger, D. Marfatia and K. Whisnant, hep-ph/0104166.

[90] See, for example, H. Minakata and H. Nunokawa, Phys. Lett. **B504**, 301 (2001); C. Lunardini and A.Yu. Smirnov, hep-ph/0106149; M. Kachelriess *et al.*, hep-ph/0108100; and many references therein.

[91] See H. Ejiri, Nucl. Phys. **B** (Proc. Suppl.) **91**, 255 (2001), and references therein for the current data; see, for example, E. Fiorini, Nucl. Phys. **B** (Proc. Suppl.) **91**, 262 (2001), for future prospects.

[92] H.V. Klapdor-Kleingrothaus, H. Pas, and A.Yu. Smirnov, Phys. Rev. **D63**, 073005 (2001); A. Wodecki and W.A. Kaminski, Int. J. Mod. Phys. **A15**, 2447 (2000); K. Matsuda, N. Takeda, and T. Fukuyama, hep-ph/0012357; S.M. Bilenky, S. Pascoli, and S.T. Petcov, hep-ph/0102265; hep-ph/0104218; and references therein.

[93] K. Ishihara, for the KamLAND Coll., talk at the NuFACT'01 Workshop in Tsukuba, Japan (May 24–30, 2001). Transparencies at `http://psux1.kek.jp/~nufact01/index.html`.

[94] A. de Gouvêa and C. Peña-Garay, Phys. Rev. **D64**, 113011 (2001).

[95] H. Murayama and A. Pierce, Phys. Rev. **D65**, 013012 (2002).

[96] J.J. Gómez-Cadenas and D.A. Harris, Ann. Rev. Nucl. Part. Sci. **52**, 253 (2002).

[97] A. de Gouvêa, A. Friedland and H. Murayama. Phys. Lett. **B490**, 125 (2000).

[98] OPERA Progress Report, LNGS-LOI 19/99, `http://operaweb.web.cern.ch/operaweb/`.

[99] ICARUS Coll. (F. Arneodo *et al.*), Nucl. Instrum. Meth. A **471**, 272 (2000); A. Rubbia, Phys. Scripta **T93**, 70 (2001); `http://pcnometh4.cern.ch`.

[100] Y. Itow *et al.* , hep-ex/0106019.

[101] M. Furusaka, R. Hino, Y. Ikeda *et al.*, KEK Report 99-4; JAERI-Tech 99-056; JHF-99-3 (1999).

[102] B. Autin *et al.*, CERN report CERN-2000-012 (2000).

[103] B. Autin, A. Blondel and J. Ellis, eds., CERN report CERN-99-02 (1999); for an updated study, see the accelerator physics part of this report.

[104] N.V. Mokhov, Fermilab-FN-628 (1995).

[105] M. Donega, graduation thesis, Milan University, unpublished.

[106] M. Mezzetto, talk presented at the 9th International symposium on Neutrino Telescopes, Venice, March 2001.

[107] Luigi Mosca, talk given in the ECFA Neutrino Oscillation Working Group, May, 10th, 2001: `http://muonstoragerings.web.cern.ch/muonstoragerings`, `http://mdonega.home.cern.ch/mdonega/lowe/homepage.html`.

[108] Super-Kamiokande Coll. (Y. Fukuda *et al.*), Phys. Lett. **B433**, 9 (1998) [hep-ex/9803006].

[109] LSND Coll., Phys. Rev. Lett. **81**, 1774 (1998).

[110] D. Casper, unpublished.

[111] M. D. Messier, UMI-99-23965 (1999).

[112] M. Shiozawa, for the Super-Kamiokande Coll., Nucl. Instrum. Meth. **A433**, 240 (1999).

[113] T. Barszczak, University of California, Irvine Ph. D. thesis (to be published).

[114] E. Kolbe *et al.*, Nucl. Phys. **A613**, 382 (1997), E. Kolbe *et al.*, Nucl. Phys. **A652**, 91 (1999).

[115] M. Mezzetto, Nufact note 060/2000 (2000); `http://mdonega.home.cern.ch/mdonega/lowe/homepage.html`.

[116] A. Cervera *et al.*, Nucl. Phys. B **579**, 17 (2000) [Erratum-ibid. B **593**, 731 (2001)].

[117] J. Burguet-Castell *et al.* Nucl. Phys. **B608**, 301 (2001), hep-ph/0103258.

[118] F. Dydak, presentation to the CERN NuFact oscillation working group, March 19, 2002.

[119] F. Vannucci, presentation to the CERN NuFact oscillation working group September 10, 2002.

[120] For an introduction, see: `http://projects.fnal.gov/protondriver`.

[121] W. Chou, C. Ankenbrandt and E. Malamud (eds.). FERMILAB-TM-2136 (2000).

[122] W. Foster, http://tdserver1.fnal.gov/foster.

[123] G. Barenboim, A. de Gouvêa, M. Szleper and M. Velasco, FERMILAB-Pub-02/066-T, nuhep-exp/2002-01, hep-ph/0204208; see also D. Ayres *et al.*, *Letter of Intent to build an Off-axis Detector to study $\nu_\mu \to \nu_e$ oscillations with the NuMI Neutrino Beam*, hep-ex/0210005.

[124] A. Blondel, M. Campanelli and M. Fechner, CERN Neutrino Factory Notes 112-2002 and 119-2002.

[125] T.K. Gaisser and J.S. O'Connell, Phys. Rev. **D34** (1986), 822.

[126] D. Casper, unpublished.

[127] Super-Kamiokande Coll. (Y. Fukuda *et al.*), Phys. Lett. **B433**, 9 (1998).

[128] D. M. Schmidt *et al.*, Nucl. Instr. Meth. Phys. Res. **A328**, 547 (1998); M. Campanelli, Ph. D. Thesis, ETH Zürich, 12742 (1998); L3 Coll., CERN-EP/98-167 (1998); M. Diehl and O. Nachtmann, Z. Phys. **C62**, 397 (1994); E. Lançon *et al.*, ALEPH 97-073 (1997).

[129] UNO proposal, Preprint SBHEP01-3, June 2001.

[130] P. Zucchelli, Phys. Lett. **B532** 166 (2002).

[131] H. L. Ravn, IEEE PAC95 proceedings, p. 858.

[132] R. Garoby, CERN/PS 2001–007 (RF) and CERN-NUFACT–Note 074.

[133] R.B. Firestone et al., *Table of isotopes on CD–ROM*, 8th edition, 1996, Wiley InterScience.

[134] D.H. Perkins, *Introduction to high energy physics*, Addison Wesley, Menlo Park, 1987, p. 210.

[135] A. Blondel, Nucl. Instr. Meth. **A451**, 131 (2000); Neutrino factory note CERN–NUFACT–07, November 1999.

[136] S. Geer, Phys. Rev. **D57**, 6989 (1998).

[137] B. Autin, A. Blondel and J. Ellis (eds.), CERN report CERN 99-02.

[138] S.Ozaki *et al.*, available from
http://www.cap.bnl.gov/mumu/studyii/FS2-report.html.

[139] R.Garoby, CERN-PS-2001-007-RF, NuFact Note 74, available from
http://muonstoragerings.cern.ch; B.Autin *et al.*, NuFact Note 103 (2001).

[140] Y.Kuno *et al.*, available from http://www-prism.kek.jp/nufactj/index.html.

[141] A.N. Skrinsky and V.V. Parkhomchuk, Sov. J. of Nuclear Physics **12**, 3 (1981).

[142] J.S. Berg, R.C. Fernow and R.B. Palmer, MUCOOL note 239, April 2002.

[143] E. Keil, CERN-NUFACT Notes 26 (triangle) and 48 (bow-tie) (2000), available from:
http://molat.home.cern.ch/molat/neutrino/nf26.pdf;
http://molat.home.cern.ch/molat/neutrino/nf48.pdf.

[144] E. Keil, CERN-NUFACT Note 54 (2000), available from:
http://molat.home.cern.ch/molat/neutrino/nf54.pdf.

[145] E. Keil, CERN-NUFACT Note 56 (2000), available from:
http://molat.home.cern.ch/molat/neutrino/nf56.pdf.

[146] A. Broncano and O. Mena, hep-ph/0203052.

[147] R. Fernow, J. Gallardo and Y. Fukui, MUCOOL-note 129, (2000);
http://www-mucool.fnal.gov/mcnotes/public/pdf/muc0129/muc0129_abs.txt;
see also: A. Blondel, M. Donega and S. Gilardoni, CERN NUFACT-Note-078 (2000),
http://nicewww.cern.ch/ molat/neutrino/nf78.pdf.

[148] C. Johnson, R. B. Palmer and E. Keil, Nucl. Instr. Meth. **A451**, 265 (2000).

[149] A. Blondel, in CERN 99-02 (1999), pp. 51-54.

[150] R. Raja and A. Tollestrup, Phys. Rev. **D58**, 13005 (1998), hep-ex/9801004.

[151] I. Papadopoulos, Proceedings of NUFACT00, Monterey, California, (2000).

[152] R. Piteira, Internal report, Stage de Magistère, Ecole Normale Supérieure de Paris, (2001).

[153] A. Cervera, F. Dydak and J.J. Gómez-Cadenas, Nucl. Instr. Meth. **A451**, 123 (2000).

[154] T. Soesbe and K. Lang, Internal report NuMI-L-356 (1998); M. Guler *et al.*, CERN SPSC/P311 (1999).

[155] M. Doucet *et al.*, Nucl. Instr. Meth. **A453**, 545 (2000).

[156] GEANT3 CERN Program Library Long Writeup W5013.

[157] M. Ambrosio *et al.*, Nucl. Instr. Meth. **A456**, 67 (2000).

[158] T. Tabarelli de Fatis, Eur. Phys. J. C24 (2002) 43.

[159] M. Selvi, Ph.D. Thesis, Bologna University (2002);
M. Selvi, talk at the Workshop on a Massive Underground Neutrino Detector with Leptonic Charge-Sign Discrimination, Sitges, November 2001:
http://www.bo.infn.it/∼selvi/monolith/NuFact.ppt.

[160] OPERA Coll. (M. Guler *et al.*), CERN-SPSC-2000-028.

[161] OPERA Coll. (M. Guler *et al.*), *Status report on the OPERA experiment*, CERN-SPSC-2001-025.

[162] A.E. Ball *et al.*, *CNGS: Update on secondary beam layout*, SL-Note-2000-063 EA.

[163] V. Barger, S. Geer, R. Raja and K. Whisnant, Phys. Rev. **D62** (2000) 013004, hep-ph/9911524

[164] A. Bueno, M. Campanelli and A. Rubbia, Nucl. Phys. **B573**, 27 (2000), hep-ph/9905240.

[165] V. Barger, S. Geer, R. Raja and K. Whisnant, Phys. Lett. **B485**, 379 (2000), hep-ph/0004208.

[166] K. Dick, M. Freund, M. Lindner and A. Romanino, Nucl. Phys. **B562** (1999) 29.

[167] A. Donini, B. Gavela, P. Hernández, S. Rigolin, Nucl. Phys. **B574** (2000) 23.

[168] A. Romanino, Nucl. Phys. **B574**, 675 (2000), hep-ph/9909425.

[169] R.Geller, presentation at the Nufact'01 workshop,
http://www-prism.kek.jp/nufact01/May28/WG1/28wg1_geller.pdf.

[170] H. Minakata and H. Nunokawa, JHEP **0110** (2001).

[171] V. Barger, D. Marfatia and K. Whisnant, Phys. Rev. **D65**, 073023 (2002).

[172] M. Freund, P. Huber and M. Lindner, Nucl. Phys. **B615**, 331 (2001), hep-ph/0105071.

[173] M. Koike, T.Ota and J. Sato Phys.Rev. **D65**(2002) 053015, hep-ph/0011387.

[174] J. Pinney and O. Yasuda, Phys. Rev. **D64** (2001) 093008, hep-ph/0105087.

[175] P. Huber, M. Lindner and W. Winter, hep-ph/0204352, to be published in Nucl. Phys. B.

[176] A. Donini, D. Meloni and P. Migliozzi, hep-ph/0206034.

[177] J. Burguet-Castell *et al.*, hep-ph/0207080.

[178] J.N. Bahcall, M.C. Gonzalez-Garcia and C. Peña-Garay, JHEP **0207**, 054 (2002), hep-ph/0204314.

[179] G. Barenboim, J.F. Beacom, L. Borissov and B. Kayser, Phys.Lett. **B537**, 227 (2002), hep-ph/0203261.

[180] K.S. Babu and S. Pakvasa, hep-ph/0204236.

[181] V. Ammosov and G. Volkov, hep-ph/0008032.

[182] A. Bueno *et al.* JHEP **0106**, 032 (2001), hep-ph/0010308.

[183] ICARUS Coll. (C. Vignoli *et al.*), Nucl. Phys. Proc. Suppl. **85**, 119 (2000).

[184] S. Bergmann, Nucl. Phys. **B515**, 363 (1998), hep-ph/9707398.

[185] S. Bergmann, Y. Grossman and D.M. Pierce, Phys. Rev. **D61**, 053005 (2000), hep-ph/9909390.

[186] S. Bergmann et al., Phys. Rev. **D62**, 073001 (2000), hep-ph/0004049.

[187] P. Huber, T. Schwetz and J.W.F. Valle, hep-ph/0111224.

[188] M. Campanelli and A. Romanino, hep-ph/0207350.

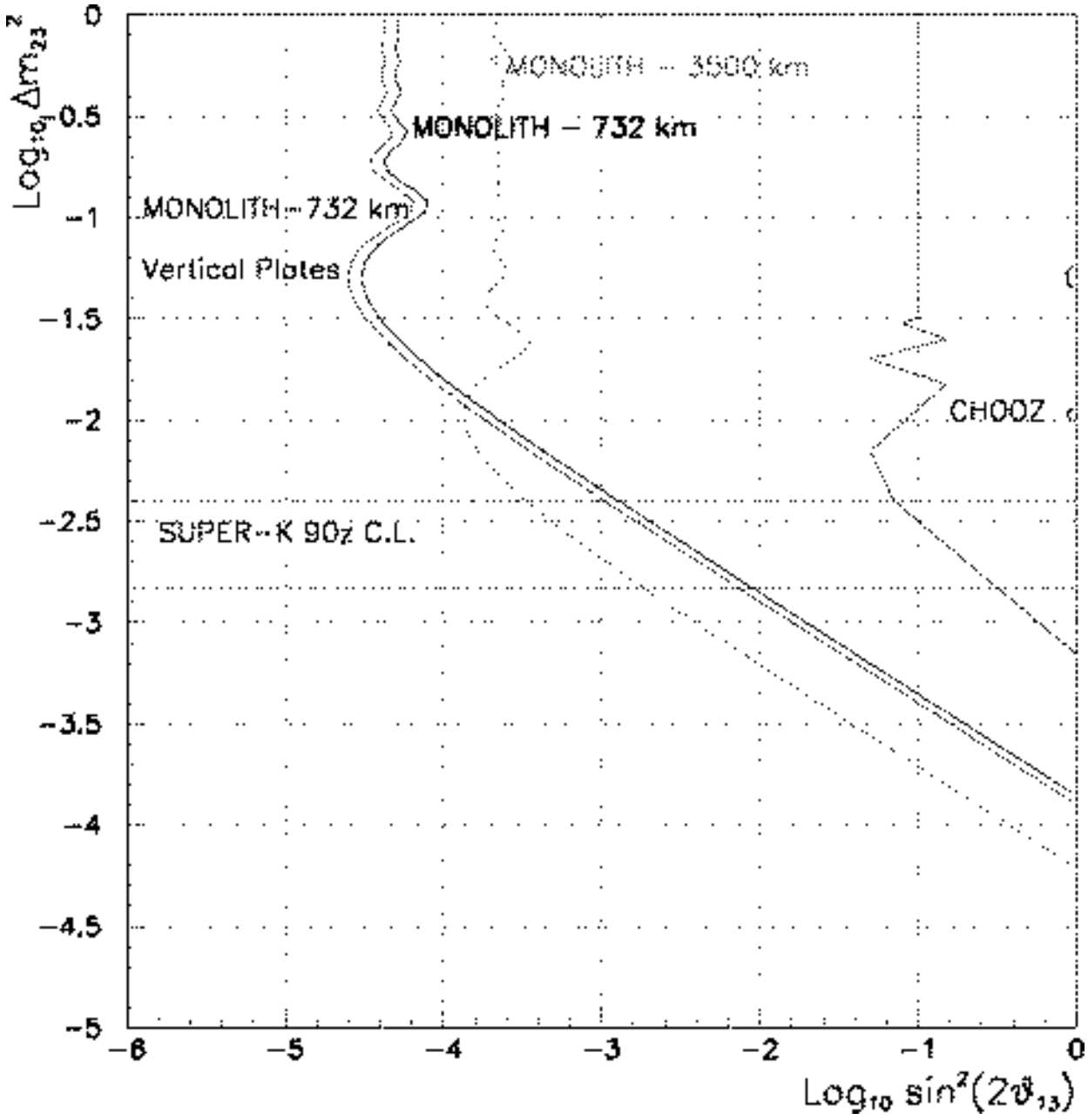
MONOLITH – 3500 km
MONOLITH – 732 km
MONOLITH – 732 km
Vertical Plates
CHOOZ
SUPER-K 90% C.L.
$\mathrm{Log}_{10}\Delta m^2_{23}$
$\mathrm{Log}_{10}\sin^2(2\vartheta_{13})$
0
−0.5
−1
−1.5
−2
−2.5
−3
−3.5
−4
−4.5
−5
−6
−5
−4
−3
−2
−1
0

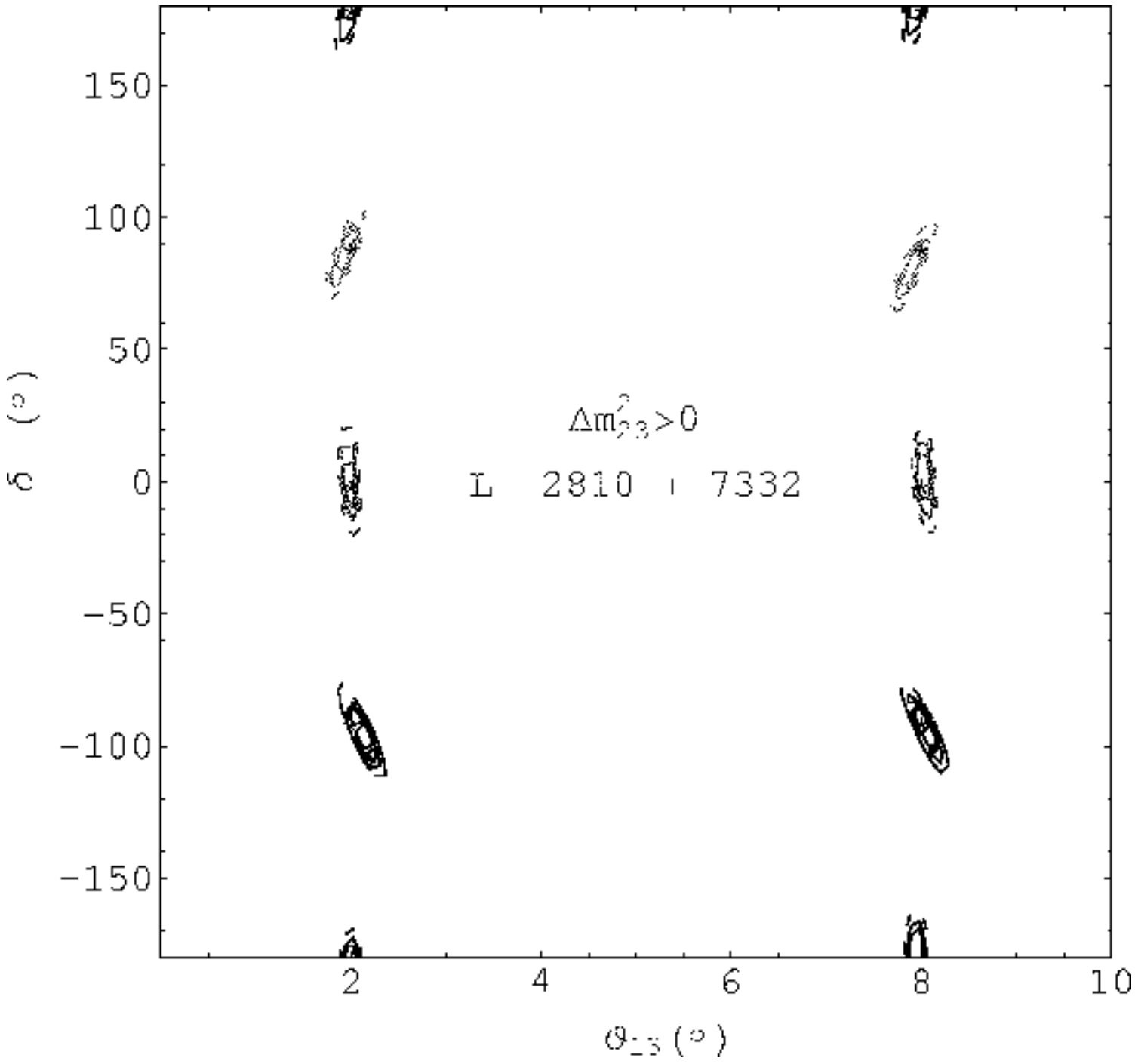
150
100
50
0
−50
−100
−150
δ (°)
$\Delta m^2_{23}>0$
L 2810 + 7332
2
4
6
8
10
θ_{13} (°)